QUANTITATIVE ANALYSES OF CADHERIN-BASED ADHESIVE FORCE

A Dissertation
Presented to
The Academic Faculty

By

Chimdimnma Chinaza Esimai

In Partial Fulfillment
Of the Requirements for the Degree
Doctor of Philosophy in Bioengineering in the
Woodruff School of Mechanical Engineering

Georgia Institute of Technology

August 2015

QUANTITATIVE ANALYSES OF CADHERIN-BASED ADHESIVE FORCE

Approved by:

Dr. Andrés García, Advisor
School of Mechanical Engineering
Georgia Institute of Technology

Dr. Susan Thomas
School of Mechanical Engineering
Georgia Institute of Technology

Dr. Thomas Barker
School of Biomedical Engineering
Georgia Institute of Technology

Dr. Cheng Zhu
School of Mechanical Engineering
Georgia Institute of Technology

Dr. Andrew Kowalczyk
Department of Cell Biology
Emory University

Date Approved: August 21, 2015

To my family, and to my many friends, who have become like family

ACKNOWLEDGEMENTS

I am completely overwhelmed at the incredible support system I have enjoyed throughout my journey. My biggest form of support has come through my family, whose constancy has sustained me, challenged me, and encouraged me. My father, Charles, was my first inspiration for pursuing engineering. My many conversations with him about engineering and his tradition of maintaining the largest library I had ever seen outside a public library kept me engaged and fascinated with the practical application of engineering. *Dalu-so.* To my mother, Grace, whose passion for and tenacity in the pursuit of excellence has kept me going, no matter how difficult the task. You are simply amazing, and you continue to lead by shining example. It's no wonder numerous people outside our family, across gender, age and many other classifications, call you "Mom." My sister, Ogenna, was truly my first role model, academically and otherwise. Thank you for setting the pace, for doing all things humbly and with a genuine heart, and for making every day of every year National Siblings' Day. May everything you touch turn to gold. My brother Obiora is so effortlessly cool and smart – I want to be like you when I grow up. You live up to your name in every single thing that you do, and I am just blown away by your inexhaustible thirst for knowledge/wisdom, for wellness, for happiness, and for authentic relationships. To my sister and second mom, Chineme, I love you and you have no idea how much you mean to me. Thank you for picking up the baton where my formal education has stopped giving me lessons, and thank you for not giving up on me. Thank you all for intervening at key times, and for paving the way. I hope to continue to do the Esimai name proud.

I must gratefully acknowledge my advisor, Dr. Andrés García, who models what it takes to be successful and to be one of the best in the field. Andrés, it is no wonder why you command utmost respect from students, peers, and superiors alike, as you take on every task with aplomb,

professionalism, and a heartfelt enjoyment for great science and interacting with great people. Thank you for giving me the opportunity to learn from you. You've been honest, encouraging, critical, and you've been patient. Perhaps what I admire the most is that you have striven to be the best in all areas of your life not just in science, and you have perfected a work-life balance that is truly exemplary. I am committed to incorporating adhesion topics into future research opportunities, and it's been helpful to observe how you've managed a successful research program and maintained healthy collaborations in many different countries. Thank you again for this experience.

Likewise, I extend gratitude to my thesis committee members for their time, reagents, and perspective toward my PhD project. I thank Dr. Andrew Kowalczyk for sharing critical reagents that are at the heart of this project. I thank you for allowing me to ask questions, to learn from your lab members, and for being a huge support over the years. I thank Dr. Thomas Barker for helpful comments and advice on protein purification and for allowing me to use your AKTA machine for protein purification. I thank Dr. Cheng Zhu for sharing perspectives on graduate school and teaching and for critical comments and probing questions throughout this process. Although she is the newest member of my committee, Dr. Susan Thomas has come on-board with timely and helpful comments. Thank you all.

Wing 2D is a popular wing in IBB. I thank David Reece for being an excellent cubicle neighbor. It has been a pleasure to converse about balancing leadership roles in various areas of our lives. You are a kindred spirit, and I'm encouraged every time we speak. Thank you for your willingness to be disturbed. And congratulations on fatherhood! Likewise, Dr. Lakshmi is a wise soul who is truly kind and generous with his time/resources. Thank you for your advice and conversations over the years. Dennis Zhou has been particularly helpful in teaching me mPAD

technology. My gratitude is sincere, as you've been so generous with your time. I pray that you accomplish everything you set your heart to. Stay encouraged! Dr. Nduka Enemchukwu (and Chinyere Enemchukwu) has been a great colleague (and friend). You both have been excellent role models. Continue to live up to your surname. I cannot wait to continue to hear great news about you guys. To Dr. Imen Elloumi-Hannachi, you're one of my favorite people in the world. Imen, *unnie,* thank you for your friendship and your timely words of encouragement.

I am grateful for the staff of the Petit Institute for Bioengineering and Bioscience (IBB). You are critical to the success of IBB's mission through your generous and professional service. Particularly, I thank the late Christopher Ruffin, who welcomed me into the Bioengineering Program and cared about the progress of every student. You are sorely missed. I acknowledge Vivian Johnson, Deidra Johnson, Floyd Wood, James Godard, Alyceson Andrews, Allen Echols, Andrew Shaw, Nadia Boguslavsky, Laura Paige, Karen Ethier, Melissa Raine, and Steve Woodard for their help and generosity. Megan McDevitt, now at Gladstone Institutes, effortlessly personified the IBB spirit, and I'm happy I got to learn how to build community from one of the best. Special thanks to Vivian and Deidra who always asked about my well-being and even sought me out to touch base. Special thanks go to Steve Woodard for lending me a critical piece of equipment to revive a part of my project. IBB custodial staff has been wonderful, including Wilhelmina, Ms. RiRi, Ms. Joyce, and Sharon, who genuinely care about the welfare of each and every student on their floors. Thank you!

Members of the broader Georgia Tech community merit special acknowledgment for facilitating my development and progress. To Dr. Comas Haynes and Dean Gary May, thank you so much for supporting special professional development opportunities for me through the FACES Fellowship and the Compact Institutes. To Dr. Raheem Beyah, Dr. Felicia Benton-

Johnson, Ms. Tia Jackson, Ms. Jacqueline Cox, Ms. Lakeita Servance, and the rest of the CEED/SURE/EBICS teams, thank you for making me an integral part of SURE 2015. To all the faculty members of the Graduate Leadership Program, including Drs. Johnna Temenoff and Ravi Bellamkonda, and former Scheller College of Business Dean Terry Blum, thank you the experience of GLP. Special thanks to Dr. Wendy Newstetter who is always a great resource and supporter, and has helped shape the IBB/Whitaker communities for the better. I thank Dr. Julia Babensee and Dr. Todd Sulchek for words of advice. I thank Dr. Rudy Gleason, who has always taken special interest in my progress. I also thank Darren Nowell, Dr. Wayne Whiteman, and Nancy Hutton for extraordinary efforts in funding matters. Staff of the Institute for Electronics and Nanotechnology (IEN) have been kind. Dr. Jie Xu trained on Biacore T200 machine for surface plasmon resonance. Gary Spinner truly embodies the IEN's collegial spirit and leads operations seamlessly with a great heart and a smile. Georgia Tech. Thank you for making me a part of the IEN family! I hope to give back to the IEN solely because of your efforts.

I am grateful for funding throughout my graduate school career. The National Science Foundation and the UNCF-Merck Science Initiative have supported me.

It would be remiss not to mention four company representatives who have been critical to the success of my projects. Donna Popp, of ThermoFisher, lobbied *tirelessly* for me to receive an expensive piece of equipment at no cost whatsoever to support my protein purification work at a critical juncture. Thank you so much! Sandra Savic, of ThermoScientific, was exceptionally responsive and frequently sent me columns, media/resin, and buffer samples to aid my protein purification work. Amy Hamilton, of Life Technologies, has just been amazing in being a great resource for all reagent needs and for amazing discounts. John Slatner, FPLC guru extraordinaire, taught me how to be an independent chromatographer.

A great cloud of witnesses surrounds me, and these giants have imparted so much to me. To Dr. George Ude and Dr. Asopuru Okemgbo – how should I begin? You have modeled how to achieve the seemingly impossible in every area of your life, and I am so grateful our paths have crossed in this life. I cannot imagine my life without you. Dr. Toyin Mafe, thank you for stepping in at such a critical time with practical words of advice and for your consistent mentoring. Dr. John Louis-Ugbo – your life is testimony that balance, excellence, and unfailing commitment to family and community are entirely possible, and that it can be accomplished flawlessly – you and your family have been so amazing to me and mine from my first year of graduate school. Thank you! To Dr. Johnson Adefila, Mrs. Mary Adefila, Dr. Lola Olufemi, the Odunade family, Saki, and the entire Family Praise Chapel team: indeed, you have been family. I count myself blessed to have found a true home with you during my time here in Atlanta. To the entire Oyeleye family (thank you for the uncannily timely and amazing phone calls from Loni!), Esther Max-Onakpoya, and the rest of the incredible BCF family, past and present, all over the world, you're family and I'm home every time I am with and within our vibrant community. I met Mr. Bayonle Akinade through a Visiting Scholar exchange program here at Tech, and in the brief time I knew him, and by extension, his family, he imparted so much wisdom and encouragement to my life before he lost a very brave battle with cancer. Thank you, sir, for your legacy. We all miss you.

My friends and my friends who have become family have made this journey truly special. Dr. Chiagozie Fawole, the sky is your limit. I'm your biggest supporter, and I'm on your team. To Dr. Christine Tolu-Ajayi, you're the hardest working and kindest person I know. And also the most hilarious. I would pay to watch your comedy show. Your reward is so very near. To He Zheng, Dr. Garth Thompson, Dr. Sharanya Arcot Desai, thank you for great memories from

graduate school! To the Black Graduate Students Association BME/BIOEs who paved the way: Dr. Nnena Adimora-Finn, Dr. Barbara Nsiah, Dr. Samantha Andrews, the aforementioned Dr. Nduka Enemchukwu – I still remember your incredible representation at NSBE Nationals that made me so happy that I would be in good company.

Utmost thanks go to my lifelong co-creators and co-conspirators – GF, JC, and HG. There are not enough words in the English language to convey my gratitude. You have been there every single step of the way, celebrating every success, comforting every sorrow, listening to every idea, and being my biggest advocates and supporters. Here's to embarking on the next adventure.

TABLE OF CONTENTS

LIST OF TABLES

LIST OF FIGURES

LIST OF SYMBOLS AND ABBREVIATIONS

2D	two-dimensional
3D	three-dimensional
AJ	adherens junction
ANOVA	analysis of variance
CHO	Chinese hamster ovary
ECM	extracellular matrix
EMT	epithelial-mesenchymal transition
HMEC-1	human microvascular endothelial cell
FBS	fetal bovine serum
FN	fibronectin
kDa	kilo Dalton

SUMMARY

Cell adhesion is a critical determinant of tissue architecture and tissue organization. Cadherin proteins mediate cell-cell adhesion in a calcium-dependent manner. The functional roles for cadherin proteins early in development and in adults, as well as the multiple disease phenotypes resulting from cadherin dysregulation, underscore the importance of cadherin proteins. Cadherin structure, force, and interaction dynamics are not yet completely understood because of lack of experimental platforms to study cadherin proteins. Engineered platforms with highly defined cadherin ligands presented in a controlled manner can be used to investigate cadherin-based adhesive force. Adhesive force measurement tools such as alkanethiols and micro-fabricated force array detectors promise to meet this challenge of elucidating how cadherin complex assembly and function develop in a spatiotemporal manner in human health and disease.

The goal of this thesis was to engineer adhesive surfaces that support cadherin-based adhesion as a model system to analyze cadherin-dependent forces. We have engineered two different types of surfaces, based on self-assembled monolayers of alkanethiols on gold surfaces as well as micro-fabricated post-array detectors that present isolated and purified VE-cadherin ligands.

We demonstrated the technology of the self-assembly of alkanethiols on gold surfaces in quantifying the adhesion strength of three different endothelial cell lines. We engineered surfaces with precisely controlled cell-adhesive areas passively adsorbed with VE-cadherin. We then evaluated adhesion strength values and perturbed cadherin binding using functional blocking antibodies or calcium chelators abrogated adhesion strength. Ligand density and contact time

mediate the strength of adhesion of a cell to its substrate. Functional blocking antibodies and calcium chelators eliminate adhesion strength.

We also demonstrated that micro-fabricated post-array detectors, or mPADs, allow for the direct measurement of cell-generated forces for cells interacting with adsorbed proteins on a surface. This work was the first system in which the traction forces of cells interacting with adsorbed cadherin ligands were measured. It is also the first system in which cadherin-dependent changes in traction forces upon exposure to different chemical agents were measured. This methodology provides insights into cadherin-based mechano-transduction events and provides a robust platform for further study.

Ultimately, future research into how cells strengthen cadherin-based adhesive force from weak homophilic interactions in the extracellular domain to strong forces intracellularly will rely on quantitative platforms with precise control of cadherin ligand density, an elimination of non-specific protein signaling through the immobilization of biomolecules or chemical chelators, as well as those that simplify the complexity of studying two cells in contact with one another. In this thesis, wee demonstrate two such systems that can accomplish all three things. Once mPAD technology becomes more standard in studies of cadherin-based adhesion, it can be applied to investigate emerging questions in the field, including the role of receptor trafficking in modulating adhesion strength and traction force generation, the interplay of cross-talk in cell-ECM and cell-cell adhesion, and the role of specific adhesion biomolecules in mediating adhesive force generation in several disease states.

CHAPTER I: SPECIFIC AIMS

Introduction

Cell-cell adhesion is critical to the functional organization of cells within tissues and the integrity of tissue architecture in developing and adult organisms. Cadherins, a family of adhesion proteins, play key roles in mediating adhesive forces and cell-cell interactions and can trigger signals that regulate migration, proliferation, differentiation, and survival. Current efforts have focused on identifying cadherin binding partners involved in the cadherin adhesion complex. Although significant progress has been made in identifying the biochemical interactions between cadherins and other molecular components, understanding the cellular mechanisms that determine the initiation and regulation of cadherin-based cell-cell adhesive force has been limited by the lack of robust, quantitative techniques to study adhesion strengthening at the cellular level. Direct, quantitative investigation of the contribution of cadherin ligand density and interaction time to overall cell adhesion strength is crucial to developing a cohesive model for how viable cell-cell contacts are formed and progressively maintained. In the context of endothelium, for example, vascular endothelial cadherin protein interactions have been implicated in maintenance of the barrier function and the preservation of tissue integrity.

Our long-term goal is to contribute to a cohesive model that describes the spatiotemporal dynamics of cadherin-based cell-cell adhesion. The objective of the project is to investigate the generation of cadherin-based adhesive force using engineered surfaces as experimental platforms. Our central hypothesis is that purified vascular endothelial cadherin ligands presented on engineered surfaces will recapitulate native structures and generate strong cadherin-based adhesive force *in vitro*. This will generate important insights into cadherin function because it

will provide a platform by which to understand how cadherin—based adhesive force is strengthened, and the variables that contribute to adhesive force generation. The rationale of the project is that a systematic analysis of adhesion strengthening between cells using integrated and quantitative approaches can provide greater understanding on the regulation of cell-cell interactions. The overall objective will be accomplished by testing our central hypothesis in the following specific aims:

1. **Investigate the influence of cadherin ligand density and contact time on the adhesive and traction force generation of endothelial cells interacting with engineered surfaces presenting purified, isolated vascular endothelial cadherin.**

   Engineered bio-adhesive surfaces of micro-patterned self-assembled monolayers of alkanethiols on gold will be functionalized with recombinant vascular-endothelial protein to control cell-cell contact area and to study the contribution of patterned cadherin ligand parameters to adhesive force generation.

2. **Investigate the vascular endothelial cadherin-dependent changes in adhesive force due to endothelial cell stimulation by tumor necrosis factor-alpha.**

   Engineered bio-adhesive surfaces of protein-coated micro-post arrays will be used to measure traction forces and to study the contribution of time and ligand density on traction force generation and cell spreading. The working hypothesis is that cells expressing endogenous VE-cadherin will exhibit greater traction forces upon binding to surfaces presenting vascular endothelial cadherin as compared to wild-type cells and smaller traction forces upon treatment by tumor necrosis factor alpha and Rho kinase inhibitors. Traction forces will be measured using quantitative micro-fabricated force-deflector arrays.

The proposed work is innovative because it focuses on complementary techniques for the quantitative assessment of adhesion strength and investigates the factors that give rise to cadherin-based adhesive force generation. We expect that the results from these experiments will integrate a quantitative characterization of adhesion strength as a function of patterned ligand geometry and will include the systematic quantification of the how perturbations of cadherin function modulates traction forces.

Project Significance

Despite the intense investigation to cadherin interaction partners, there still exists no model for understanding the cellular mechanisms that determine the initiation and regulation of cadherin-based cell-cell adhesive force. The goal of understanding the mechanics of cell-adhesion events is critical. Understanding cadherin adhesion has major implications in several disease states and is fundamentally important in defining architecture and integrity in tissues. Investigations so far have focused on initial receptor-ligand binding interactions or qualitative adhesion assays [1]. Progress has been retarded by the lack of robust, quantitative techniques to study adhesion strengthening at the cellular level. The challenge, therefore, is to develop an experimental model system that assesses adhesion strength quantitatively while probing the underlying structure of the cadherin complex through biochemical assays. The proposed research is significant because it focuses on creating a robust, quantitative experimental platform to study the formation of the cadherin complex in vitro and integrates a quantitative understanding of cell mechanics [2-6]. The proposed research is also significant because it focuses on engineering

adhesive surfaces with well-defined ligands that direct cell function through cell-cell interactions for defined geometries. This work is fundamentally different from current approaches (qualitative assessments of adhesion, micromanipulation, and centrifugation assays) in that it concentrates on examining longer-term adhesion phenomena (adhesion strengthening response), a critical stage in cadherin dynamics [7]. This is a key consideration because understanding how cadherins transform weak binding interactions in their extracellular domain to strong intracellular forces is necessary to elucidating cadherin regulation, which will be key in developing therapeutic platforms for associated disease states. Indeed, the transduction of mechanical stress is a critical cell adhesion-associated signal, a major contributor to health and disease in developing and adult organisms. This project is significant because it expands the knowledge gap in the field regarding mechanotransduction at cadherin-mediated cell-cell contacts. We measure the forces transduced at cell-cell contacts and show that these analysis platforms are versatile for future studies in addressing mechanical stresses associated with various adhesion receptors coated on engineered surfaces or correlating cadherin-associated protein dynamics with local forces by incorporating real-time fluorescence microscopy. Our validated approach provides a good strategy to understand the variables that promote adhesion strength at cadherin-based cell-cell contacts.

CHAPTER II: LITERATURE REVIEW

2.1. Cell Adhesion Overview

Cell adhesion to the extracellular matrix (ECM) and to other cells is a fundamental requirement for embryonic development and adult homeostasis [8-15]. Cell adhesion complexes are classified by the protein composition, protein localization, as well as their functional capabilities. These adhesive complexes are not static entities but undergo changes in both composition and structure as cells respond to extracellular cues. Several signaling proteins mediate these dynamic changes under tight spatiotemporal control, dictating the type, location, and duration of the ensuing adhesive contact.

2.1.1. Cell-Matrix Adhesion

Cell-matrix adhesion structures can take many forms [16, 17]. Early investigation into cell adhesive structures identified three classical formations, namely focal complexes (FCs), focal adhesions (FAs), and fibrillar adhesions (FBs) [16, 18-20]. Briefly, FCs are short-lived, assembling and disassembling on the order of minutes, and probe local ECM environment before disassembling or forming a more mature contact. FAs are larger and more stable, composed of multiple proteins, transmit forces to and from the ECM, and persist for lifetimes on the order of tens of minutes. FBs run parallel to fibronectin (ECM protein) bundles and are enriched in tensin and α5β1 integrin. Common to the initiation and stability of these adhesive structures are the integrin family proteins, heterodimeric trans-membrane receptors that bind the ECM, recruit proteins to their cytoplasmic face, and link the cell exterior to the interior. Upon integrin binding

to the ECM, several actin-binding proteins such as vinculin, talin, filamin, and α-actinin bind in tandem. [20, 21]. Stress fibers are initiated upon this complex formation, which provides a mechanical scaffold. In addition, each recruited protein to the integrin tail recruits other proteins such as Src and focal adhesion kinase (FAK), contributing to the signaling cascade and the stabilization of the structure, extending the lifetime of the adhesive contact.

2.1.2. Cell-Cell Adhesion

Cell-cell adhesion provides direct mechanical linkages between adjacent cells and helps in the formation of structural components between cells that maintain tissue integrity of intact epithelial and endothelial cell layers *in vivo*. Mechanical stability, cell polarity, and tissue architecture is generated and actively maintained by the selective adhesions that cells make and progressively adjust [22-26]. In development, cell adhesion events provide spatiotemporal cues or "addresses" to direct differentiation and organization for specific tissues, and are involved in the phenomenon of cell sorting [27]. In one canonical experiment by Townes and Holtfreter, cells from the three primary germ layers are dissociated and mixed in an *in vitro* cell culture experiment [28]. With nothing other than cell-cell adhesion cues, the cells, over a specified time, are able to recapitulate structures that resemble their original microenvironment [29-31]. This experiment showed that tissue structure is actively stabilized by "selective affinities" that cells have for one another and for the ECM. Adhesion is mediated by trans-membrane proteins with extracellular domains that interact with other cells and intracellular components that can recruit and organize molecular components for specialized functions within the cell. Thus, cell-cell adhesion molecules can also act as sensors for cell signaling through their connections with the cytoskeletal network.

Dysregulation of mature adhesive contact formation or premature disassembly of established contacts is a common attribute of certain disease contexts [32-36]. Cell-cell adhesion-mediated integrity is important for preserving the barrier function in tissues and is implicated in pathologies such as cancer [5, 6, 37-39]. A hallmark of cancer, apart from abnormal cell growth, is the detachment, invasion, extravasation, and metastasis of a tumor cell from the tumor mass into another tissue or organ. The events of this process are regulated by adhesion and can trigger survival signals through cell-cell and cell-ECM interactions and up-regulation of signaling cascades that promote migration and angiogenesis. Cell-cell adhesion is also implicated in the context of injury and the immune response.

Despite significant work in identifying key players of cell-cell adhesive complexes, the mechanisms of cell-cell contact formation and intracellular protein recruitment and localization are not fully understood. Force transmission that drives tissue-level organization is long-range (across multiple cells). As such, it has been difficult to precisely understand how force transmission is propagated through cell junctions to affect downstream biological processes. New studies, aided by recent progress in force measurement tools, have begun to appreciate the interplay (crosstalk) and similarities between cell-ECM and cell-cell force transmission.

2.2. History of Cadherin Proteins: Discovery and Investigation

In 1977, while Dr. Masatoshi Takeichi was investigating the role of divalent cations in cell adhesion, he serendipitously stumbled upon the presence of cadherin proteins [40]. The use of trypsin, a serine protease used to proteolytically remove adherent cells from a tissue culture dish, to disrupt cell adhesion caused a temporary loss of adhesion before cells re-aggregated. While repeating these adhesion assays, he observed a permanent disruption of cell adhesion upon

treatment of cells and was puzzled by the result. Upon further inquiry, he noticed the inclusion of EDTA, a known scavenger of metal cations, in the trypsin formulation. Using Chinese hamster V79 cells, fibroblasts from the lung tissue, he tested various groups systematically: cells with trypsin, cells with trypsin plus calcium, cells with trypsin plus EDTA, and then cells with EDTA alone. This experiment elucidated calcium-independent and calcium-dependent adhesion pathways. His seminal paper in 1977 showed that the disruption of adhesion via a calcium-dependent pathway (at physiological temperatures) could be protected from trypsinization by calcium [41]. Takeichi also observed that they calcium-dependent adhesion pathway was characterized by "cell deformation resulting in the increase of contact area between adjacent cells." Furthermore, Takeichi identified a cell surface protein, of size 150 kDa that was only present in cells with calcium-dependent adhesiveness.

Using teratocarcinoma (F9) cells, the team of Yoshida and Takeichi identified E-cadherin as the first cadherin family member. The so-called ***ca***lcium-dependent ***adh***esion molecules, or cadherins, were shown to regulate adhesion, morphogenesis, and tissue structure and architecture. Notably, Takeichi and colleagues observed morphological differences linked to impaired cadherin adhesion, which led to hypotheses of cadherin's functional role in mediating cell architecture and behavior. Over time, other seminal papers by Takeichi confirmed that cadherins bind in homophilic manner and could be regulated by phosphorylation [42-44].

2.3. Cadherin Family Proteins

Twelve distinct cadherin families specify cadherin sequence characteristics, structure, and function: classical and desmosomal cadherins, PCDH15/CDHR15 and CDH23/CDHR23, 7D-cahderins, protocadherins, fat and deschsous, flamingo/celsr, calsyntenins, Ret and T-

cadherin (**Figure 2.1**) We limit our discussion of cadherin family proteins primarily to classical cadherins. The classical cadherin family proteins are a group of approximately 20 surface proteins that mediate cell-cell adhesion [45-48]. These cadherins are classified further into either type I subfamily members and type II subfamily members. Type I cadherins have broad distribution and are segregated by germ layer or tissue type, whereas type II cadherins often have overlapping expression patterns.

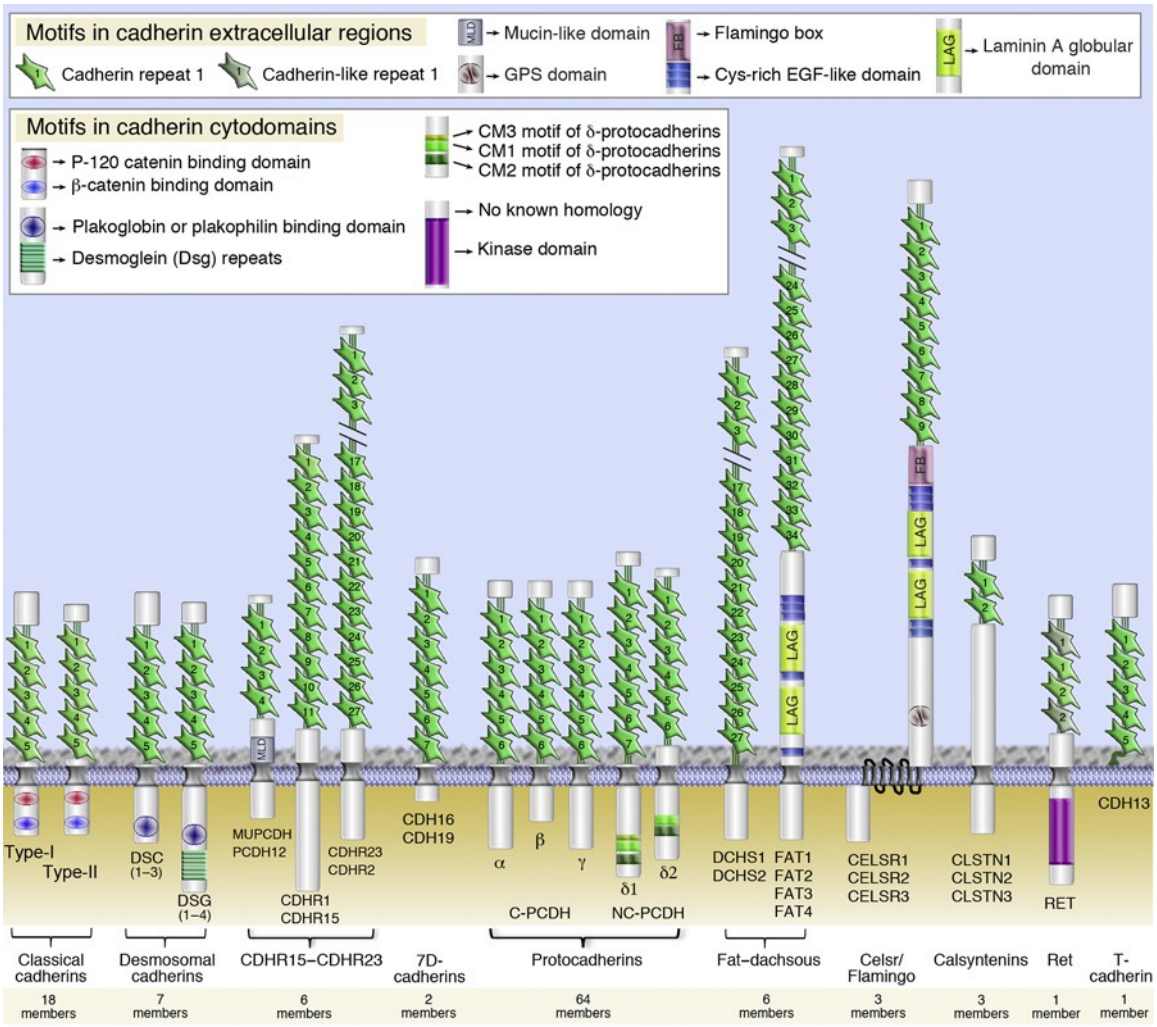

Figure 2. 1: Members of the cadherin superfamily. From [49]. There are 12 distinct cadherin family proteins, specified by their sequence characteristics, structure, and function.

Cadherins in the classical family are similarly organized, being comprised of an extracellular cadherin (EC) domain, which confers adhesive function and contains five beta-barrel ectodomains, a single-pass trans- or juxtamembrane domain, and an intracellular domain, or cytoplasmic tail. Three calcium-binding regions occupy and stabilize each inter-domain region of the ectodomains. These ectodomains are numbered EC1-5, beginning from the N-terminus. Cadherins typically bind in a homophilic mechanism, binding to other cadherin receptors to form cadherin-cadherin bonds in the extracellular space. This homophilic binding is calcium dependent [50, 51]. The cytoplasmic tail links the actin cytoskeletons of adjacent cells by the recruitment of anchor proteins that mediate signaling and help stabilize the adhesion complex.

2.3.1. Functional Role of Cadherins

Absolute lethality at early embryonic stages with the deletion of cadherin proteins supports their functional importance [52-54]. Indeed, cadherin expression levels correlate with the formation of discrete tissue structures and the delineation of cell layers and other architectures. Additionally, cadherin proteins play critical roles in tissue remodeling events during development. This process requires that cells remain attached to one another while undergoing morphological changes that enable movement. Sometimes, normal development calls for disassembly of cell-cell contacts, requiring precise coordination of cell adhesion. Historically, the adhesive functionality of cadherins was discovered when cadherin expression promoted calcium-dependent cell aggregation into tissue-like clumps [28, 55, 56]. Mentioned earlier, cells from the three primary germ layers were able to recapitulate their structure *n vitro* after thorough mixing through homotypic cell sorting, meaning that cells of one subtype are able to bind to one another with no other external cues other than the selective affinities that cell adhesion molecules

have for one another. Cadherin downregulation correlates with the progression of the metastatic pathway in cancer cells, arising from the decrease in their adhesive properties and their transition to a more migratory phenotype. There are several other disease states arising from dysregulation of cadherin or cell-cell adhesion molecules, underscoring their functional importance in directing tissue architecture, tissue organization, and coordinated cellular processes [34-36, 57-61].

2.3.2. Vascular Endothelial Cadherin

Vascular endothelial cadherin (VE-cadherin), originally called cadherin-5, was discovered in 1991 alongside 7 other cadherins using RT-PCR [62-64]. Following up on their excellent work, Tanihara and colleagues also cloned the entire human cDNA sequence of these 8 cadherins, showcasing the diversity of sequences in the cadherin cytoplasmic tails and clear homology in the extracellular receptors. Shortly after, Dejana and colleagues identified cadherin-5 by monoclonal antibodies as a protein that made contact with endothelial cells. Renaming the protein vascular endothelial cadherin, Dejana and colleagues showed that Chinese Hamster Ovary (CHO) cells transfected with the protein aggregated through a calcium-dependent mechanism [65, 66]. Soon after, mouse VE-cadherin was cloned, implicating its importance in endothelial tissue specificity during embryonic development [67]. Furthermore, the Dejana group released the chromosomal map and genomic structure of mouse VE-cadherin, paving the way for more genetic analysis of the VE-cadherin gene [68-72]. Functionally, VE-cadherin's role was first established through the use of polyclonal anti-VE-cadherin antibodies that disrupted endothelial cell-cell contacts *in vitro* and confirmed earlier *in vivo* experiments. Namely, the Vestweber, Takeichi, Vernet and Dejana groups conducted key experiments detailing how antibodies against VE-cadherin impaired function by inducing vascular permeability or

inhibiting cellular adhesion by binding to VE-cadherin ectodomains [73-77]. These experiments then paved the way for intense investigation into the structural basis for the homophilic interactions of VE-cadherin, detailed in later sections.

2.3.3. Vascular Endothelial cadherin and Vascular Permeability

It has been increasingly appreciated that intracellular junctions are dynamic structures that are continuously remodeled in order to respond to the demands of the tissue micro-environment. During morphogenesis, or in confluent or resting cells in response to agents that increase permeability, recycling and remodeling of adherens junction components allow for rapid remodeling of the complex. In response to the dynamic environment of the endothelium, including but not limited to pressure changes as a result of blood flow, vessel contraction and dilation, and complex hemodynamics, junctions and endothelial cadherin complexes need to reshape in order to be adaptable to the ever-changing conditions. VE-cadherin plays a very important role in controlling vascular permeability and vascular integrity. There are several pathways to the induction of vascular permeability [78]. Stimuli such as growth factors, thrombin, and histamine may increase endothelial cell permeability by affecting cell contractility and phosphorylating myosin light chain. Histamine, tumor necrosis factor (TNF), platelet activating factor, and vascular endothelial growth factor (VEGF) also phosphorylate cadherin complex components including VE-cadherin, p120-catenin, and β-catenin. This increase in phosphorylation correlates with an induction in permeability in cell culture systems. VE-cadherin-specific phosphatases whose inactivation impaired VE-cadherin formation in embryos suggests that constant phosphorylation of VE-cadherin increases barrier function in vascular endothelium. VE-PTP, among other phosphatases such as Src, Dep-1, SHP2 may play a critical

role in modulate VE-cadherin phosphorylation. Kinases such as Csk also modulate vascular permeability. VE-cadherin cleavage by enzymatic proteolysis also induces vascular permeability. For our experiments, we focus on stimuli such as TNF to investigate cadherin-dependent changes in traction forces as a function of induced vascular permeability [79].

2.4. Cadherins in Disease

The mammalian genome has over 120 genes encoding cadherin and cadherin-like proteins [80, 81]. Many inherited disorders have been linked to defects in about 25 of these proteins, including but not limited to psychiatric disorders, skin and hair disorders, cardiomyopathies, and deafness and blindness [49, 82, 83]. Investigations continue into the pathogenicity of these conditions and the model systems that may reveal how the contributions of adhesive strength and intracellular signaling pathways give rise to a variety of associated phenotypes.

2.4.1. Cadherins in Psychiatric Disease

The function of the mature (adult) brain derives from neural circuitry that originates from embryonic patterning and the differentiation of the neural tube. The adhesive cues that cadherins provide play major roles in embryonic patterning, circuit formation, synaptogenesis, synaptic plasticity, and mature architecture [84-91]. In fact, the expression profiles of cadherins in neuronal development point to distinct functions for neural tube regionalization, neuronal migration, gray matter differentiation, neural circuit formation, spine morphology, synapse formation, and synapse remodeling.

Perhaps most widely recognized for their role in tissue morphogenesis, cadherins' earliest role in neuronal development occurs during neural tube formation where they are dispersed throughout the radial glia[1] of neuro-epithelium [92, 93]. After mitosis, neural precursor cells migrate to the pial surface and differentiate into early neurons that comprise the mantle layer. Differential cadherin expression helps form aggregates of neurons that become brain nuclei, gray matter, basal ganglia, and other complex structures [94, 95]. Brain connectivity stems from the functional differentiation of gray matter. Cadherin expression profiles direct the migration of neurons and integrate them into distinct target regions so much so that isocortical regions, which differ in histology, surprisingly, show similar layer-specific cadherin profiles in different systems of the brain [96-101]. Specialized gray matter structures that define functional systems in the brain, such as visual, auditory, or motor systems are typically connected by fiber tracts and form neural circuits. Circuit- and sub-circuit-specific cadherin expression profiles underscore their importance in neuronal maintenance, and cadherins have also been shown to regulate axonal outgrowth and navigation [102-105].

[1] Radial glial cells are cells that span the width of the cortex in the developing brain, readily identified by their unique morphology. They serve as progenitors for neurons and glia during development and direct outgrown of

Table 1 – Cadherin subfamilies (Hulpiau and van Roy, 2009) and their association with neuropsychiatric disorders.

Cadherin subfamily	Members	Association with neuropsychiatric disorders		
		Cadherin	Disease	Reference
Classic cadherins				
Type I	CDH1–4, 15	CDH15	Intellectual disability	Bhalla et al. (2008)
Type II			Autism	Willemsen et al. (2010)
	CDH5–12, 18–20,22, 24	CDH5	Autism	O'Roak et al. (2012)
		CDH7	Bipolar disease	Sklar et al. (2008) and Soronen et al. (2010)
		CDH8, 9, 10	Autism	Pagnamenta et al. (2011) and Wang et al. (2009)
		CDH11	Alcoholism	Johnson et al. (2006) and Edenberg et al. (2010)
			Bipolar alcoholism	Lydall et al. (2011)
		CDH12	Bipolar alcoholism	Lydall et al. (2011)
		CDH12, 18	Schizophrenia	Singh et al. (2009)
Clustered protocadherins	PCDHA1-A13, PCDHAC1-C2,	PCDHa	Bipolar disease	Pedrosa et al. (2008)
(α-, β-, γ-protocadherins)	PCDHB1-B16, PCDHGA1-A12, PCDHGB1-B7, PCDHGC3-C5	PCDHb4	Autism	O'Roak et al. (2012)
Non-clustered protocadherins				
δ1-Protocadherins	PCDH1, 7, 9, 11	PCDH10	Autism	Morrow et al. (2008)
δ2-Protocadherins	PCDH8, 10, 17, 18, 19	PCDH19	Epilepsy with or without mental retardation	Dibbens et al. (2008), Jamal et al. (2010), Marini et al. (2010), Depienne and LeGuern (2012), Camacho et al. (2012), Vincent et al. (2011) and Higurashi et al. (2012)
		PCDH19	Dravet syndrome	Depienne et al. (2009) and Camacho et al. (2012)
		PCDH19	Autism	Depienne and LeGuern (2012) and Camacho et al. (2012)
Others	PCDH12, 15, 21, 24	PCDH12	Schizophrenia	Gregorio et al. (2009)
FAT and FAT-like cadherins		FAT	Bipolar disease	Blair et al. (2006) and Abou Jamra et al. (2008)
Flamingo/CELSR cadherins	CELSR1, 2, 3			
Other cadherins	CDH13, 16, 17, 26	CDH13	Autism	Chapman et al. (2010) and Sanders et al. (2011)
		CDH13	Alcohol dependence	Johnson et al. (2006) and Treutlein et al. (2009)
		CDH13	Methamphetamine dependence	Uhl et al. (2008a,b)
		CDH13	ADHD	Lesch et al. (2008), Neale et al. (2008), Lasky-Su et al. (2008), Zhou et al. (2008) and Franke et al. (2009)

Table 2. 1: Cadherin subfamilies in neuro-psychiatric disease. From [82].

Cadherins also play major roles at the synapse: CDH2 (Cadherin-2, N-cadherin, or neural cadherin), for example, regulates dendritic spine morphogenesis and density, mediates long-term spine stabilization, is required for long-term potentiation, and alongside catenin proteins, help maintain synaptic function overall [106-109]. Among others, mutations in cadherin and cadherin-like proteins have been linked to mental retardation, autism-spectrum disorders, language problems, schizophrenia and bipolar disorders. Cadherins have been also been linked to

drug dependence, alcoholism, violent suicide, and attention deficit hyperactivity disorder [82, 110]. A table linking members of the cadherin superfamily and known psychiatric disorders is included above.

2.4.2. Cadherins in Skin and Hair Disease

During hair follicle morphogenesis, the expression levels of cadherin proteins switch from E-cadherin (epithelial cadherin) to P-cadherin (placental cadherin). When mutations occur in the P-cadherin gene, hypotrichosis[2] occurs, with macular dystrophy as a co-morbidity, or ectodermal dysplasia[3], as well as cleft palate and ectrodactyly.[4]

Desmogleins and desmocollins maintain specialized cell-cell junctions called desmosomes that are under stress, including that of the skin and heart. Tissue-specific abnormality in the four desmogleins and three desmocollins give rise to cardiac and skin disease, including palmoplantar keratoderma (desmoglein-1 disorder), hair loss, and the periodic thinning of hair (desmoglein-4 and desmocollin-3 disorders). Of note, palmoplantar keratoderma, with phenotypes of woolly hair and cardiovascular disease, which is also known as Naxos disease, affects about 1 in 1000 residents on the island of Naxos, off the coast of Greece, and more recently has been identified in Jerusalem and Spain. It is evidenced by a desmocolin-2 mutation, in addition to a mutation in plakoglobin, a cadherin complex protein. Naxos patients often have steely hair, sever tachycardia and cardiac abnormalities, and experience sudden death [34, 111].

---

[2] Hypotrichosis is any condition specified by abnormal hair patterns, including but not limited to hair loss, spiky hair, baldness, or hair thinning.

[3] Ectodermal dysplasia are abnormalities in tissues derived from the ectoderm, including hair, teeth, skin, nails, sweat glands, digitation, cranial-facial features, dryness of the eye, vision defects, etc.

[4] Ectrodactyly is the absence of one or more central digits of the hand or foot.

2.4.3. Cadherins in Cardiovascular Disease

In the heart, arrhythmogenic right ventricular cardiomyopathy can occur, with progressive cardiomyocyte loss that results in tachyarrhythmia and sudden death. Ultimately, phenotypes arise of small desmosomes, desmosome gap widening, fibro-fatty tissue substitution, and inappropriate localization of desmosomes. Additionally, biventricular cardiomyopathy, aneurysms, and myocyte necrosis can occur, as well as elevated markers for cardiac stress, remodeling and heart failure. For intercalated discs, adherens junctions, and gap junctions, appropriate assembly of desmosomal protein and plakoglobin, N-cadherin and catenin protein complex, and connexin-43, respectively, are required for mechanical and electrical coupling in cardiomyocytes. Associated phenotypes for dysregulation of these proteins include expression of adipogenic genes, which replaces cardiomyocytes with fatty issue and ultimately results in tachycardia and sudden death.

2.4.4. Cadherins in Ear and Eye Diseases

Outer hair cells and inner hair cells in the ear process sound pressure waves and transmit sound information to the brain. Mechanotransduction occurs at the hair bundle, which has up 300 cilia, filled with F-actin and organized into three rows of cilia, connected by fibrous links. These links control have been suggested to control mechano-electrical transduction of ion channels. Structurally, tip links (150-200 nm long) interact with other links by cadherin heterodimers of cadherin-23 and protocadherin-15 and withstand up to 10 pN of force per link. Amino acid residues involved in the binding mechanisms of classical cadherin proteins are not conserved in non-classical cadherins, and thus these proteins may depend on the additional calcium-binding

site that they have to facilitate cadherin complex assembly, stability and maturation. Structural studies and molecular dynamics simulations are necessary to investigate how the heterodynamic bond between protocadherin-15 and cadherin-23 can withstand forces from sounds of moderate to high intensity.

Usher syndrome, which has three clinical subtypes, features severe deafness and blindness. Two of the five causal genes identified encode for cadherin-23 and protocadherin-15. Specifically, USH1 protein defect is the primary cause of hearing impairment, with retinitis pigmentosa and imminent blindness as co-morbidities. USH1 defects affect the fibrous links that bind cilia, which contain cadherin-23 and protocadherin-15, causing them to be misshapen. Links, consisting of heterodimers of cadherin-23 and protocadherin-15, limit adaptation of mechano-electrical transduction and activates adaptation motors. Conditional knockout mice of cadherin-23 show considerably shortened cilia and interrupted F-actin polymerization. A table summarizing all cadherin-related disorders explained so far is included below [49, 83, 112].

Usher syndrome also affects the retina. Although no visual defect has been observed in Ush1 mutant mice, analyses of human patients show that disease phenotype includes dystrophy of rods and cones, with rapid and gradual degradation, respectfully. USH1 proteins (including protocadherin-15 and cadherin-23) are present in photoreceptor cells and non-sensory cells. They localize to junctions between photoreceptor segments as well as in the F-actin-rich microvilli that wrap around the basolateral area of the outer segments of photoreceptors. Thus. These proteins form stabilizing adhesive contact for photoreceptors.

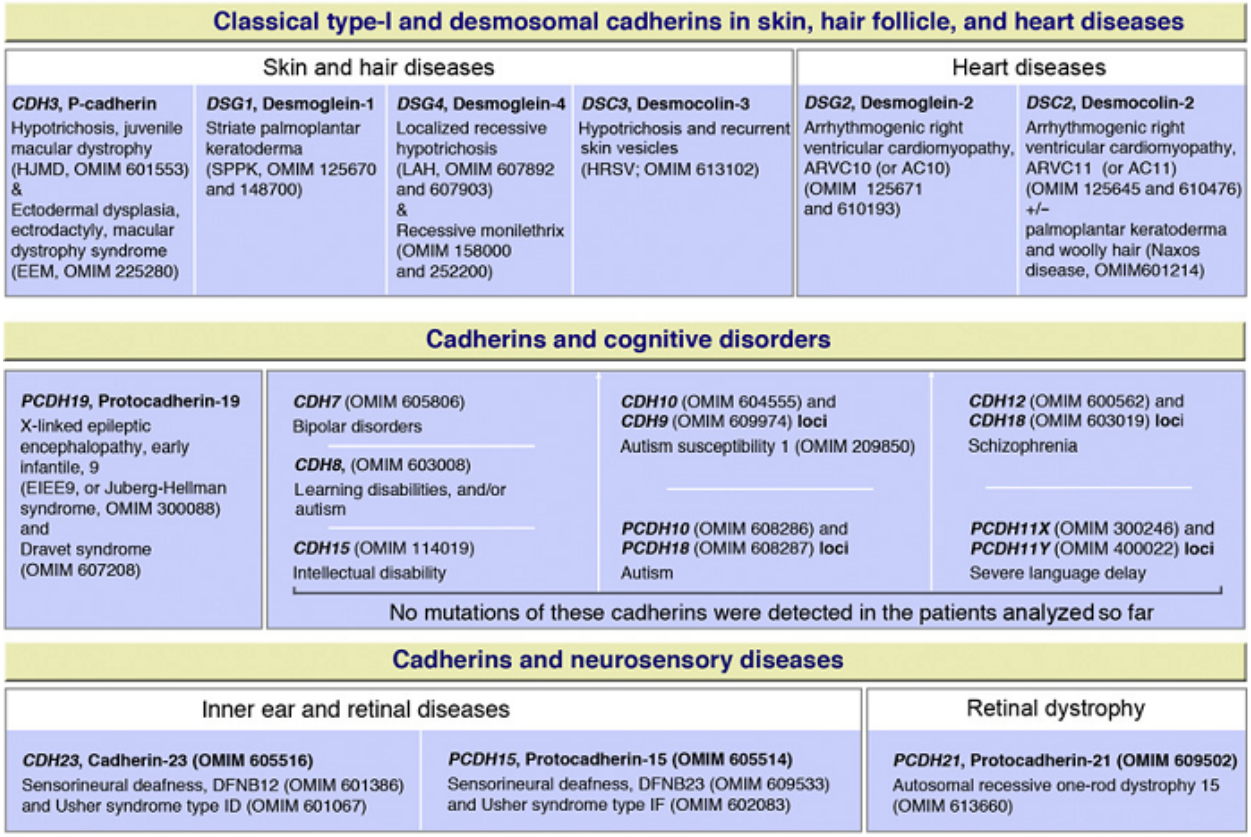

Figure 2. 2: Cadherin family superfamily members and their association in skin, hair, heart, cognitive, and sensory disease. From [49].

2.4.5. Cadherins in Cancer

Myriad reports detail the role of cadherins in tumorigenicity and the metastatic cascade. Epithelial cadherin (CDH1, cadherin-1, or E-cadherin) has been most widely studied with respect to cancer, being a growth and invasion suppressor. Epithelial cells are progenitors of carcinomas, which constitute 70% of human tumors worldwide. E-cadherin is a tumor suppressor through the maintenance of tissue organization and by blocking apoptosis [113-115]. E-cadherin does this by a complex mechanotransduction-based intracellular signaling that inhibits oncogenes such as β-catenin and epidermal growth factor receptor [114, 116]. Indeed, the evidence is

overwhelming for many tissue-specific cancers: loss of (epithelial) cadherin expression or mutations in (epithelial) cadherins are implicated in tissue disorder, cell de-differentiation, increased invasiveness, and the epithelial-to-mesenchymal transition [117, 118]. Given the structural diversity of cadherins and the multiplicity of cadherin superfamily members, new roles – synergistic, antagonistic, tumor-suppressing, and more - are emerging for cadherin proteins with relevance to cancer relevance.

Type I cadherin protein member CDH2 (Cadherin-2, neuronal cadherin, or N-cadherin), has often taken the spotlight as a 'mesenchymal cadherin,' switching expression patterns with CDH1 during epithelial-to-mesenchymal transition, however, CDH2 has distinct, complex roles in tissue-specific contexts [119-121]. Reduction in CDH2 expression has been correlated with neuroblastoma metastatic dissemination [122]. CDH2 also stimulates fibroblast growth factor receptor 1 (FGFR1), binding to FGFR1 ectodomains and preventing its internalization, ultimately sustaining FGFR1-associated membrane signaling and subsequent malignancy. CDH2 also allows epithelial cells to bind other cell types (including stromal and endothelial cells) through heterotypic cell-adhesion, possibly contributing to dissemination of carcinoma cells [123-125]. Experiments in the intestine that successfully combine tissue-specific *Cdh1* knockouts with ectopic expression of *Cdh2* knock-in show that CDH2 substituted for CDH1 for initial tissue organization but phenotypic abnormalities, including dysplasia, reduction in differentiated cell types, and impaired cell signaling. Experiments of CDH1-CDH2-switched alveolar cells in the mammary gland also showed severe abnormalities, including high malignancy and FGF-based initiation of CDH2-driven EMT [126-129]. In pancreatic cancer, CDH2 promotes tumor cell survival, migration, invasion and metastasis. Taken together, these

studies show that CDH2 has dual roles as tumor-suppressor and tumor-promoter in a context-dependent manner.

CDH3 (Cadherin-3, placental cadherin, or P-cadherin) also has complex roles in its cancer-related functions. Co-expression of CDH3 and CDH1 typically occur, and induction of CDH3 is associated with CDH1 repression and CDH2 induction. This so called 'cadherin switch,' however, has also been shown to promote adhesion in an anti-invasive role similar to that of CDH1 in malignant melanomas [130-133]. In colon carcinomas, CDH3 behaves similarly to CDH1, and its knockdown features cell dissociation, migration and invasion [134]. Contradicting reports support roles for CDH3's expression as a marker for tumor cell proliferation and not malignant tumor progression in contrast to colon cancer metastasis. Several mechanisms delineating CDH3's possible stimulation of tumor malignancy have been proposed, including the involvement of metalloproteinases, which excise a soluble, pro-invasive extracellular fragment from CDH3 [135]. CDH3 has also been shown to complex with insulin-like growth factor 1 receptor, resulting in tyrosine phosphorylation and activation of cytoplasmic p120-catenin to promote tumor invasion. Cytoplasmic localization of p120-catenin occurs in tumors with co-expression of CDH1 and CDH3, trending with poor patient survival [136, 137].

The cancer-related properties of CDH4 (Cadherin-4, retinal cadherin, or R-cadherin) are also complex, and at times, conflicting. CDH4 is not expressed in normal myoblasts, and its ectopic expression induced tumorigenicity in myoblasts via RAC1 activation [138]. In breast cancer, however, CDH4 expression is downregulated in carcinomas, and its overexpression confirmed suppressor roles for CDH4 [139]. Taken together, these data underscore the importance of tissue-specificity in delineating cadherin function.

PCDH type	Tumour type*	Reported tumour-specific changes*	Activity	Refs
PCDH1	Medulloblastoma	Decreased expression	Shorter survival	89
	Pancreatic	Epigenetic silencing	TSG?	86
PCDH7	Breast	Increased expression in brain metastatic tumour cell populations	Metastasis gene?	118
	Breast	Upregulated in bone metastatic primary tumours	MPA, MWH, MIA and XMC	119
PCDH8	Colorectal, mantle cell lymphoma, pancreatic, renal cell and nasopharyngeal	Epigenetic silencing	TSG? MCF and MWH	86, 97–100
	Breast	Epigenetic silencing and/or somatic mutations	AIG and MWH	112
	Prostate	Homozygous deletion‡	TSG?	111
PCDH9	Glioblastoma multiforme and other gliomas	Decreased expression	TSG in glioblastoma multiforme? Higher tumour grade, shorter survival, APO, CCA and AIG in glioma	94,113, 142
	Colorectal, endometrial, oesophageal and prostate	Somatic mutations‡ (mostly substitution missense)	TSG?	110,111
PCDH10	Breast, gastric, colorectal, pancreatic, cervical, testicular germ cell tumours, various lymphoma types, multiple myeloma, B cell and T cell acute lymphoblastic leukaemia and reactive follicular hyperplasia	Epigenetic silencing	TSG? For multiple myeloma: MCF, CCA and CAM. For acute lymphoblastic leukaemia: chemotherapy resistance	86,87,93, 101–104, 108,143, 144
	Nasopharyngeal, oesophageal, breast, gastric, hepatocellular, non-small-cell lung	Epigenetic silencing	TSG? MCF, AIG, MWH and MIA. In addition, for gastric: shorter survival, MPA, APO and XTG	91,95, 105,106
	Medulloblastoma	Epigenetic silencing and/or homozygous deletion	TSG? MWH	107
	Lung, gastric and colorectal	Somatic mutations‡ (mostly substitution missense)	TSG?	110,111
PCDH11X	Prostate	Missense mutations	Lethal metastatic tumours	145
	Lung, oesophageal, gastric, as well as head and neck	Somatic mutations‡ (mostly substitution missense)	TSG?	110,111
PCDH11Y‖	Prostate	Upregulated	Androgen-independent growth, anti-apoptotic, neuroendocrine transdifferentiation and resistance to cytotoxic drugs	114,115, 117
PCDH17	Pancreatic and gastric	Epigenetic silencing	TSG?	86,109
	Oesophageal squamous cell	Epigenetic silencing and/or homozygous deletion	Poorer differentiation status of tumours; MPA, CCA, MWH and MIA	92
	Gastric and colorectal	Epigenetic silencing and/or homozygous deletion	TSG? MCF, AIG, APO, AUT and XTG	96
	Colorectal, oesophageal, gastric, lung, skin cutaneous melanoma and prostate	Somatic mutations‡ (mostly substitution missense)	TSG?	110,111
PCDH18	Skin cutaneous melanoma, oesophageal and gastric	Somatic mutations‡ (mostly substitution missense)	TSG?	110,111
PCDH19	Gastric and endometrial	Somatic mutations‡ (mostly substitution missense)	TSG?	110,111
PCDH20	Non-small-cell lung	Epigenetic silencing	Shorter survival, MCF and AIG	90
	Prostate and skin cutaneous melanoma	Homozygous deletion‡	TSG?	111

Table 2. 2: Cadherin subfamily proteins and their association with cancer phenotypes. From [113].

Cadherin type	Tumour-suppressing activities*		Tumour-promoting activities‡		Refs
	Tumour type§	Putative mechanism‖	Tumour type§	Putative mechanism‖	
Type I cadherins					
CDH1	Numerous types of carcinomas; germline mutations in hereditary diffuse gastric cancer families	Morphogenetic by multiple mechanisms	Inflammatory breast, ovarian, squamous cell carcinoma and glioblastoma multiforme	Microemboli formation, collective cell invasion and pro-survival EGFR signalling	2,4,17, 140,141
CDH2	Neuroblastoma	Morphogenetic?	Melanoma and many carcinoma types	EMT, heterotypic adhesion, FGFR signalling and the induction of several genes that are implicated in cancer progression	11,13–16, 18,19,22, 24,25
CDH3	Skin and colon	Complements CDH1 defects; anti-invasive	Colon cancer metastasis, alveolar rhabdomyosarcomas and numerous invasive carcinomas	Distorts CDH1 function in the case of co-expression; IGF1R signalling; cytoplasmic p120-catenin; downmodulation of other cadherins?	27,28, 31–33,35–41
CDH4	Breast	Morphogenetic?	Rhabdomyosarcomas	RAC1 activation	42–44
Type II cadherins					
CDH11	Osteosarcoma, melanoma, head and neck, and several other carcinomas	Multiple signalling pathways (AKT, RHOA, β-catenin, apoptosis and EMT)	Prostate and breast cancers with bone metastases; glioblastoma multiforme	Homophilic, heterotypic interactions with CDH11 in bone tissue; signalling?	46–53
CDH5	Not known (essential for endothelial integrity)	Blocks VEGFR2 signalling; stimulates TGFβ signalling; inhibits formation of FGFR1–CDH2 complexes	Expression in breast cancer cells and aggressive melanomas	Increased intravasation; vascular mimicry; TGFβ-driven EMT; CDH2 induction	55,56,59–61
Other cadherin types					
DSGs and DSCs	Numerous carcinoma types	Mainly strong cell–cell adhesion? EMT inhibition; extranuclear sequestration of armadillo proteins; preserved PERP activity	DSG2 in certain cancers of the skin; DSG3 in head and neck	Stimulation of proliferation and invasion; inhibition of apoptosis	62,63,65
CDH13	Various (expression in cancer cells)	EGFR inhibition; cell cycle arrest	Numerous cancer types (expression in tumoural microvasculature)	AKT activation leading to increased cell proliferation and survival; migration due to β1 integrin endocytosis	66–68
CDH16	Renal cell carcinomas and thyroid carcinomas	EMT inhibition?	Not known	NA	69,70
CDH17	Not known	NA	Malignant GIT tumours	NF-κB signalling; β-catenin signalling; integrin signalling	71–74
Protocadherins¶					
cPCDHs	Several α-PCDH, β-PCDH and γ-PCDH members in breast, colorectal and pancreatic, as well as Wilms' tumours	Pro-apoptotic, anti-proliferative; blocks WNT and mTOR signalling	Not known	NA	82–88
ncPCDHs#	Most δ-PCDHs in numerous cancer types	Inhibition of cell proliferation, AIG, cell migration and invasion; speculated inhibition of mesenchymal cadherins, association with NAP1–WAVE and the proteasome	PCDH7 in metastasizing breast cancers; PCDH-PC (PCDH11Y isoform) in castration-resistant prostate cancers	PCDH7: stimulation of cell proliferation, cell migration, invasion and bone metastasis. PCDH-PC: WNT signalling, inhibition of androgen receptor and neuroendocrine differentiation	
Cadherin-related proteins					
FAT1	Glioblastoma multiforme, colorectal, head and neck	Inhibition of cell proliferation, AIG and xenograft growth; sequestration of β-catenin outside the nucleus; actin reorganization; Hippo signalling?	Breast (high-grade DCIS), melanomas and leukaemias	Cancer-specific production of a FAT1 fragment with nuclear function?	134,135
FAT4	Breast, pancreatic and melanoma	Tumour suppression *in vivo*; DCHS1 *trans* interaction; Hippo signalling, which inhibits YAP	Not known	NA	134,136
CDHR23	None known	Not known	Breast	Invasion by heterotypic adhesion to stromal cells	138
CDHR5 isoform M	Colon	AIG; *in vivo* growth; inhibition of β-catenin signalling	Not known	NA	139

Table 2. 3: Protocadherins and their association with cancer phenotypes. From [113].

Overall, members of the cadherin family proteins undergo cancer-related changes and in turn affect tumor progression. Their roles as oncogenes or tumor suppressors are context-specific, depending on cadherin, cell, tumor, primary tumor tissue, and disseminated tumor types. Homophilic and heterophilic cadherin binding promotes crosstalk between cancer cells and tumor-associate cells. More importantly, cadherin proteins affect downstream signaling pathways involved in EMT and cancer progression, but can also be modulated by co-expression of different cadherins. Cadherin proteins present great potential for therapeutic targets in cancer phenotypes, although the poorly predictable interactivities and crosstalk between cadherin proteins makes such targeted therapies challenging [113].

2.5. Cadherin Structure, Complex Assembly, and Interaction Dynamics

2.5.1. Cadherin Structure

The extracellular domains of the classical cadherin family are characterized by five repeating "immunoglobulin-like" units of approximately 110 amino acid residues each called cadherin repeats, or ectodomains. Although some atomic force microscopy (AFM) and force spectroscopy data show multiple distances at which adhesive states can occur (discussed under 'Quantitative Force Measurements' below), the large body of data that exists on cadherins through crystallography, crosslinking, electron tomography, and fluorescence studies suggests that adhesive binding occurs through the membrane-distal EC1 domain [140]. An elegant study by former Secretary of Energy, Steven Chu, labeled EC1 and EC5 domains with fluorescent dyes and measured the fluorescence resonance energy transfer (FRET) between cadherin molecule pairs [141]. They show that cadherins bind by association of their EC1 domains.

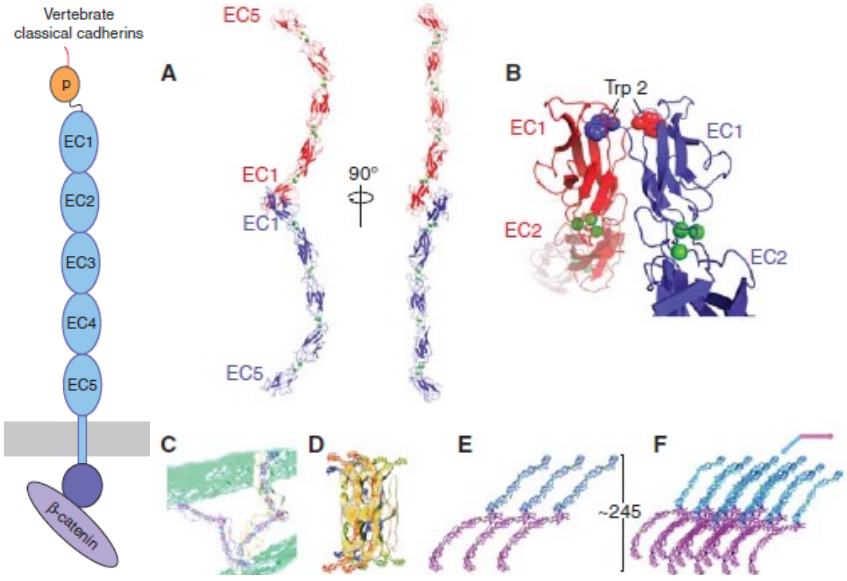

Figure 2. 3: Domain structure of "classical" cadherins, in which a pro-domain (P) linked to a signal sequence, is proteolytically cleaved to create a mature extracellular cadherin (EC) domain. The EC domain is composed of five repeat units, a single-pass trans-membrane region, and a cytoplasmic tail, which interacts with β-catenin and other associated proteins. Figure 2: Structure of cadherins in show that A) the adhesive interface is formed by the a strand-swap between EC1 domains; B) bound calcium ions mediate the adhesive interaction; C-F) junction structures are made up of intersecting lines of cadherin proteins arranged in lattice layers to form a two-dimensional array.

Structurally, cadherins contain a signal sequence and a pro-domain that precedes EC1 (**Figure 2.3**) [140]. Removal of the pro-domain by proteolysis yields a mature ectodomain with five cadherin repeats. Thus, the adhesive capacity of cadherins depends on the proteolytic removal of the pro-domain. Each EC domain has seven β-strands, which are arranged into two opposed sheets with their C- and N-termini at opposite ends so that they can be repeated one after the other. Cadherin-based cell adhesion is calcium-dependent. Structural studies reveal that calcium localization between successive EC domains make their connection rigid, a process in which three calcium ions are coordinated between amino acids at the base of one domain, the linker region between them, and the top of the next domain (**Figure 2.3**). Studies also reveal

strong curvature in the calcium-bound (active) state of the full-length EC domains, putting EC1 and EC5 nearly orthogonal to one another. Calcium removal disrupts EC domain structural integrity, makes cadherins susceptible to proteolytic activity, and reduces rigidity of the cadherin structure.

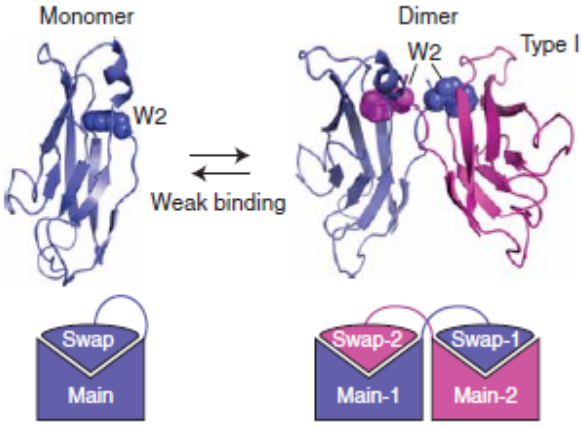

Figure 2. 4: Strand-swapping by classical cadherins allows for homophilic interactions because of near-equivalent binding interfaces. A protein consisting of a "main" domain and a "swapping" domain, connected by a flexible region, can form a "closed" monomer or a dimer, in the case of cadherins. The monomer and dimer molecular configurations compete with one another and lead to weak binding affinities. W2 represents the conserved tryptophan-2 residue crucial to strand-swapping.

The adhesive interface is most uniquely characterized by a "strand swapping" between the N-terminal β-strands of EC1 pairs, called the A strands. This interaction is denoted by the insertion of an A strand side chain from the conserved tryptophan-2 (Trp2) residue from one ectodomain into the hydrophobic core of another ectodomain (**Figure 2.4**). Removal of the Trp-2 interaction by mutation abrogates cadherin adhesive function in all cadherins tested. The parallel binding of ectodomains between cadherins, despite the cadherin orientation being anti-parallel, is a consequence of symmetric A strands swapping. This parallelism is critical to provide near-equivalent interfaces at adhesive binding sites, enabled by the curvature of the cadherin ectodomain. Conservation of key elements of the adhesive interface (most notably the Trp2

residue) promotes evidence for heterophilic binding of cadherins within the same subfamily, although different levels of affinity exist for these interactions.

2.5.2. Cadherin Complex Structure and Assembly

It is important to note that through their association with other co-receptors, structures, and protein complexes, cadherin proteins may regulate and may in turn be regulated by other proteins. Integrins may regulate cell-cell adhesion and have recently been proven important at stabilizing cell-cell junctions. Results from the study show that CD151-α3β1 integrin complex hyper-activates Rho A GTPase, which in turn remodels epithelial cell junctions. Notably, key signaling proteins directly involved in regulating cell-ECM adhesions have been identified as key regulators of cell-cell contacts. Vinculin, for example, has been shown as a binding partner for β-catenin at cell-cell junctions. Vinculin loss decreased E-cadherin at junctions without changing total E-cadherin. Mutant vinculin could not rescue E-cadherin levels or support the formation of intact junctions upon lack of binding to β-catenin. Microtubule (MT) structures have been implicated in the integrity of cell-cell junctions. Depolymerizing MTs or disrupting plus-end dynamics (without disassembling MTs) affect junctional integrity. Future mechanistic experiments for cadherin adhesion should consider these potential contributions to adhesion dynamics. The synergistic effects to cadherin dynamics through its association with integrins, signaling proteins, actin, MTs, or other proteins must be taken into account (**Figure 2.5**).

Initial immunoprecipitation studies revealed three main cytoplasmic partners for cadherin proteins: α-, β-, and γ-catenin (also known as plakoglobin). Indeed, catenins are the major cytoplasmic binding partners for cadherin proteins, alongside accessory proteins. Characterization of binding interactions showed that the cadherin cytoplasmic tails bind either β-

catenin or plakoglobin, which then binds to α-catenin. It is still unclear what causes β-catenin and plakoglobin to bind in a mutually exclusive manner (**Figure 2.5**).

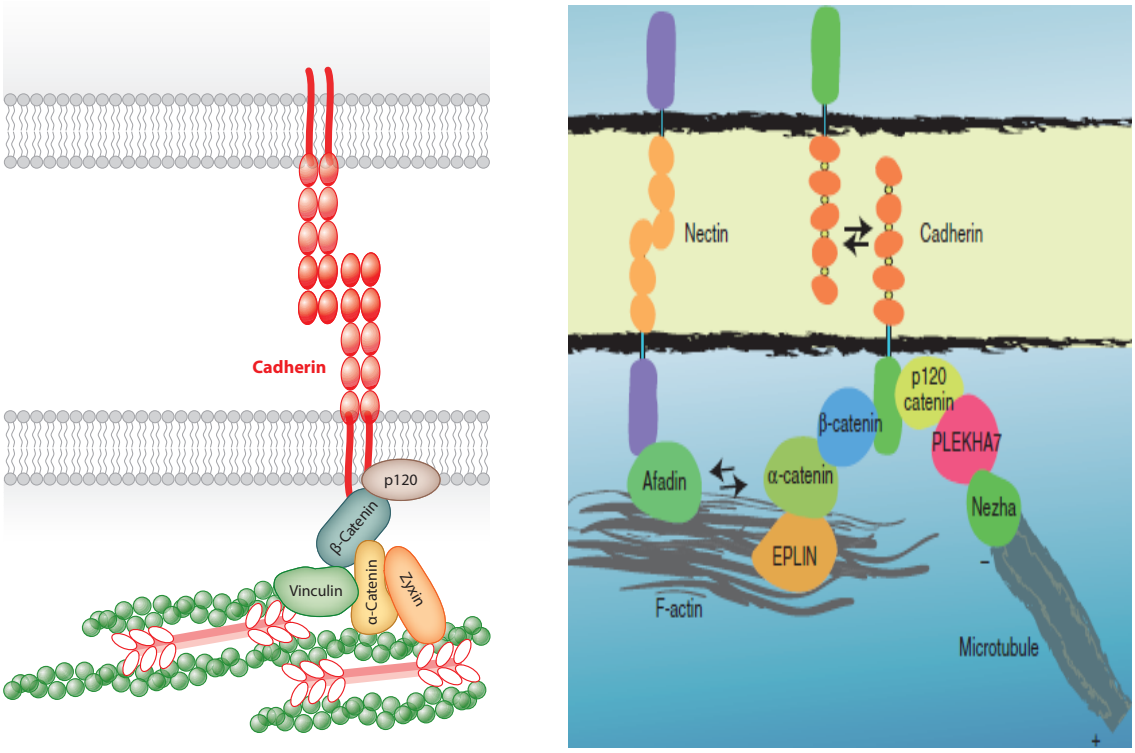

Figure 2. 5: Schematics of protein interactions within endothelial intercellular junctions [4] and representative constituents of the adherens junction [142].

Additionally, α-catenin binds the actin cytoskeleton, which has implications for cytoskeletal interactions and downstream signaling. Catenin proteins can regulate junction dynamics and mechanics directly. p120-catenin binds to the juxta- or trans-membrane region of the cytoplasmic tail [4]. Additionally, p120 has been associated with other structures such as microtubules via their minus ends through complex formation with PLEKHA7 and Nezha, which may, in turn, sustain cadherin complex architecture (**Figure 2.5**) [142]. Studies reveal three distinct roles for p120: first, to regulate cadherin levels by controlling cadherin turnover, and

second, to control GTPases that regulate actin cytoskeleton organization. Specifically, p120 catenin binding masks an ubiquitination sequence that signals cadherin endocytosis, and regulates cadherin availability/abundance at the membrane Finally, p120-catenin regulates the inside-out signaling of cadherin adhesion [143, 144].

Of the 150 amino acids (AAs) that comprise the highly conserved cytoplasmic domain of cadherin proteins, 100 AAs bind β-catenin and plakoglobin. The cytoplasmic tail is intrinsically unstructured: without catenin recruitment to the cytoplasmic tail and subsequent phosphorylation, which help anchor them, cadherins may be targeted for cellular destruction machinery. Previous studies with purified recombinant proteins showed that β-catenin inhibits α-catenin-actin binding, initially rejecting the notion that α-catenin links the cadherin complex to the actin skeleton. Previous FRET studies also showed that deletions of the actin-binding and cytoplasmic domain of α-catenin do not alter the dynamics of cadherin proteins. α-catenin, therefore, did not appear to be required for the stability of cadherin clusters at sites of cell-cell contacts. Weis and colleagues rationalized these observations through a model that posited that transient contacts between cadherins within lamellipodia (extensions of actin polymerization at the leading edge of a cell) lead to cadherin clustering, which produced a high local concentration of α-catenin at the immature junction [140]. When α-catenin concentration became high, it dissociated from β-catenin to suppress actin polymerization. This arrested lamellipodia movement, matured and stabilized the cell-cell contact, and reorganized actin into linear cables. This model initially supported the mechanical linkage between actin and adhesion molecules and allows dynamic junction remodeling

Recently, Weis and colleagues revised their initial findings to elucidate the minimal cadherin-catenin junctional proteins required to bind to the actin cytoskeleton using an elegant

optical trap assay [145]. In epithelia, cytoplasmic cadherin binds β-catenin, which binds αE-catenin, an F-actin binding protein. αE-catenin binds strongly to the cadherin-catenin complex but binds weakly to F-actin. Force transmission studies *in vitro*, however, show weak affinity of αE-catenin to F-actin, possibly eliminating the validity of the model of αE-catenin-F-actin binding. Furthermore, vinculin, as well as EPLIN, or epithelial protein lost in neoplasm, α-actinin, and afadin, have been shown to bind to both αE-catenin and F-actin and could serve as constituents of a valid model for cadherin-catenin/F-actin binding. To investigate the role of actomyosin-generated tension in cell-cell adhesion and the hypothesis that tension stabilizes a direct link between the cadherin-catenin complex and F-actin, Buckley, Weis and colleagues used an optical trap assay that recapitulated the geometry of the adherens junction and probed the mechanical forces between actin filaments and junction components [9, 146-153]. During the experiment, bond lifetimes of cadherin-catenin complex and actin filaments were measured under tension. Briefly, actin was tied to two optically trapped beads and suspended above immobilized cadherin-catenin complexes. By moving the stage on which the immobilized complexes were mounted parallel to the actin filament, tension was generated and the beads were displaced from their trap if bond attachments were successful. Bond lifetime distributions were plotted with respect to applied force, and kinetic parameters were fit to the curves. Ultimately, bond lifetimes were observed to have a biphasic dependence on force, such that a two-state catch bond model could be used to approximate the presence of two bond lifetime populations. In other words, based on this experiment, Weis posit that bonds between cadherin-catenin complex and actin form very weakly and quickly dissociate from their bound state but rapidly enter a strongly bound state as applied force increases. Long bond lifetimes in this strongly bound state persist until a high force threshold is reached and the cadherin-catenin bond dissociate from actin.

2.5.3. Adhesive and Kinetic Properties of Cadherin Bonds

Previous mention has been made of structural features of cadherin binding, echoing consensus views that cadherin-based adhesion involves a single *type* of binding interface between N-terminal regions of cadherin ectodomains. Far from it, multiple homophilic cadherin bond types exist, and we detail their structural specificity and biological consequences here. Historically, cadherin-binding studies have investigated structure determinations, solution-binding measurements or adhesive force measurements and have therefore yielded apparently contradictory results/interpretations, recent studies have reconciled the nuances inherent of these experimental platforms and has helped present a more unifying understanding of cadherin adhesion.

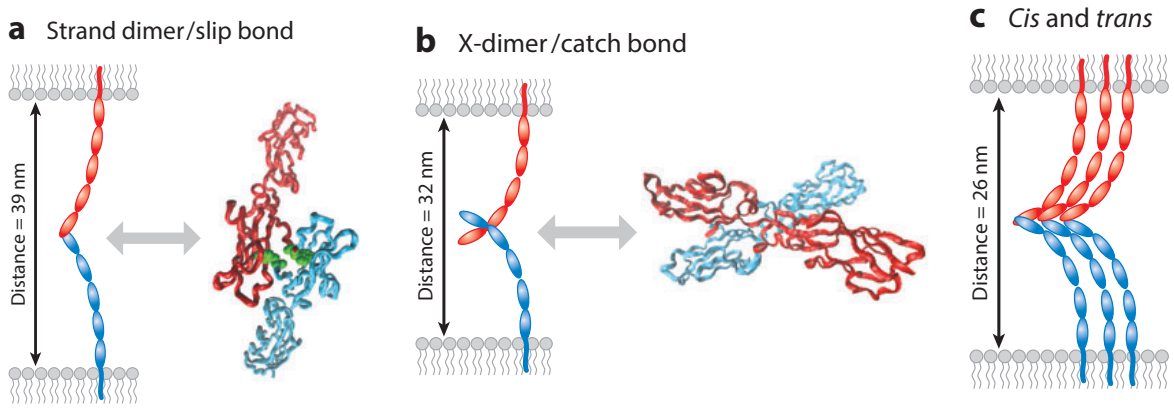

Figure 2. 6: Types of cadherin adhesive bonds and their configurations. From [154].

Strand Dimers. We have already detailed the primary adhesive interface of type-I classical cadherins. This so-called strand-dimer, in which there is mutual exchange of tryptophan at position 2 and their insertion into hydrophobic pockets of the first ectodomain of the apposing

protein, is critical for cadherin adhesion. Mutations of the Trp2 residue (a tryptophan-to-alanine switch, W2A) abrogate cadherin-mediated adhesion [155-158].

Using force versus distance measurements, Leckband and colleagues quantified attractive and repulsive forces between apposing cadherin proteins that were membrane-bound and their inter-membrane distance. These studies showed that ectodomains adhere at three membrane separations, distances that mapped to spatially distinct bonds in the ectodomains [159]. Force rupture studies, increasing the force on a particular bond until it ruptures, similarly identified multiple distinct types of cadherin bonds and associated strengths and dissociation rates. Ectodomain force rupture studies showed three distinct bonds with kinetic and mechanical properties, corresponding to the strand dimer bond and other bonds we will discuss in detail[160].

X-dimers. T-cadherin (CDH13, Cadherin-13, Heart-cadherin, H-cadherin, or 'truncated' cadherin) is the only cadherin family member that lacks both a trans-membrane and a cytoplasmic domain. GPI-anchored to the cell membrane and lacking the conserved cytoplasmic region of classical cadherins as well as the Trp2 residue necessary for strand-swapping, T-cadherin was previously thought to be uninvolved in cell-cell adhesion. It is adhesion-competent, however, as recent studies have proven [161, 162]. T-cadherin's EC1 and EC2 ectodomains associate in an anti-parallel, crossed configuration (called the X-dimer), with inter-protein contact at the EC12 junction. Even the W2A mutant of E-cadherin forms X-dimers in crystal form [163].

Solution-binding experiments, including surface plasmon resonance (SPR) and analytical centrifugation measurements (AUC) quantified association and dissociation rates of soluble and immobilized EC12 fragments of T-cadherin, as well as its equilibrium constants. A lysine-to-

glutamic acid (K14E) mutant ultimately showed that association and dissociation rates, but not the equilibrium constant were affected (increased activation barrier) and that this mutation prevents cadherins from exiting intercellular junctions (slower dissociation rates). In other words, this X-dimer formation in T-cadherin lowers the activation energy and accelerates strand dimer formation that is more stable [164-166].

Finally, single-bond force-rupture experiments using the atomic force microscope (AFM) have been critical in revealing that X-dimers rupture more slowing when force applied increases. This behavior changes after a certain force threshold (29 pN), after which X-dimers rupture more quickly. In other words, X-dimer bond lifetimes increase under tension, resisting forces more effectively, a behavior known as catch-bond behavior before converting to slip-bond behavior, in which bond lifetime decreases, rupturing more quickly and resisting tension less effectively under higher applied forces. X-strand dimers, therefore, exhibit more catch-bond behavior and strand-dimers exhibit more slip-bond behavior. This dual role and bond-behavior switch could be critical for dual roles for cadherins in tissue-specific contexts, including contractile or static tissues [164, 167].

***Cis* dimers.** Lateral cadherin interactions, different from the *trans* adhesions of the X-dimers and strand dimers, are also important to the stability of junctions. Based on functional blocking antibody studies, VE-cadherin junctions bind laterally at EC3 and EC4, while E-cadherin binding regions cluster between EC2-EC3. However, the full ectodomains may have additional binding interfaces, as evidenced by micropipette measurements (discussed later), or structural studies [168-171]. Extracellular domains that are densely packed form antiparallel strand dimers, which allow for a binding interface between EC1 on one protein and EC2-3 on

another protein, but numerous attempts to study this interaction have failed, including methods by NMR, AUC, single-molecule FRET, and SPR [141, 172, 173].

2.6. Quantitative Force Measurements

2.6.1. Adhesion Assays

Cell-cell adhesion events are highly regulated and complex processes with initial receptor-ligand interactions and subsequent strengthening response. The notion that receptor-ligand interactions, clustering, intracellular protein recruitment, cytoskeletal association, and adhesion complex assembly results in an increase in adhesion strength over time is accepted in the field, but neither the contributions of each of these processes to overall adhesion strength nor the specific molecules that mediate the strengthening response has been elucidated. Part of the problem has stemmed from lack of robust quantitative platforms to provide reproducible, calibrated, and appropriately large detachment forces, as well as the spatiotemporal and molecular complexity of adhesion events [174].

Typically, adhesion assays measure the ability of cells to remain adhered to surface when exposed to a detachment force. Early adhesion strength analyses were strictly qualitative. These "wash" assays were useful, however, in identifying key adhesion proteins. "Wash" assays involve seeding cells onto a substrate (a cell culture dish, for example), washing cells off using a pipette or other means of applying reagent buffers over the cells, and counting the remaining fraction of adherent cells. These early assays were severely limited in magnitude of applied forces able to be generated to detach cells within adequate time and often yielded inconclusive or contradictory results.

Quantitatively speaking, a variety of adhesion assays have been able to apply controlled forces to adherent cells. There are three main classes of these adhesion assays, namely micromanipulation, centrifugation, and hydrodynamic force. Briefly, micromanipulation assays apply normal or tangential force to the cells with micropipettes, AFM, or laser tweezers to yield pico-range forces for sensitive, real-time, force-displacement analysis. Micromanipulation is advantageous in analyzing isolated or few receptor-ligand interactions but is limited to studying very short-term adhesion phenomena (receptor-ligand interactions) because the forces required to examine long-term adhesion phenomena (subsequent strengthening response) far exceeds the equipment force thresholds possible (hundreds of pN) [175]. Micromanipulation experiments are difficult to conduct because they are time-intensive due to their nature of single-cell analysis and require highly calibrated equipment, which may affect their reproducibility. Centrifugation assays apply a constant detachment force perpendicular to the cell adhesive area of a substrate (tissue culture dish, for example) with adherent cells on top of it. Centrifugation assays are advantageous because they have low set-up and maintenance costs and yield population-average values of adhesion strength. However, they apply low detachment forces ($< 10^{-3}$ dynes/cell) and are limited to short attachment times. More importantly, they apply a single force per experiment and thus require multiple iterations at different speeds to yield mean adhesion strength data.

There are three main types of hydrodynamic flow assays, all of which generate shear forces by the mechanism of fluid flow over adherent cells on a substrate. The parallel plate setup (two rectangular substrates separated by gap distance) applies a constant shear stress (determined by flow rate between the plates) in a single experiment: similar to the centrifugation assay, multiple experiments at different flow rates must be conducted to quantify mean adhesion strength. Although this apparatus allows direct observation of the attachment/detachment process

and easily validated flow patterns, the detachment forces generated are usually still insufficient to detach spread cells. Radial flow systems (two radial plates separated by gap distance) apply a range of shear stresses to the surface of the substrate. Although the radial flow system allows for direct observation of attachment/detachment processes and applies a gradient of forces to adherent cells, the shear stress applied is inversely proportional to radial position from the center of the disk, which yields very complex hydrodynamic conditions at the center of the disk (fluid impingement point). The spinning disk assay, detailed in the following section, is advantageous because it generates and applies a wide range of forces, has a linear gradient of applied forces, and has uniform conditions at the substrate surface.

2.6.2. Quantitative Measurement Tools for Cadherin-Based Mechanotransduction

Previous studies in cadherin-based cell-cell adhesion had largely been limited to micromanipulation experiments [1, 22, 47, 169, 176-182]. They proved useful, however, in elucidating short-term kinetics, energetic, and binding mechanisms of cadherin proteins during their initial receptor-ligand binding, as well as underscoring their functional importance in disease states. For example, Leckband and colleagues use *micropipette* to measure kinetics of binding between single cell pairs by plotting the probability of binding event occurring given (as a function of) specified contact time [183]. Experimentally, a micropipette holding Chinese Hamster Ovary (CHO) cells expressing wild-type cadherin was brought into contact with a red blood cell (RBC) modified with immobilized C-cadherin bound covalently to the RBC surface through monoclonal antibodies. Binding probability, calculated as the ratio of number of detected binding events to total number of cell-cell contacts, can be used to determine kinetic rates and two-dimensional affinity constants (strength of interaction) when plotted against time

allowed for the binding event to occur. Leckband discovered that C-cadherin receptor-ligand interactions occur in a biphasic manner. In other words, two cadherin-binding states exist, with a weak low-probability state occurring very rapidly (within the first 2 seconds), followed by 2-5 second lag, after which a stronger higher-probability state emerges. Using cadherin mutants, they also find that the initial state of the biphasic behavior can be attributed to ectodomain (EC) 1 and 2 binding, and that the lag and transition to the second higher-probability state both require EC3.

To quantify the strengths and dissociation rates associated with cadherin proteins, Leckband and colleagues also use the *bio-membrane force* probe (BFP) to delineate four different cadherin bonds, which differ in strength and dissociation rate. Briefly, BFP experiments bring two beads in contact – one immobilized with cadherins is fused biochemically to the surface of a RBC and another is coated with complementary cadherin. Upon contact, the two beads are pulled apart at a specific loading rate until bond failure occurs, as determined when the RBC recoils back to its original (unperturbed) state. Leckband's final contribution uses the *surface force apparatus* (SFA) to quantify the inter-membrane distances at which cadherin ectodomain adhesion occurs. Briefly, SFA quantifies interaction potentials, or energy per unit area, as a function of distance between two cadherin monolayers within a resolution of ±1 Å (or 0.1 nm). Strongest adhesion occurs when ectodomains fully overlap (EC1-5) in anti-parallel fashion at an inter-membrane gap distance of 39nm. Intermediate adhesion occurs at 38nm with EC3-5 overlapping and weak adhesion occurs at 53nm with binding between EC1 domains. Consistent with their micropipette results, they found that eliminating EC3 removes strongest adhesive bonds. These studies are useful in delineating the different kinetic and adhesive states that require different EC domains in initial receptor-ligand binding.

In addition, Wirtz and colleagues conducted single-molecule force spectroscopy to show that α-catenin reduces adhesive force between individual epithelial cadherin pairs (E-cadherin) on parental breast cancer cells [184]. Re-expressing α-catenin in these cancer cells restores intracellular E-cadherin bond strength and could delay or prevent the epithelial-to-mesenchymal transition, a hallmark of the onset of the metastatic process characterized by reduced cadherin expression levels, loss of cell adhesion, and a more migratory phenotype of cells. AFM then correlates the deflection of the cantilever to the forces associated interaction dynamics. Notably, Chen and colleagues, instead, have used 3D-microneedle array posts with specified bending moduli to study the responsiveness of cell-cell junctions to tugging force, showing that junction size increases with increased force in a Rac1-dependent manner. This underscores the important interplay of sites of adhesion as mechano-transducers of force and effectors of downstream signaling events. The micromanipulation assays described above cannot provide any insight to dynamics of the strengthening response, however, because the forces required in examining long-term adhesion phenomena far exceeds the force generation thresholds possible. To our knowledge, no one has performed population-based mean adhesion strength assays to study the initiation and progression of *adhesion strengthening.*

2.7. Adhesive Force Generation

The goal of our experiments is to measure adhesive force generation for cadherin-based cell-cell interactions. We base our understanding of adhesive force generation on McClay's early model [7]. Briefly, following the initial receptor-ligand binding event, strengthening arises from increases in cell-substrate contact area (spreading), receptor recruitment and clustering to anchorage sites, and interactions with cytoskeletal components (complex assembly), resulting in

rapid increases in adhesion strength. Although we control for cell spread area in our assays, in order to control increases in bond number due to receptor number increases at the interface, we expect that protein recruitment and complex assembly will generate strong adhesive forces. The model posits that protein recruitment will increase bond density within specified adhesive area. Indeed, recruitment and clustering may modulate adhesion strength more than contact area increase because increasing bond density per unit area reduces the effects of non-uniform loading due to membrane tension. Cytoskeletal interactions and complex assembly are also important because they increase the rigidity of adhesive structures at anchoring sites, requiring higher adhesion strength to cause bond failure at sites of adhesion. Thus far, the molecular binding partners involved in the adhesion process have been extensively studied. Mechanisms initiating, stabilizing, and modulating overall adhesion strengthening of cadherin complexes merit further investigation. We propose a combined approach of a hydrodynamic assay, engineered substrates, and quantitative biochemical assays to probe the contributions of protein recruitment or complex assembly to overall adhesion strengthening dynamics.

2.7.1. Spinning Disk Assay

We use a hydrodynamic flow assay called the spinning disk, in which we can apply a range of shear forces to the cells on the surface of this coverslip to measure the adhesion strength of a population of cells in a robust and sensitive manner (**Eq. 1**) [2, 174, 185-187]. During the experiment, coverslips of engineered adhesive surfaces with adherent cells seeded onto islands of controlled geometries are mounted on the device, immersed in fluid spin buffer, and spun at constant speed for 5 minutes with constant ramp up and ramp down times. The shear stress on

the surface of the coverslip, which is well defined and varies linearly with radial position from the center of the coverslip, is given by the following equation:

$$\tau = 0.8r\sqrt{\rho\mu\omega^3}\,, \qquad \text{(Equation 1)}$$

where τ is the shear stress applied, r is the radial position from the center of the coverslip, ρ is the fluid density, μ is the fluid viscosity, and ω is the rotational speed. Fluid flow over the cells produces a detachment force given above, where shear stress at the center of the coverslip is negligible and is maximized at the edge of the coverslip. The disadvantage of the spinning disk assay is that this is an end-point assay - there is no real-time analysis of the detachment process. Additionally, fluid flow patterns have to be validated. A major advantage of the spinning disk, however, is that within a single experiment, a wide range of detachment forces can be applied through a linear gradient to a population of approximately 75,000 cells with uniform and constant chemical conditions at the surface of the coverslip and with consistent reproducibility.

What we expect for a population of cells is that each cell will have its own adhesive signature and will be sheared from its original position on the coverslip. Probabilistically, the fraction of adherent cells should decrease non-linearly with applied shear stress (**Eq. 2**). We plot the resultant detachment profile, or the adherent cell fraction as a function of shear stress. When fit to the following sigmoid:

$$f = \frac{f_0}{1+ e^{b(\tau-\tau_{50})}} \qquad \text{(Equation 2),}$$

where is $f_0$is the normalized asymptote, b is the slope at the inflection point of the sigmoid, τ is the shear stress applied, and τ_{50} is the shear stress at 50% detachment. We define the adhesion strength as the shear stress at which 50% of the cells in the experiment remain adherent, or the mean shear stress. By proper experimental design, this population parameter can be used to report the adhesive signature of cells in response to various perturbations, such as substrate

chemistry, adhesive area, ligand density, contact time, and reagents to modulate the strengthening process.

2.8. Traction Force

Studies seeking to understand the interaction between cells and their surrounding environment have employed a set of micro- and nano-technological tools to investigate how physical factors in the micro-environment can affect downstream function, including adhesion, proliferation, migration, and survival. Traditionally, traction force measurements have been used study how cells respond to focal adhesion formation and maturation. Cell-ECM traction forces are generated by the cross-bridge cycling between actin and myosin and allow cells to migrate, spread, and maintain its shape. Traction forces provide insight as to how cells respond to their mechanical and chemical environment, as they allow the stresses induced below and around an adhered cell to be measured by tracking the displacements of structures or sensors at the adhesive interface (see next section). It must be noted that they do not provide a direct measurement of the strength of an adhesive interaction between a cell and its matrix or between a cell and an engineered surface presenting proteins at different ligand densities. The strength of the adhesive interaction, adhesion strength, quantifies the force or stress required to detach a cell from a substrate on which it is adhered [188].

2.8.1 Quantitative Measurement Tools for Traction Forces

Bead displacements on thin films were first use to measure traction forces for highly contractile cells, but using elastic films limited the range of traction force able to be measured by

the system and thus limited the range of cultured cells able to be studied. Polyacrylamide gels have also been used to study traction forces, in that fluorescent nano-beads embedded in cross-linked acrylamide/bisacrylamide substrate (whose stiffness could be finely tuned by adjusting the monomer-cross linker ratio) could be imaged after cellular traction forces displace the beads. Traction stresses are then calculated by quantifying displacement vectors of deformed beads from their un-deformed positions using elasticity theory. Known as traction force microscopy, or TFM, the imaging of beads randomly dispersed in these substrates introduced some uncertainty in solving for traction forces when the density of beads was slow. Improvements to the technique by spatially organizing the beads complicated analysis even further, as the possible solutions for the vector fields for traction forces became reduced. One limitation of TFM is that local forces can distort the substrate, which can generate secondary forces that in turn act on the adhesive structures being studied. In other words, it is difficult to decouple the physical parameters being studied from the cellular response.

Micro-fabricated cantilevers were the first tools that could measure local traction forces independently of the physical parameters of the systems. Horizontal cantilevers fabricated from silicon wafers, whose lateral deflection can be used to quantify traction force by multiplying by the stiffness of the cantilever, were improved upon by the fabrication of an array of vertical elastomeric cantilevers. These posts, fabricated through soft lithography and replica molding of silicone rubber, deflect independent of each other and cells spread on top of the posts. One of many advantages of using these vertical elastomeric arrays, also termed micro-fabricated post-array detectors (mPADs) are that the top of the posts can be functionalized by different chemistries to allow for cells to be patterned, organized, or confined in any arrangement [189, 190].

CHAPTER III: P120-CATENIN AND β-CATENIN DIFFERENTIALLY REGULATE CADHERIN ADHESIVE FUNCTION[5]

3.1. Abstract

Vascular endothelial (VE)-cadherin, the major adherens junction adhesion molecule in endothelial cells, interacts with p120-catenin and β-catenin through its cytoplasmic tail. However, the specific functional contributions of the catenins to the establishment of strong adhesion are not fully understood. Here we use bioengineering approaches to identify the roles of cadherin–catenin interactions in promoting strong cellular adhesion and the ability of the cells to spread on an adhesive surface. Our results demonstrate that the domain of VE-cadherin that binds to β-catenin is required for the establishment of strong steady-state adhesion strength. Surprisingly, p120 binding to the cadherin tail had no effect on the strength of adhesion when the available adhesive area was limited. Instead, the binding of VE-cadherin to p120 regulates adhesive contact area in a Rac1-dependent manner. These findings reveal that p120 and β-catenin have distinct but complementary roles in strengthening cadherin-mediated adhesion.

3.2. Introduction

Cell adhesion enables tissues to maintain their structural integrity and withstand mechanical stress [143]. Cadherins are a family of trans-membrane adhesion receptors that enable cells to form cell contacts that mature into adherens junctions as cytoplasmic binding partners are recruited to facilitate cytoskeletal linkages [191]. The vascular endothelium, which

[5] Adapted from: Oas RG, Nanes BA, Esimai CC, Vincent PA, García AJ, Kowalczyk AP. p120-catenin and β-catenin differentially regulate cadherin adhesive function. Mol Biol Cell. 2013 Mar; 24(6):704-14.

forms a thin layer lining the interior of blood vessels, must sustain strong intercellular adhesion in order to maintain vascular barrier function and prevent hemorrhage and edema. However, the adhesion between endothelial cells must be dynamically regulated to enable angiogenesis during growth and development and to allow the passage of leukocytes from the vascular lumen to surrounding tissue at sites of inflammation. The major cadherin family member found in endothelial cells is vascular endothelial (VE)-cadherin, which mediates homophilic, calcium-dependent adhesion through its extracellular domain and binds to Armadillo-family proteins p120-catenin (p120) and β-catenin inside the cytoplasm through its juxtamembrane and catenin-binding domains, respectively. β-Catenin provides linkage between adherens junctions and the actin cytoskeleton through interactions involving α-catenin [192], whereas p120 regulates cadherin stability at the plasma membrane by masking an endocytic signal on the cadherin cytoplasmic tail to prevent cadherin internalization [193-197]. Studies using mouse models have demonstrated a requirement for both p120 and β-catenin to maintain vascular barrier function, and the conditional endothelial knockout of either catenin results in hemorrhages, particularly in areas subject to increased vascular flow during development [198, 199].

In previous studies involving C-cadherin and E-cadherin, the cadherin juxtamembrane domain and its specific interaction with p120 were implicated in the strengthening of cell adhesion [26, 200]. However, the mechanisms by which strong cadherin-based adhesion is achieved in endothelial cells, and the contribution of catenins to this process, are not fully understood. The loss of endothelial p120 in vivo results in a reduction in VE-cadherin levels [199], consistent with a role for p120 in regulating cadherin turnover. Studies using cultured endothelial cells demonstrated that the interaction between p120 and VE-cadherin at the plasma membrane is required for the maintenance of endothelial barrier function [201, 202]. However,

the knockout of VE-cadherin is recessive embryonic lethal [70, 203], and the reduction of VE-cadherin levels by 50% in the heterozygotes did not lead to hemorrhaging or other vascular defects. This raises the question of whether p120 could be acting to strengthen VE-cadherin–dependent adhesion independently of cadherin levels alone. In addition, p120 is a potent regulator of the Rho family of small GTPases, which regulate actin cytoskeletal dynamics and play important roles in the establishment of cell–cell contacts and vascular barrier function [204, 205]. Specifically, p120 activates Rac1 and inhibits RhoA [206, 207]. Moreover, the adhesion defects introduced by blocking p120 binding to the E-cadherin tail can be rescued by expression of constitutively active Rac1 [200]. Therefore it is likely that the contribution of p120 to strong adhesion through VE-cadherin involves not only the stabilization of the cadherin at the cell surface, but also the localization of p120 near the membrane to locally regulate Rho family GTPases.

Adhesive strength is modulated by a number of factors, including contact area and cytoskeletal linkages [2]. Previous studies examining cadherin adhesion strengthening used model systems in which cells both adhere and spread onto surfaces [26, 208-210]. Thus the contributions of cadherin tail domains and catenins to adhesion strengthening independent of contact area and cytoskeletal coupling have not been resolved. We used a combination of two approaches to overcome these limitations. First, to examine the role of p120 and β-catenin in endothelial cell adhesion, we expressed chimeric proteins in which the interleukin-2 receptor (IL-2R) extracellular domain was fused to the cytoplasmic domain of VE-cadherin. We then introduced mutations that selectively uncoupled the cadherin tail to either p120 or β-catenin. Second, we used micro-patterned coverslips that limited cell–substrate contact area, thereby controlling cell geometry independent of cytoplasmic linkages. Using a hydrodynamic assay to

measure the strength of cell adhesion, we found that the interaction between p120 and the cadherin tail did not alter adhesion strength. In contrast, the β-catenin–binding domain was crucial to strengthening adhesion. Furthermore, we found that the interaction between p120 and VE-cadherin was necessary to promote Rac1-dependent cell spreading. These findings support a model in which p120 and β-catenin modulate cadherin-based adhesion through complementary and experimentally distinguishable mechanisms to independently regulate adhesive contact area and adhesion strength.

3.3. Results

3.3.1. Chimeric adhesion receptors enable functional separation of cadherin intracellular domains

To examine the functional significance of the cytoplasmic domains and interactions of the VE-cadherin cytoplasmic tail in endothelial adhesion strengthening, we used adenoviral vectors to express a series of chimeric receptor proteins in primary human micro-vascular endothelial cells (MECs; **Figure 3.1A**). The cytoplasmic tail of VE-cadherin was fused with the extracellular and trans-membrane domains of IL-2R to generate the IL-2R– VE-cad$_{cyto}$ construct. Similar chimeric receptors have been used in studies of cell adhesion mediated by cadherins as well as integrins [208, 211-213].

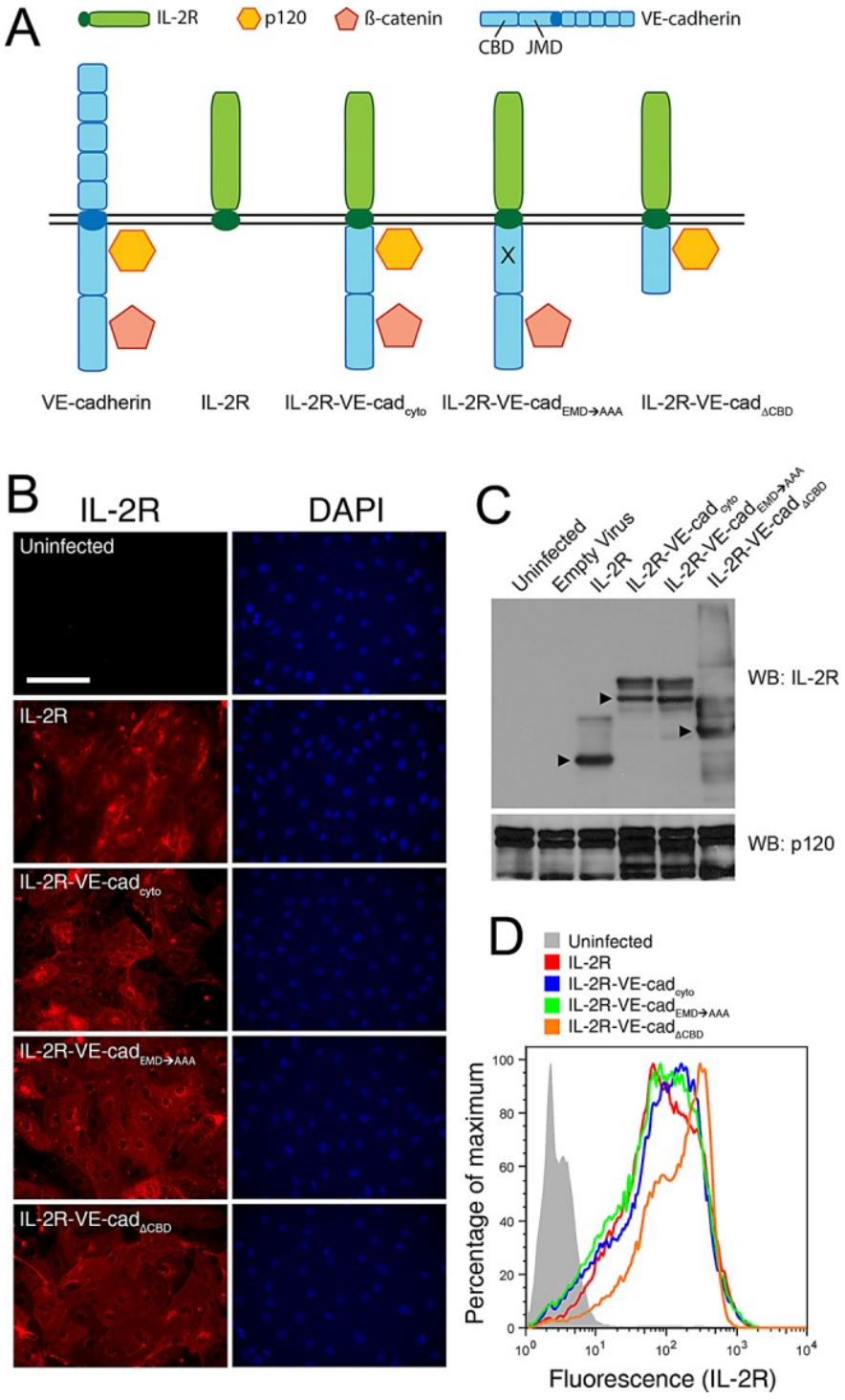

Figure 3. 1: Chimeric receptors are expressed at comparable levels at the plasma membrane. (A) The four chimeric constructs used in this work as adhesive receptors are depicted, along with wild-type VE-cadherin. The extracellular domain of VE-cadherin is replaced with IL-2R to generate IL-2R–VE-cad$_{cyto}$. A triple-alanine mutation in the p120-binding site that uncouples the cadherin tail from p120 is introduced to generate IL-2R–VE-cad$_{EMD\rightarrow AAA}$. The catenin-binding domain is deleted to generate IL-2R–VE-cad$_{\Delta CBD}$. The four constructs are introduced into cells

by way of adenoviral vectors. (B–D) Human micro-vascular endothelial cells were transduced with chimeric constructs containing the IL-2R extracellular domain fused to the cytoplasmic domain of VE-cadherin. (B) Expression of the constructs was verified by immunofluorescence microscopy. Cells were stained for IL-2R to detect the receptors and DAPI to show the cell nuclei and enable evaluation of infection rates. IL-2R staining was absent in uninfected cells, and for all four constructs we observed infection rates of 80% or higher. Scale bar, 100 μm. (C) Expression levels were also assessed by Western blot in which whole-cell lysates were probed for IL-2R and with p120 as a loading control. Arrowheads indicate main bands. Higher–molecular weight bands result from IL-2R glycosylation. (D) The levels of expression of the chimeric receptors at the cell surface were assessed using flow cytometry. Unpermeabilized cells were fixed and stained for IL-2R and tested for their peak fluorescence values as compared with those of uninfected control cells. Peak values for each construct occurred within a similar range, indicating that their surface expression was comparable.

To examine the contri-bution of specific domains of the VE-cadherin tail in cell adhesion, we generated two additional variants by mutating the VE-cadherin cytoplasmic domain: a triple-alanine mutation at amino acids 562–564 in the juxtamembrane domain, which blocks binding to p120 (IL-2R– VE-cad$_{EMD\rightarrow AAA}$) and a deletion of the catenin-binding domain (amino acids 620–702), which eliminates β-catenin interactions (IL-2R– VE-cad$_{\Delta CBD}$; [194]. IL-2R alone without a cytoplasmic tail was used as a control. Expression of the receptors in MECs was verified by immunofluorescence (**Figure 3.1B**) and Western blot (**Figure 3.1C**), which confirmed that the constructs were expressed at comparable levels. Flow cytometry was performed to further verify that cell surface expression levels of each IL-2R construct were comparable among groups (**Figure 3.1D**).

To verify that the chimeric receptors were able to interact with p120 and β-catenin despite the absence of the cadherin extracellular domain, we performed immunoprecipitations using antibodies against IL-2R. The catenins did not associate with IL-2R, whereas p120 formed complexes with IL-2R– VE-cad$_{cyto}$ and IL-2R– VE-cad$_{\Delta CBD}$. In contrast, β-catenin formed complexes with IL-2R– VE-cad$_{cyto}$ and IL-2R– VE-cad$_{EMD\rightarrow AAA}$. These results demonstrate that the chimeric cadherins associate in the predicted manner with p120 and β-catenin (**Figure 3.2A**).

We next sought to determine whether the chimeric cadherins were able to recruit β-catenin and p120 to sites of adhesion mediated by the IL-2R extracellular domain. Cells expressing the chimeric constructs or IL-2R were seeded on micro-patterned coverslips, which presented an array of 20-μm adhesive islands prepared as previously described [21]. The adhesive areas were coated with antibodies directed against the IL-2 receptor, and cells expressing the chimeric constructs were seeded onto the micro-patterned surfaces. Because the area of the islands was smaller than the fully spread area of the cells, the cells were maintained in a uniform geometry and spaced regularly across the surface of the coverslip (**Figure 3.3B).** Uninfected cells and cells transduced with an empty adenoviral vector failed to adhere to either patterned (unpublished results) or unpatterned surfaces (see discussion of **Figure 3.5A** later in the paper).

Using immunofluorescence microscopy, we verified that cells expressing IL-2R– VE-cad$_{cyto}$ and IL-2R– VE-cad$_{\Delta CBD}$ exhibited colocalization between IL-2R and p120 (**Figure 3.2, B and D**), whereas samples expressing IL-2R– VE-cad$_{cyto}$ and IL-2R– VE-cad$_{EMD\rightarrow AAA}$ displayed colocalization between IL-2R and β-catenin (**Figure 3.2, C and E**), Cells expressing IL-2R alone did not yield demonstrable colocalization with either catenin. Although both catenins can also be observed in other regions, presumably representing interactions with endogenous cadherin or other binding partners, these results show that the chimeric receptors expressing cytoplasmic VE-cadherin domains are able to selectively recruit catenins and specifically mediate adhesion to patterned surfaces.

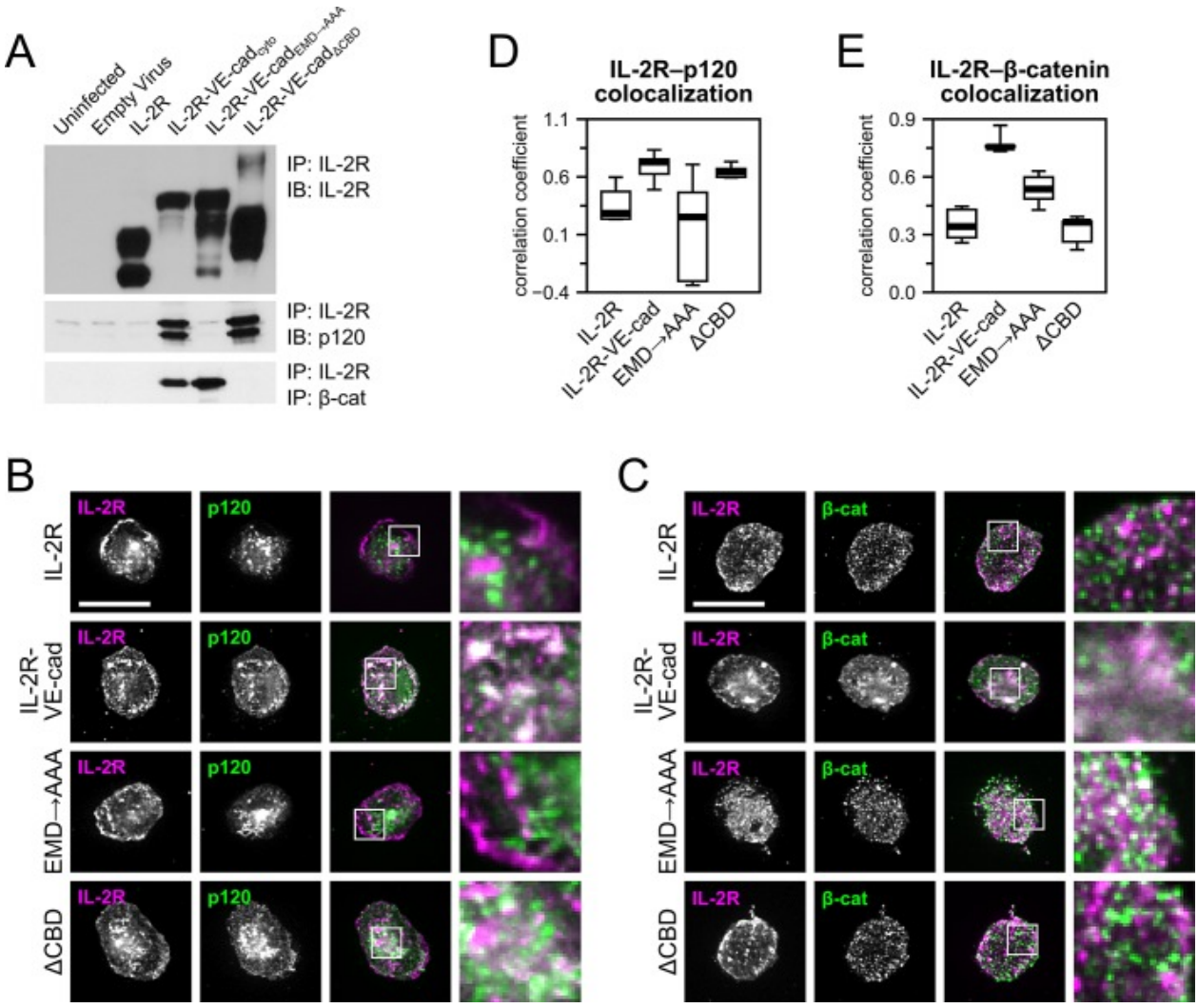

Figure 3. 2: Cytoplasmic domains of chimeric receptors recruit p120 and β -catenin to the site of adhesion. (A) Immunoprecipitations were performed to verify that the chimeric receptors were able to complex with the appropriate catenins. Magnetic beads conjugated to antibodies against IL-2R were used to pull down the chimeric receptors, which were subsequently probed for p120 and β-catenin. p120 coprecipitated with IL-2R–VE-cadcyto and IL- 2R–VE-cadΔCBD, and β-catenin was pulled down by IL-2R–VE-cadcyto and IL-2R–VE-cadEMD→AAA. (B, C) To ensure that catenins were recruited to the sites of adhesion mediated by the chimeric constructs, cells expressing the constructs were seeded on micro-patterned coverslips (see Figure 3) using IL-2R antibodies as an adhesive ligand. The cells were then extracted using Triton X-100 in a cytoskeleton stabilization buffer and stained for p120, β-catenin, and IL-2R. p120 colocalized with IL-2R–VE-cadcyto and IL-2R–VE-cadΔCBD (B), whereas β-catenin colocalized with IL-2R–VE-cadcyto and IL-2R–VE-cadEMD→AAA (C). Bars, 20 μm. (D, E) Colocalization of IL-2R chimeras with p120 (D) and β-catenin (E) was quantified as Pearson's *r*. Thick line, median (n = 5–6 cells per group); box, interquartile range; whiskers, full range.

3.3.2. The catenin-binding domain of VE-cadherin is necessary for strong adhesion

To define the contributions of the VE-cadherin cytoplasmic domains to cell adhesion strengthening, we tested cells expressing the chimeric receptors for their ability to remain attached to a surface when subjected to a range of shear forces. Measurements of adhesion strength were made using a spinning-disk apparatus that applies hydrodynamic shear force to a large population of cells attached to patterned coverslips (**Figure 3.3B**) by rotating them in a fluid-filled chamber, generating a well-characterized range of shear forces that increase with radial position along the surface of the coverslip (**Figure 3.4A**). Cells expressing the IL-2R constructs were seeded on patterned coverslips and exposed to shear forces using the spinning-disk system. This approach, which has been extensively discussed in previous reports [2, 174, 214], yields detachment profiles such as the representative data shown in **Figure 3.4B**. The chart shows the fraction of adherent cells in regions of the coverslip subject to increasing shear force relative to the fraction of adherent cells near the center, where there is no shear force.

A sigmoidal curve is then fitted to the resulting data points to obtain the shear stress needed for 50% detachment (τ_{50}), which is used as a measure of cell adhesion strength. Cells expressing IL-2R– VE-cad$_{cyto}$ exhibited 50% higher adhesion strength values (τ_{50}) than those cells expressing the IL-2R alone, demonstrating the importance of the cadherin cytoplasmic tail in mediating strong attachment (**Figure 3.4, B and C**). Unexpectedly, the cells expressing the IL-2R– VE-cad$_{EMD\rightarrow AAA}$ construct produced adhesion strength values statistically indistinguishable from those obtained with the wild-type cadherin tail. In contrast, cells expressing the IL-2R– VE-cad$_{\Delta CBD}$ construct yielded adhesion comparable to the IL-2R. Taken

together, these results indicate that the p120 binding site in VE-cadherin does not contribute to adhesion strength but that the β-catenin-binding domain is required.

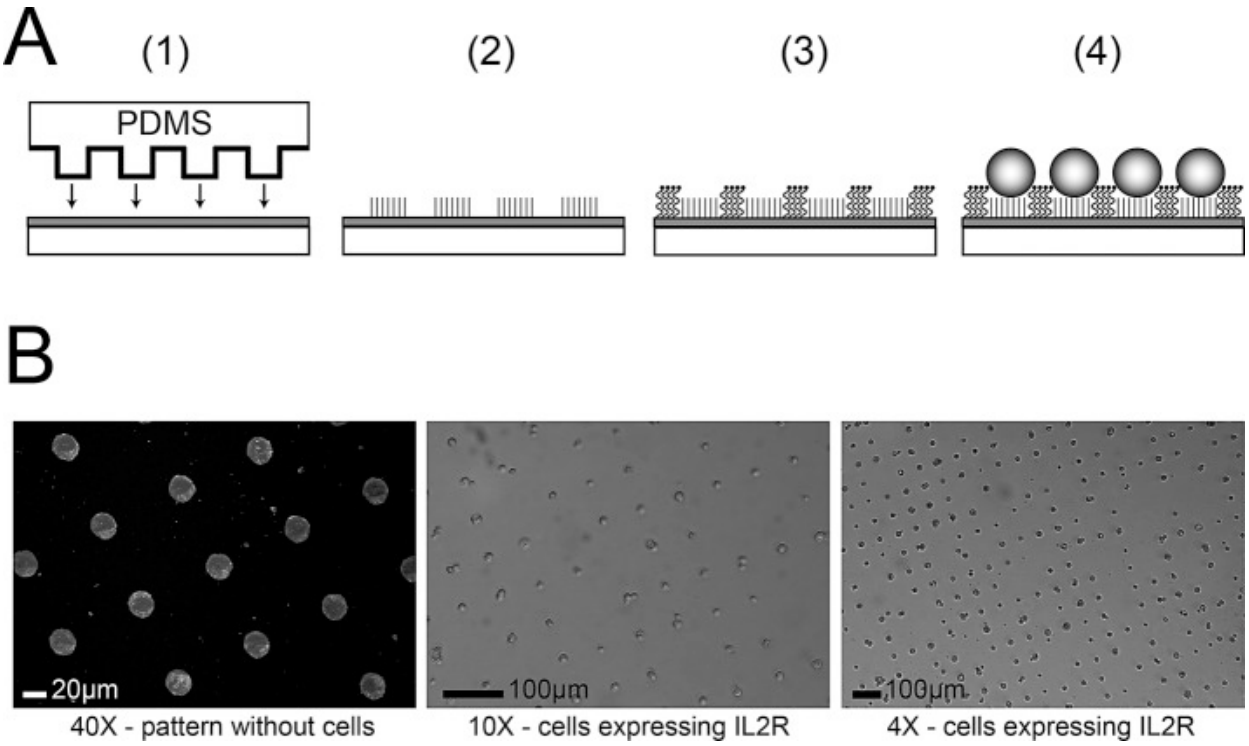

Figure 3. 3: Micropatterned coverslips feature adhesive islands that allow for the generation of regular arrays of evenly spaced cells with well-defined morphologies. Micropatterning occurs through a stepwise process. (A) Glass coverslips are coated with titanium and gold using an electron beam evaporator, and then a PDMS stamp is used to print islands of the self-assembling monolayer across the surface of the coverslip (A, 1). This generates adhesive islands that can passively adsorb ligands that will interact specifically with adhesive receptors on the surface of cells (A, 2). Spaces between the adhesive islands are backfilled with polyethylene glycol to create nonadhesive surfaces around sites of cell adhesion (A, 3). Cells are seeded on the micro-patterned coverslips and adhere individually to adhesive islands (A, 4). (B) Cells expressing IL-2R and chimeric constructs adhere to adhesive islands. Micropatterned coverslips are treated with immunoglobulin G directed against the IL-2 receptor, which can be detected with fluorescently labeled secondary antibodies. Cells expressing IL-2R seeded on the micro-patterned surfaces form a regular array of single cells attached to adhesive islands.

To verify that p120 levels in the cells were not limiting, we coexpressed exogenous p120 with IL-2R– VE-cad$_{cyto}$ and IL-2R– VE-cad$_{EMD\rightarrow AAA}$. The overexpression of p120 did not

increase the adhesion strength of cells expressing IL-2R– VE-cad$_{cyto}$ compared with those expressing IL-2R– VE-cad$_{EMD\rightarrow AAA}$ (Supplemental Figure S1), indicating that p120 was not limiting. This result suggests a requirement for linkage to the actin cytoskeleton through the catenin-binding domain and its association to β-catenin in order to produce strong steady-state adhesion but that p120 appears to be dispensable. Taken together, these results indicate that the loss of p120 binding to the VE-cadherin juxtamembrane domain does not significantly reduce cell adhesion strength, whereas the β-catenin–binding domain is essential for strong adhesion.

3.3.3. p120 binding to the VE-cadherin tail is necessary to promote cell spreading

Because we were unable to demonstrate a requirement for the interaction between p120 and VE-cadherin in establishing strong adhesion to patterned surfaces, we next tested the ability of cells expressing the chimeric constructs to spread on unpatterned substrates that did not constrain the adhesive area. Primary microvascular endothelial cells expressing IL-2R and the three chimeric receptors were able to adhere to the surface, whereas control uninfected cells or cells expressing empty adenoviral vector were unable to form attachments and were easily removed from the surface.

The typical diameter of fully spread IL-2R– VE-cad$_{\Delta CBD}$ - and IL-2R– VE-cad$_{cyto}$ – expressing cells was approximately 30 μm, whereas the typical diameter of fully spread IL-2R– and IL-2R– VE-cad$_{EMD\rightarrow AAA}$ –expressing cells was approximately 20 μm. Of interest, whereas IL-2R– VE-cad$_{\Delta CBD}$ –expressing cells did not exhibit a significant spreading defect compared with those expressing IL-2R– VE-cad$_{cyto}$, the p120-uncoupled chimera was statistically indistinguishable from IL-2R, suggesting a key role for p120 in modulating cell spreading (**Figure 3.5B**).

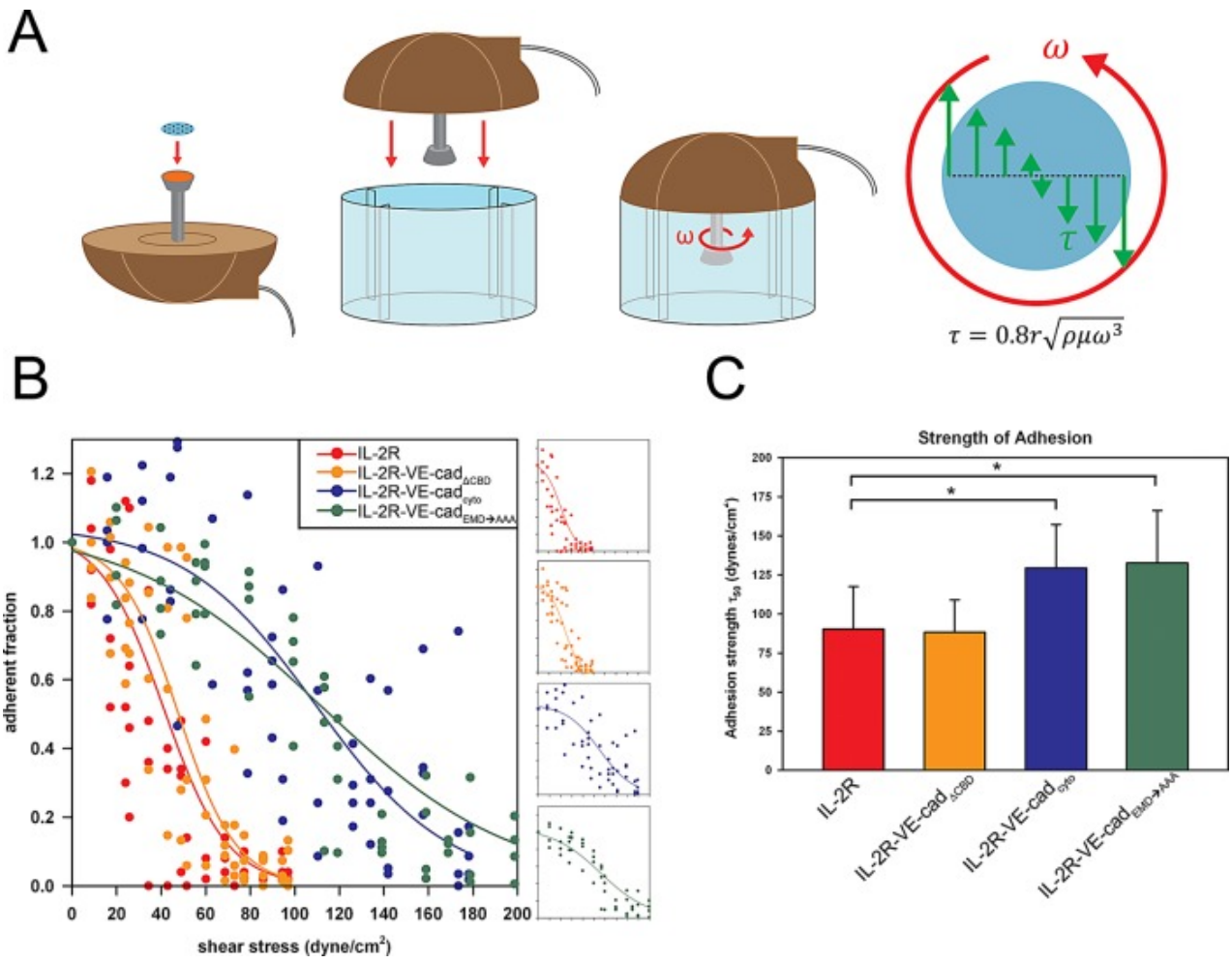

Figure 3. 4: Linkage between cadherins and the actin cytoskeleton is necessary to strengthen steady-state adhesion. (A) A hydrodynamic spinning-disk device was used to measure the adhesive strength of populations of cells. Cells were seeded onto micro-patterned coverslips and allowed to adhere for 16 h. A coverslip with adherent cells was mounted onto the spinning-disk apparatus, and a vacuum pump was used to hold the sample in place. The sample was then submerged into the spin chamber filled with PBS+ with 2 mM dextrose. The chamber was equipped with baffles at the edges, which prevented the spinning motion of the sample from creating a vortex. The sample was then spun for 5 min at a controlled speed (ω), resulting in a gradient of shear force (τ) proportional to the distance from the coverslip center (r). Samples were then fixed, permeabilized, and stained for microscopy and quantification of adherent cells remaining on the coverslip. (B) The cells remaining attached to the coverslip were counted at various positions across the coverslip, and the values were plotted and sigmoid curves were fitted to the combined count totals. (C) Comparisons of adhesion strength values (τ50) among the chimeric constructs. IL-2R was significantly less adhesive than IL-2R–VE-cad$_{cyto}$ and IL-2R–VE-cad$_{EMD\rightarrow AAA}$ (Tukey test; $p < 0.050$) but not significantly different from IL-2R–VE-cad$_{\Delta CBD}$.

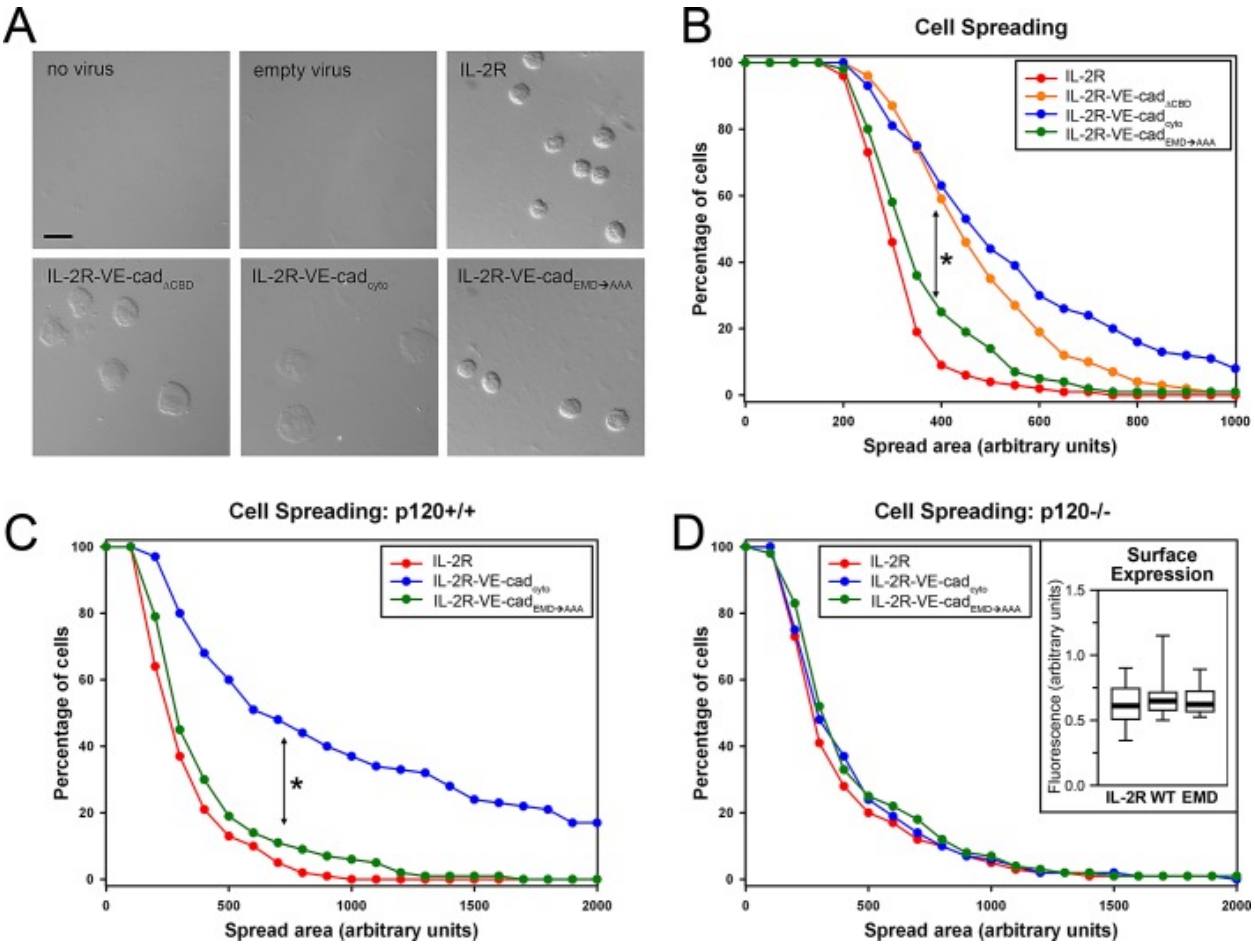

Figure 3. 5: The interaction between p120 and the cadherin juxtamembrane domain is require to promote cell spreading. (A, B) Cells expressing the chimeric constructs were seeded sparsely on unpatterned coverslips coated with antibodies against IL-2R. The cells were allowed to adhere for 30 min before fixation. (A) Representative images of adherent cells expressing the IL-2R constructs. Uninfected cells and those infected with an empty adenoviral vector were not able to attach to the IL-2R–antibody-coated coverslips. Bar, 20 μm. (B) The spread areas of 100 cells per condition, chosen at random, were measured and plotted by quantifying the number of cells per condition whose spread areas were larger than a given area in microns. On these inverse cumulative distribution plots, each data point indicates the percentage of cells (*y*-axis) that have spread areas greater than a given value (*x*-axis). Thus a population of cells exhibiting comparatively larger spread areas will generate data points that fall further to the right on the graph than the other populations being compared. The median values of the different groups were found to be statistically different (Kruskal–Wallis test; $p < 0.001$). IL-2R and IL-2R–VE-cad$_{EMD\rightarrow AAA}$ were not statistically different from each other, and IL-2R–VE-cadcyto and IL-2R–VE-cad$_{\Delta CBD}$ were not statistically different from each other. However, both members of the former pair were statistically different from both members of the latter pair (Tukey test; $p < 0.05$). (C, D) IL-2R, IL-2R–VE-cadcyto, and IL-2R–VE-cad$_{EMD\rightarrow AAA}$ were expressed in mouse endothelial cells that were either control or p120 null, and their spreading ability was measured as in the previous experiment. (C) In control cells, IL-2R–VE-cad$_{cyto}$ exhibited significantly

increased spreading over IL-2R and IL-2R–VE-cad$_{EMD→AAA}$ (Kruskal–Wallis test; $p < 0.001$; Tukey test; $p < 0.05$). (D) In p120-null cells, the increased spreading observed in IL-2R–VE-cad$_{cyto}$ was lost (Kruskal–Wallis test; $p = 0.230$). (D, inset) Surface expression levels of the various chimeras were similar, as measured by immunofluorescence. Thick line, median ($n = 28$–38 cells per group); box, interquartile range; whiskers, 90% range.

3.3.4. Rac1 activity regulates cell spreading but not adhesion strength

Binding of p120 to the juxtamembrane domain of cadherins is believed to locally activate the small GTPase Rac1 at the plasma membrane, which in turn induces membrane ruffling and allows for the extension of lamellipodia through the localized regulation of actin dynamics [215-217]. A prediction based on these previous findings and our results presented thus far is that p120-dependent cell spreading would require Rac1 activity but the acquisition of strong adhesion, which is mediated by β-catenin, would be Rac1 independent.

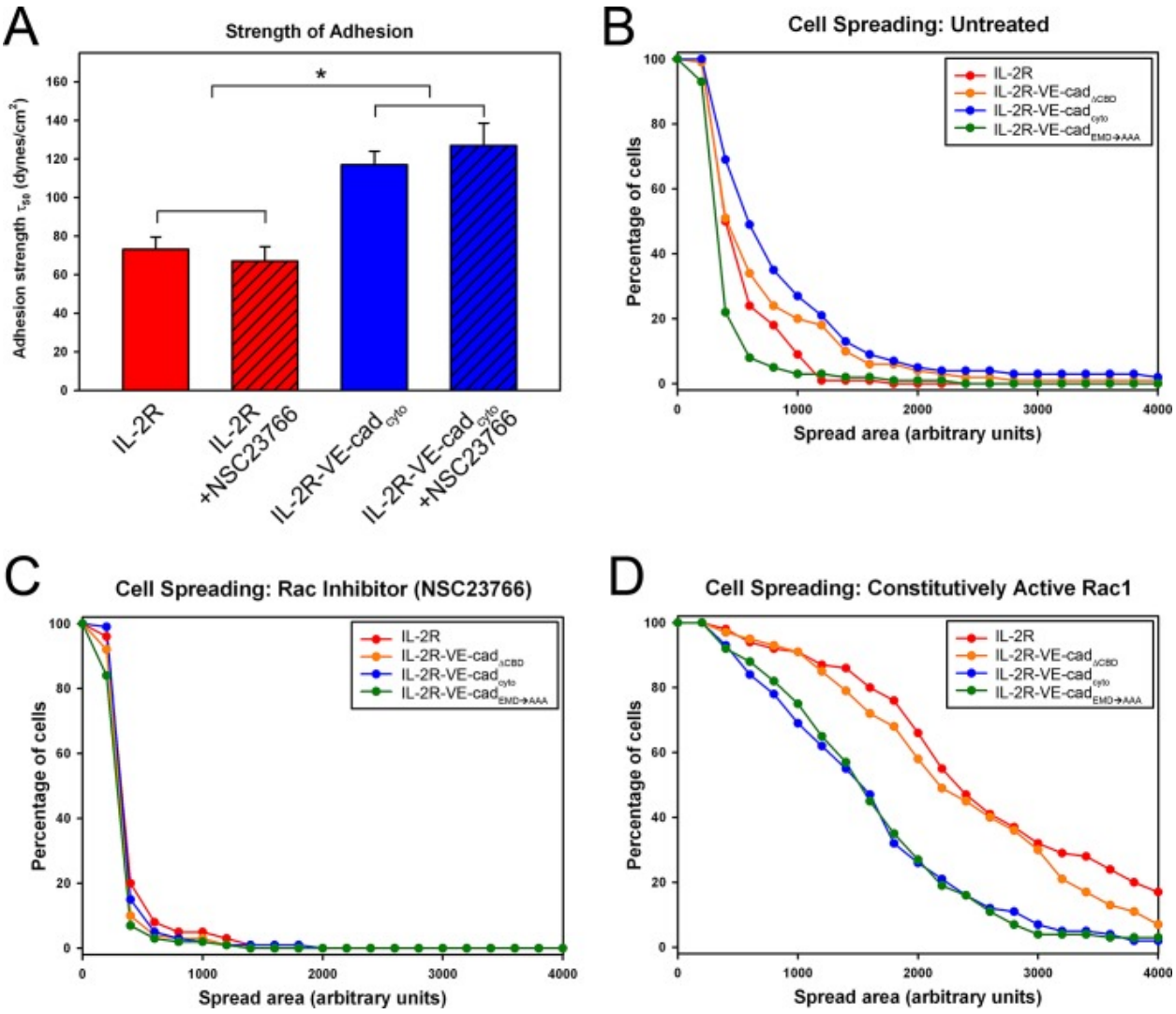

Figure 3. 6: Rac1 inhibition phenocopies the p120-dependent spreading defect. (A) The adhesion strength of primary microvascular endothelial cells expressing IL-2R and IL-2R–VE-cad$_{cyto}$ with and without Rac1 inhibitor NSC23766 treatment was assayed using the hydrodynamic spinning-disk device. The addition of NSC23766 did not significantly affect adhesion strength mediated by the VE-cadherin cytoplasmic tail (Tukey test; $p < 0.050$). (B–D) Cell spreading was measured in untreated endothelial cells (B), NSC23766-treated endothelial cells (C), and endothelial cells expressing a constitutively active Rac1 mutant (D). Rac1 inhibition prevented cell spreading and eliminated differences between chimeras, whereas constitutively active Rac1 increased spreading.

To test this model, we determined adhesive strength mediated by the IL-2R– VE-cad$_{cyto}$ chimera in the presence or absence of the Rac1 inhibitor NSC23766, using the hydrodynamic spinning-disk assay. Inhibition of Rac1 had no discernible effect on adhesion strength mediated

by the IL-2R– VE-cad$_{cyto}$ chimera (**Figure 3.6A**). In contrast, inhibition of Rac1 dramatically reduced spreading mediated by the IL-2R– VE-cad$_{cyto}$ chimeras (**Figure 3.6C**). Furthermore, when cells expressing IL-2R constructs were cotransduced with constitutively active Rac1, the spread areas of all four groups were dramatically increased, regardless of the ability of p120 to bind the cadherin tail (**Figure 3.6D**). Of interest, constitutively active Rac1 expression caused cells expressing the β-catenin–uncoupled constructs to spread more than those expressing β-catenin–coupled chimeras, suggesting that actin associations limit spreading in this context. These findings indicate that p120-mediated cell spreading occurs through a Rac1-dependent pathway but that the acquisition of adhesive strength mediated by the β-catenin–binding domain of the cadherin tail occurs through a Rac1-independent process.

3.4. Discussion

The results presented here indicate that the p120- and β-catenin–binding domains of the cadherin tail function differentially to regulate adhesion. Whereas p120 modulates the ability of cells to spread and increases the area of the adhesive contact, β-catenin binding to the cadherin tail modulates the strength of cadherin-mediated adhesion independent of contact area. Thus p120 and β-catenin both contribute to the overall adhesive potential of cadherin-based cell–cell contact but in mechanistically distinct manners.

Several studies have examined the contributions of cadherin tail domains and signaling pathways to cadherin-mediated adhesion strength [26, 197]. [26] demonstrated that the cadherin juxtamembrane domain and p120 are important in strengthening cell adhesion. Using a laminar flow assay, they allowed cells expressing C-cadherin constructs to adhere to a tube coated with the C-cadherin extracellular domain and subjected to fluid shear force. Cells expressing wild-

type C-cadherin showed an increase in adhesion strength. However, this adhesion-strengthening effect was lost in those cells in which the p120 binding site was deleted or mutated [200]. An important distinction between these previous studies and our present analysis is that we controlled the geometry of cells exposed to shear forces using micro-patterned surfaces, thus allowing us to discriminate between cell spreading and adhesion strength. Indeed, [26] reported reduced spreading in cells expressing C-cadherin constructs lacking the cadherin juxtamembrane domain. Similarly, we observed defects in cell spreading when binding of p120 to the cadherin tail was abrogated either by mutation of the juxtamembrane domain or the loss of endogenous p120 (**Figure 3.4, B and C**). As shown previously, contact area is a key factor in controlling adhesive strength [2]. Furthermore, it is likely that in a shear flow–based adhesion assay, cells that flatten and spread reduce their relative exposure to shear stress. Cells expressing cadherins that are uncoupled from p120 do not flatten and are thus subjected to higher shear forces. Consistent with this interpretation, when we controlled cell shape using micro-patterned surfaces to constrain cell spreading and thus control cell geometry, we found that p120 had no significant role in modulating the strengthening of cadherin-based adhesion. We conclude that p120 does not directly regulate cadherin strengthening but instead regulates the area of the cadherin contact zone.

As mentioned previously, p120 binding stabilizes cadherins at the cell surface. Because surface expression levels of the different chimeras were similar (**Figure 3.1D**), disrupting p120 binding did not affect adhesion strength by reducing the amount of cadherin available to form adhesive contacts. However, the localization of p120 near the plasma membrane also influences actin dynamics through the Rho-family GTPases. p120 has been well characterized as a potent regulator of Rho-family GTPases RhoA, Rac1, and Cdc42 [204]. In particular, the initiation of

adhesion by cadherins was found to stimulate Rac1 activity [218, 219], and this activation is dependent on binding of p120 to the cadherin tail [200]. Rac1 activity at the plasma membrane causes actin reorganization and membrane ruffling [215] and is known to be important in the formation of lamellipodia [216, 217], particularly at newly formed adhesive contacts [209]. The adhesive defects reported by [200] when p120 binding to the E-cadherin tail was blocked were rescued when constitutively active Rac1 was expressed. Consistent with these results, we found that inhibition of Rac1 impaired cell spreading even in cells in which p120 was able to bind to the cadherin tail (**Figure 3.6C**). Likewise, constitutively active Rac1 rescued the spreading defect in cells expressing p120-uncoupled cadherin (**Figure 3.6D**). However, in the hydrodynamic spinning-disk assay, in which spreading area is limited, inhibition of Rac1 did not decrease adhesion strength (**Figure 3.6A**). Collectively, these findings indicate that the cadherin–p120 complex regulates the size of the adhesive contact area in a Rac1-dependent manner, although we cannot rule out the possibility that, in some circumstances, Rac1 might influence cadherin-based adhesion independently of cell spreading.

In contrast to the role of p120 in modulating adhesive contact area, β-catenin binding is dispensable for cell spreading but required for cadherin-based adhesive strength (**Figure 3.5**). β-Catenin associates with α-catenin and is believed to participate in coupling the cadherin–catenin complex to the actin cytoskeleton, although the precise mechanism by which cadherins associate with actin is not fully understood [9, 151].

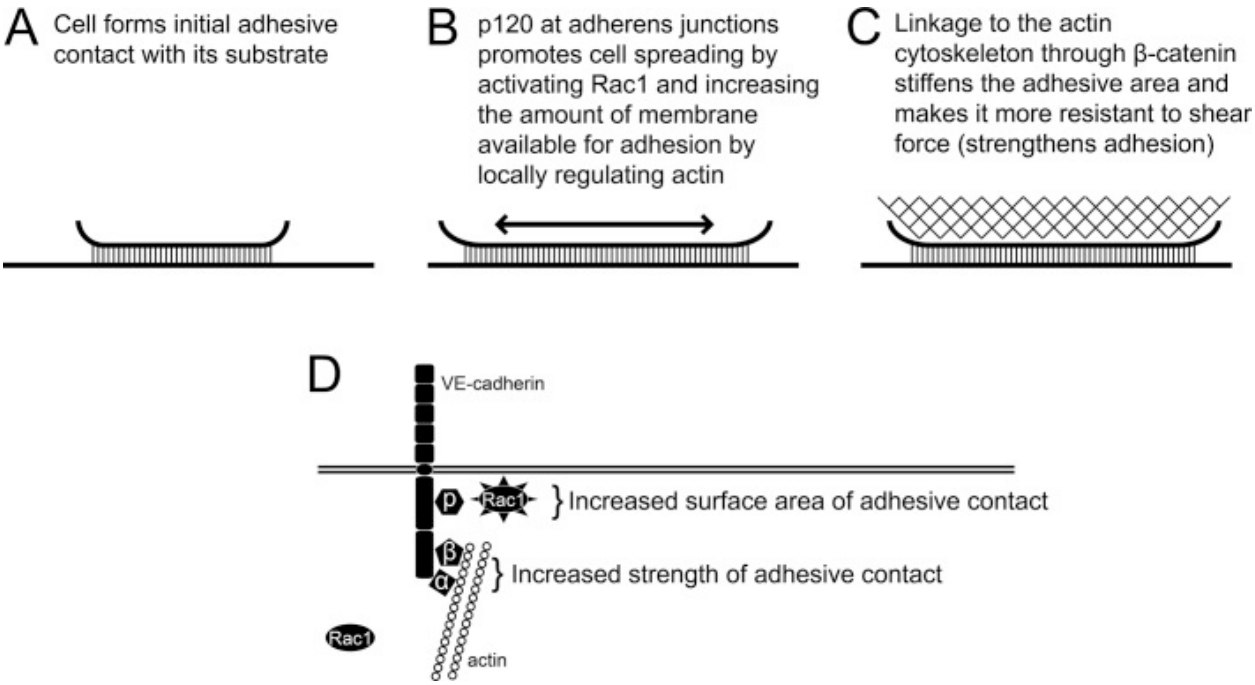

Figure 3. 7: Interaction between p120 and cadherins strengthens cell adhesion by promoting cell spreading. A proposed model demonstrating the distinct contributions of p120 and β-catenin to strengthening adhesion.

On the basis of our findings, we propose a model (**Figure 3.7**) in which p120 binding to the cadherin tail drives expansion of the cadherin contact in a Rac1-dependent manner. β-Catenin serves to strengthen the adhesive contact by recruiting actin-binding proteins that couple the cadherin–catenin complex to the actin cytoskeleton, thus stiffening the adhesive contact zone. Localized cytoskeletal stiffening enhances adhesion strength by increasing the shear force needed to peel off the leading edge of an adherent cell [2, 220]. Thus p120 and β-catenin both contribute to the overall adhesive potential of cadherins at the cell surface, but they do so through distinct and complementary mechanisms. These findings have important implications for understanding the mechanistic basis for loss-of-function mutations in the cadherin tail domain and catenins in various model systems. Further in vivo analysis of p120-uncoupled cadherins, in parallel with the use of Rac1-uncoupled p120 gene replacement studies, will be critical for

understanding how the cadherin–pl20 complex regulates cell–cell contact size and adhesion strength during development and other complex biological processes.

3.5. Materials and Methods

3.5.1. Cell culture

Primary cultures of dermal microvascular endothelial cells (MECs) from human neonatal foreskin were isolated and cultured in Microvascular Endothelial Cell Growth Media-2 (EGM-2MV; Lonza, Basel, Switzerland) supplemented with cAMP (Sigma-Aldrich, St. Louis, MO). Heart endothelial cells were isolated from mice harboring a floxed allele of p120 as previously described [199] and immortalized by transduction with SV40 DNA according to a previously published method [221]. Clonal cell populations were expanded, and a cell line was selected on the basis of morphology and the expression of endothelial markers VE-cadherin and PECAM-1. To induce p120 knockout, the cells were infected with an adenovirus expressing Cre (gift from L. Yang, Winship Cancer Institute, Emory University School of Medicine, Atlanta, GA) so that parallel wild-type and p120-null lines were generated. These cells were cultured in high-glucose DMEM (Mediatech, Herndon, VA) with 20% fetal bovine serum (Sigma-Aldrich), antibiotic/antimycotic solution (Mediatech), 100 μg/ml heparin (Sigma-Aldrich), 100 μg/ml endothelial cell growth supplement (ECGS; Biomedical Technologies, Stoughton, MA), 1 mM nonessential amino acids (Invitrogen), 1 mM sodium pyruvate (Invitrogen), 2 mM l-glutamine (Mediatech), and 25 mM 4-(2-hydroxyethyl)-1-piperazineethanesulfonic acid (HEPES; Mediatech). All endothelial cells were grown on 0.1% gelatin-coated plates to □80% confluency

for experiments. Rac1 inhibitor NCS23766 was obtained from Tocris Bioscience (Bristol, United Kingdom) and used at a concentration of 200 μM at 30 min before assays were performed.

3.5.2. Adenoviruses

The IL-2R– VE-cad$_{cyto}$, IL-2R– VE-cad$_{\Delta CBD}$, and IL-2R–VE-cad$_{JMD\text{-}AAA}$ (here designated as IL-2R– VE-cad$_{EMD\rightarrow AAA}$) constructs were generated as described previously [194]. These were subcloned into the pAd-Track vector that coexpresses green fluorescent protein (GFP), and they and the IL-2R and wild-type p120 constructs were added to cells 16–20 h before seeding for experiments, and infection rates of ≥80% were used as monitored by GFP expression. Constitutively active RhoA adenovirus [222] was provided by D. Kalman (Emory University, Atlanta, GA).

3.5.3. Micropatterned surfaces

Micropatterned coverslips with adhesive islands surrounded by a nonadhesive background were prepared as previously described [2]. Briefly, to generate a regular array of adhesive islands 20 μm in diameter and 75 μm from center to center, a polydimethylsiloxane (PDMS) stamp was prepared from a template [21] and used for microcontact printing of self-assembled monolayers of alkanethiols on gold-coated coverslips. Glass coverslips 25 mm in diameter were cleaned and then coated with titanium (100 Å) and then gold (2000 Å) using an electron beam evaporator (Thermionics, Hayward, CA). Before microcontact printing, the stamp was sonicated in 70% ethanol for 15 min and allowed to dry. Using a cotton swab, the patterned surface of the PDMS stamp was coated with 1.0 mM hexadecanethiol in ethanol, dried using a

nitrogen stream, and laid on the gold-coated coverslip for 30 s under 50–100 g of weight to ensure uniform contact. This process generates a surface with regularly spaced adhesive islands that adsorb ligands such as extracellular matrix proteins or cell membrane–associated adhesive receptors. To prevent adhesion to the areas between islands, patterned coverslips were incubated for 2 h in tri-(ethylene glycol)-terminated alkanethiol to create a nonadhesive and nonfouling background. The coverslips were then washed three times with absolute ethanol, once with sterile double-distilled H2O, and once with phosphate-buffered saline plus calcium and magnesium (PBS+/+) before coating with IgG2a directed against the IL-2 receptor (purified from American Type Culture Collection [Manassas, VA] hybridoma HB8784) at a concentration of 20 μg/ml for 1 h. After ligand adsorption, the patterned coverslips were blocked in heat-inactivated bovine serum albumin (1% wt/vol) for 30 min and incubated in PBS until seeding. Cells expressing IL-2R–containing constructs were removed from culture plates using trypsin/EDTA and seeded onto the micro-patterned coverslips at a density of 225 cells/mm^2. The coverslips were returned to the 37°C incubator for 16 h.

3.5.4. Hydrodynamic spinning-disk assay

Cell adhesion strength was measured as previously described [2, 186]. With the use of a spinning disk, a micro-patterned coverslip with adherent cells was mounted on the spinning platform, stabilized by vacuum pressure, submerged in a solution of 2 mM dextrose in PBS+/+, and spun for 5 min (**Figure 3.4A**). The hydrodynamic forces present on the surface of the coverslip are described by the equation

$$\tau = 0.8r\sqrt{\rho\mu\omega 3},$$

where τ is the applied shear stress (force/area), r is the radial position relative to the center of the

coverslip, ρ is the density of the solution, μ is the viscosity of the solution, and ω is the speed of rotation. After being spun, the samples were fixed in 3.7% formaldehyde, permeabilized in 0.1% Triton X-100, and stained with ethidium homodimer-1 (E1169; Life Technologies, Carlsbad, CA). The remaining adherent cells were counted on a fluorescence microscope with a motorized stage, ImagePro image analysis software (Media Cybernetics, Silver Spring, MD), and an algorithm that analyzed 61 fields of view per sample ranging from the center of the coverslip to the outer edges. The fraction of adherent cells (f) was calculated by comparing the number of cells present at each field with the number present at the center, where the shear forces are close to zero. Detachment profiles (f vs. τ) were fitted to a sigmoidal curve,

$$f = \frac{f_0}{1 + e^{b(\tau - \tau_{50})}},$$

where τ_{50} is the value of shear stress at which 50% of the cells remain adherent. This value was used as a measure of mean adhesion strength. For comparisons between groups, analysis of variance was used, and if significant differences were detected, the Tukey test was used to perform pairwise comparisons, in which $p < 0.05$ was considered significant.

3.5.5. Cell-spreading assay

Adhesive substrates were generated using the same method as for the micro-patterned samples described earlier, except that instead of stamping, the entire coverslip was coated with 1 mM hexadecanethiol in ethanol before incubation in the IL-2R IgG2a ligand. Cells expressing the constructs containing IL-2R were seeded sparsely on these surfaces and allowed to attach at 37°C for 30 min. The samples were then gently washed in PBS, fixed with paraformaldehyde, and mounted on microscope slides. Light microscopy was used to photograph fields at random, and for each condition, the spread areas of a total of 100 individual cells (not bordering any other

cell) were measured. To determine whether the difference in median values between groups was statistically significant, we performed the Kruskal–Wallis test (with $p < 0.001$ indicating significance), followed by pairwise comparisons between groups using the Tukey test (with $p < 0.05$ indicating significance).

3.5.6. Immunofluorescence staining

Cells were fixed using methanol (Acros Organics, Geel, Belgium) or 3.7% paraformaldehyde (Electron Microscopy Sciences, Hatfield, PA) in phosphate-buffered saline with calcium and magnesium (PBS+/+) containing 2% bovine serum albumin (Fisher Scientific), followed by permeabilization with 0.1% Triton (Roche Diagnostics Corporation, Indianapolis, IN) in PBS+/+, and then stained using antibodies against IL-2R (MAB223 clone 22722; R&D Systems, Minneapolis, MN) and 4′,6-diamidino-2-phenylindole (DAPI). Cells attached to micro-patterned coverslips were washed with PBS+/+ and washed once in cytoskeleton buffer (CSK) containing 10 mM 1,4-piperazinediethanesulfonic acid buffer, 50 mM NaCl, and 3 mM MgCl2. Protease inhibitors (1 mM phenylmethylsulfonyl fluoride, 1 μg/ml aprotinin, and 1 μg/ml pepstatin) were added immediately before use. The cells were then washed twice in CSK containing 0.5% (vol/vol) Triton X-100 and fixed in 4% paraformaldehyde. Cells were subsequently blocked in 5% goat serum with 0.01% NaN3 and stained using antibodies against IL-2R (R&D), p120 (610135; BD Biosciences, San Diego, CA), and β-catenin (A5441; Sigma-Aldrich).

3.5.7. Immunoprecipitation

Immunoprecipitations were carried out as described previously [196], without cross-linking. Briefly, HeLa cells were grown to confluency and infected with IL-2R–containing chimeric constructs. On the day of the experiment, cells were placed on ice, rinsed with PBS, and lysed with buffer A (150 mM NaCl, 10 mM HEPES, 1 mM ethylene glycol tetraacetic acid, and 0.1 mM MgCl2, pH 7.4) plus 0.5% TX-100, scraped from the dish, and incubated on ice for 30 min. Cell lysates were centrifuged at 16,100 × *g* for 10 min, and supernatants were diluted to 1 mg/ml in 0.5 ml of buffer A plus 0.5% Triton X-100. The supernatants were incubated overnight at 4°C with sheep anti-mouse Dynal magnetic beads (Invitrogen) conjugated to monoclonal antibodies against IL-2R (N-19; Santa Cruz Biotechnology, Santa Cruz, CA). The beads were then washed with buffer A plus 0.1% Triton X-100 and eluted with SDS–PAGE sample buffer at 75°C for 5 min before performing Western blots, which were probed with antibodies against p120 (SC-1101; Santa Cruz Biotechnology) and β-catenin (A5441; Sigma-Aldrich).

3.5.8. Western blotting

Cells were cultured in complete growth medium and infected with adenoviruses for 16–24 h before being harvested in Laemmli sample buffer (Bio-Rad Laboratories, Hercules, CA), and samples were boiled for 5 min before loading on 7.5% SDS–PAGE gel for protein separation. Proteins were transferred to nitrocellulose membrane for immunoblotting and probed with antibodies against IL-2R (N19; Santa Cruz Biotechnology), and p120 (SC-1101; Santa Cruz Biotechnology). Horseradish peroxidase–conjugated secondary antibodies (Bio-Rad Laboratories) were used at 1:3000 dilution, and blots were developed with Amersham ECL

Western Blotting Detection Reagents (RPN2106; GE Healthcare, Piscataway, NJ) or Amersham ECL Plus (RPN2132; GE Healthcare).

3.6. Acknowledgements

We thank Christopher Caughman, Sean Coyer, David Dumbauld, and Krystalyn Hudson for their technical assistance and advice. This work was supported by funding from the National Institutes of Health through Grants T32EY007092 (R.O.), F30HL110447 (B.A.N.), R01HL77870 (P.A.V.), R01GM065918 (A.J.G.), and R01AR050501 (A.P.K.), the National Science Foundation through Grant BES0827719 (A.J.G.), and a National Science Foundation Graduate Research Fellowship Award (C.E.).

CHAPTER IV: INFLUENCE OF CADHERIN LIGAND DENSITY AND CONTACT TIME ON THE ADHESION STRENGTH OF HUMAN ENDOTHELIAL CELLS INTERACTING WITH ENGINEERED SURFACES PRESENTING ISOLATED VASCULAR ENDOTHELIAL CADHERIN

4.1. Summary

Investigating the contributions of the physical parameters of the tissue micro-environment on cellular function, such as ligand density and contact time, on the strengthening response of endothelial cells is important for understanding cadherin function. Engineered surfaces presenting purified cadherin ligands were used to measure the adhesion strength of both human micro-vascular endothelial cells (HMEC-1s), wild-type Chinese hamster ovary cells as well as VE-cadherin-expressing Chinese hamster ovary cells (CHOs).

4.2. Introduction

The endothelium, a single-cell layer lining blood vessels, establishes the barrier function, a semi-permeable barrier between the circulatory system and adjacent tissue. This role is critical, and blood vessel formation depends on cell adhesion to the underlying extracellular matrix and to adjacent cells. Endothelial cells actively sense and respond to changes in their tissue microenvironment, which includes soluble factors, adhesive proteins and neighboring cells. Understanding endothelial cell adhesion has implications for health and disease, as dysregulation

of endothelial cell adhesion and migration affects wound healing, angiogenesis, tumor-initiated vasculogenesis, as well as successful integration and optimization of biomaterial and medical device therapeutic platforms. Recapitulating the tissue microenvironment requires knowledge of the precise encoding of the composition and organization of adhesive ligands at different length scales. This encoding is critical, as this determines the identity and duration of the adhesive complex formed. Indeed, the spatial presentation of adhesive cues as well as the organization of cells on surfaces can direct the physiological and tissue-specific functions of these cells. Our understanding of the mechanisms that regulate cell function is incomplete because of a lack of experimental platforms that allow for the direct manipulation of key parameters that specify the adhesive microenvironment.

In order to reduce the complexity of the adhesive microenvironment between two cells, we set out to engineer an adhesive surface that would precisely control cell shape, ligand density, and spatial positioning of cell-cell contacts. Another goal of the project was to maximize the maximize the signal of the cell-cell adhesive contact, so we set out to isolate of the cadherin-based adhesive cues and leave purified ligands on these surfaces. We engineered self-assembled monolayers of alkanethiols on gold surfaces in order to present purified cadherin ligands in a well-defined system in order to measure adhesive force generation and the factors that direct cadherin function.

4.3. Materials and Methods

4.3.1. Protein Expression, Purification, and Storage

Plasmid constructs of VE-cadherin, fused with fragment crystallizable region (Fc) of the human immunoglobulin protein IgG_1, were received as a gift from Peter A. Vincent of Albany Medical College. Recombinant proteins were expressed in the HEKPlus Expression System (ATCC, ACS-4800-K). For protein transfection, HEK293T/17 SF suspension cells were cultured in HEK Plus serum-free media (ATCC ACS-4002) supplemented with 8 mM L-glutamine (ATCC 30-2115) at 130rpm in an 8% CO_2 controlled-humidity environment (**Figure 4.1)**. Conditioned media from the transfected HEK293T/17 SF suspension cells from multiple collection cycles were pooled and purified using 6x-His-tag affinity chromatography columns (Thermo Scientific 90094) on an AKTA Pure 25 FPLC system (GE Healthcare, Piscataway, NJ). After Western blotting, protein samples were then desalted using PD-10 desalting columns (GE Healthcare 17-0851-01), concentrated using Millipore (UFC810024), Thermo Scientific (89921) and Pall Corporation (MAP030C7) concentrators, flash frozen in liquid nitrogen, and stored at -80˚ C in Ringer's Buffer (10mM HEPES, pH 7.4; 154 mM NaCl; 7.2 mM KCl) at high concentration and low volumes. All protein sample concentrations were determined using an ND1000 nanodrop spectrophotometer (ThermoScientific, Wilmington, DE).

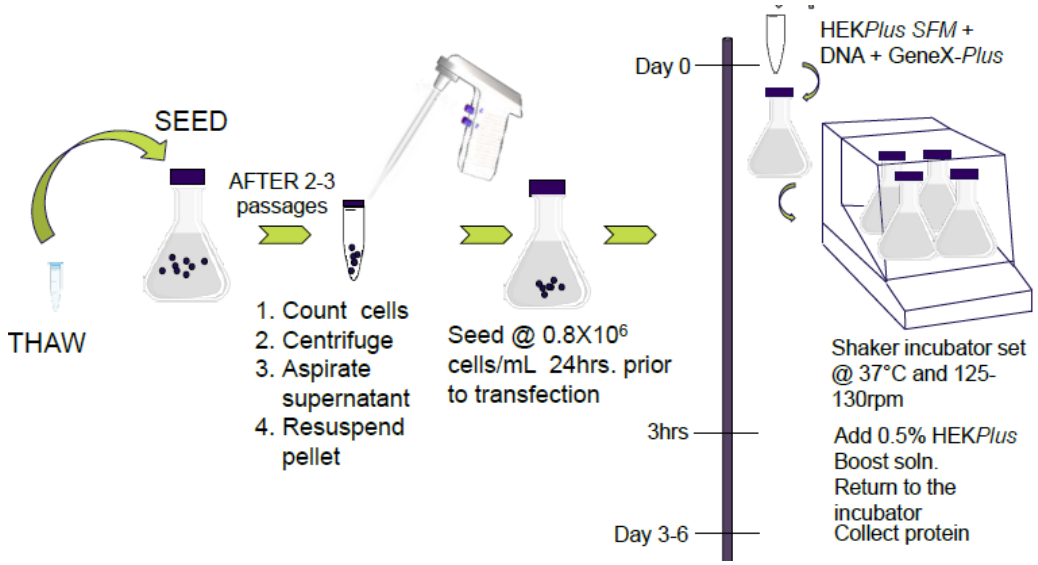

Figure 4. 1: Protein purification process flow using the HEKPlus system. Suspension cells are cultured in an 8% CO_2 environment. Protein is collected and purified with an AKTA Pure FPLC system.

4.3.2. Western Blotting

Purification efficiency was verified through Western blotting under reducing conditions. Briefly, samples were prepared according to Nu-Page Novex instructions for either 3-8% Tris-Acetate gels or 4-12% Bis-Tris gels (Life Technologies EA03752BOX, NP0321BOX) and were transferred onto PVDF, or a non-reactive artificial membrane, for immunoblotting (Millipore IPVH00010, ISEQ00010). Membranes were probed with either Cad-5 (BD Biosciences 610252, 0.5 µg/mL) or GG-7 (Sigma-Aldrich I6260, 1.0 µg/mL) mouse monoclonal antibodies with reactivity against the extracellular domain of VE-cadherin or the Fc portion of human IgG, respectively. Cell lysate of HUVECs (Lonza) lysed in RIPA Buffer (10mM Tris-Cl (pH – 8.0), 1mM EDTA, .5mM EGTA, 1 % Triton X-100, .1 % SDS, and 140mM Nacl) was used as a positive control for VE-cadherin. For cells used as VE-cadherin positive control during Western Blotting, human umbilical vein endothelial cells (HUVECs, Lonza) were grown on tissue culture plates coated in 0.1% gelatin (Millipore ES-006-B) using EBM-2 Media (Lonza cc-3156), supplemented with bullet kit components (Lonza cc-2517). Blots were imaged with the Odyssey Infrared Imaging System (LI-COR, Lincoln, NE) using the IRDye 680 Goat Anti-Mouse IgG secondary antibody (LI-COR 926-68020). Total protein was visualized using SYPRO Ruby Protein Gel Stain (Life Technologies S-12000) and the IRDye Blue Protein Stain (LI-COR 928-40002).

4.3.3. Bio-Adhesive Surfaces of Self-Assembled Monolayer Alkanethiols on Gold

Self-assembled monolayers of hexadecanethiol (HDT, Sigma-Aldrich 674516, 1.0 mM in absolute ethanol) were coated on coverslips with thin films of titanium (100 Å) and gold (200 Å) deposited using an electron beam evaporator (Thermionics, San Leandro, CA). Coordinated by the gold, these methyl-terminated alkanethiol SAMs promote protein adsorption and cell adhesion. HDT was incubated for 30 minutes, followed by washing thoroughly with ethanol, water, and PBS (Life Technologies 14040-133) to promote protein adsorption. Each sample was coated with appropriate ligand density of purified VE-cadherin:Fc protein for 1 hour before blocking with 1% (w/v) 62º C-heat-denatured bovine serum albumin (BSA, Sigma-Aldrich A9647) to prevent sites of non-specific protein adsorption. If surfaces were those on which proteins were captured, samples were first coated with protein A (Pierce 21181) before coating with VE-cadherin:Fc. Human microvascular endothelial cells (HMEC-1) received from the CDC were removed from tissue culture plates using 0.05% Trypsin-EDTA (Life Technologies 25300-054) and seeded onto coverslips at a density of 175 cells/mm^2. Coverslips were incubated in a 5% CO2 incubator for either 4 or 16 hours.

4.3.4. Surface Plasmon Resonance of Protein Adsorption on SAM Surfaces

The surface densities of purified VE-cadherin proteins adsorbed to engineered SAM surfaces were monitored real-time and measured using a Biacore T200 system (GE Healthcare, Piscataway, PA), housed in the Georgia Institute of Technology's Institute for Electronics and Nanotechnology (IEN). Biacore chips were either purchased (GE Healthcare BR100405) or prepared using a multi-step process, which involved hot etch decontamination by Piranha

cleaning, e-beam deposition, and SAM preparation. Briefly, 9mmx11mm glass coverslips, hereafter "chips," were cut and cleaned by complete immersion into a mixture solution of 70:30 (v/v) concentrated sulfuric acid (Sigma 320501) and hydrogen peroxide (Sigma 216763) and gently agitated for 30 minutes in Pyrex containers. *Extreme* precaution must be taken during Piranha cleaning, as the reaction is dangerously volatile. After several serial rinses in DI H_2O, coverslips were dried with filtered nitrogen and deposited with titanium (65 Å) and gold (500 Å). Chips were incubated overnight in HDT alkanethiols (1.0 mM in absolute ethanol), similar to the procedure used to prepare coverslips for adhesion assays. Chips were rinsed in absolute ethanol to remove excess HDT SAMs then rinsed with DI H_2O before SPR experiments.

All experiments were conducted in triplicate. For all experiments, a reference flow cell was used for baseline absorbance signal tracking to subtract bulk refractive index changes and injection noise from final analyses. Cadherin-specificity of interactions was verified by a calcium switch assay, in which the SPR experiment running buffer was changed to PBS without divalent cations to indicate that cadherin interactions persist only in the presence of calcium (data not shown).

The following SPR protocol was used for the "passively adsorbed" configuration experiment: 50 μL injection of VE-cadherin of appropriate ligand density over the surface at 50 μL/min (association phase, 60 seconds), followed by a dissociation phase of 60 seconds. The "captured" configuration experiment included: 150 μL injection of protein A (Pierce 21181) or protein G at a concentration of 100 μg/mL at 50 μL/min ('immobilization' phase, 180 seconds), 50 μL injection of VE-cadherin of appropriate ligand density over surface at 50 μL/min (association phase, 60 seconds), followed by a dissociation phase of 60 seconds. Homophilic interactions between cadherin proteins were also analyzed using SPR. The passively adsorbed

configuration included: 50 μL VE-cadherin of sub-saturating density (chosen from previous experiment) at 50 μL/min (association phase, 60 seconds), 50 μL BSA at 50 μL/min to block unoccupied adhesion sites, 50 μL VE-cadherin of appropriate density at 50 μL/min (association phase, 60 seconds), followed by a dissociation phase of 60 seconds. Similarly, we will measure the absorbance of cadherin ligands and their self-association in the "captured" configuration with the following protocol: 150 μL of protein A at a concentration of 100 μg/mL at 50 μL/min ('immobilization' phase, 180 seconds), 50 μL injection of VE-cadherin at sub-saturating density (chosen from previous experiment) at 50 μL/min (association phase, 60 seconds), 50 μL BSA at 50 μL/min to block unoccupied adhesion sites, 50 μL VE-cadherin of appropriate density at 50 μL/min (association phase, 60 seconds), followed by a dissociation phase of 60 seconds.

4.3.5. Cell Sourcing and Cell Culture

For adhesion strength analyses, human micro-vascular endothelial cells (HMEC-1) were received from the Center for Disease Control (CDC) through an institutional materials transfer agreement (MTA) and expanded according to instructions. We selected the immortalized HMEC-1s as our candidate cells because we wanted cells that were easy to isolate and grow in culture as compared to primary cells, retained endothelial cell characteristics, and were easy to manipulate with reagents [221]. Briefly, cells were grown on tissue culture plates coated with 0.1% gelatin (Millipore ES-006-B) using EBM-2 Media (Lonza cc-3136), supplemented with bullet kit components (Lonza cc-4147). All adherent cells were detached in the presence of warm 0.05% Trypsin-EDTA (Life Technologies 25300-054), and were either lysed with RIPA Buffer

for Western blot positive control or seeded onto coverslips at a density of 175 cells/mm^2 for quantitative adhesion studies on bio-adhesive surfaces.

4.3.6. Micro-patterned Surfaces of Self-assembled Monolayer Alkanethiols on Gold

Bio-adhesive arrays of circular islands that promote protein adsorption surrounded by regions of non-adhesive background were prepared as previously described [2, 223, 224]. Briefly, a mask template of 10 or 20μm circles with center-to-center spacing of 75μm was created using soft-lithography techniques. A 10:1 poly(dimethysiloxane) (PDMS):curing agent mixture was well-mixed, degassed for long period, poured over the template, cured overnight at 110C, and cut into "stamps" for micropatterning (Dow Corning Sylgard 184). Stamps were characterizated using a Nikon TE300 microscope with a Spot-RT camera and Spot Basic software to resolve feature morphology and verify consistency of feature sizes. Before micropatterning, stamps were sonicated for at least 15min in 70% ethanol (Decon Labs 2716) to remove surface impurities from the feature-side of the elastomer surface. Self-assembled monolayers of hexadecanethiol (HDT, Sigma-Aldrich 674516, 1.0mM in absolute ethanol) were inked on the stamp and brought into conformal contact with a coverslip previously deposited with titanium (100Å) and gold (200Å) using an electron beam evaporator (Thermionics, San Leandro, CA). Coordinated by the gold, these methyl-terminated alkanethiol SAMs promote protein adsorption and cell adhesion. Test patterns were visualized with a 0.1M potassium cyanide wet etch technique (Sigma-Aldrich 11813) and characterized by imaging passively adsorbed proteins to island arrays. To prevent cell adhesion to non-island regions, coverslips were incubated in a solution of (HO(CH2CH2O)3-(CH2)11SH), or tri(ethylene glycol)-

terminated SAMS (Prochimia, TH001-M11.n3-1, 1.0mM in absolute ethanol), for 2 hours to create a non-fouling and non-adhesive background. Washed thoroughly with ethanol, water, and PBS (Corning 21-030) to promote protein adsorption, each sample was coated with appropriate ligand density of purified VE-cadherin: Fc protein for 1 hour before blocking with 1% (w/v) 37C-heat-denatured bovine serum albumin (BSA, Sigma-Aldrich A9647) to prevent sites of non-specific protein adsorption. If surfaces were those on which proteins were captured, samples were first coated with protein G (Sigma-Aldrich 19459) before coating with VE-cadherin:Fc. Human microvascular endothelial cells (HMEC-1) received from the CDC were removed from tissue culture plates using .05% Trypsin-EDTA (Life Technologies 25300-054) and seeded onto micropatterned ccoverslips at a density of 225 cells/mm^2. Coverslips were incubated in a 5% CO2 incubator for either 4 or 14 hours.

4.3.7. Adhesive Force Measurements using Hydrodynamic Spinning Disk Assay

We used a hydrodynamic flow assay based on a disk spinning in a large (‘infinite’) fluid, in which we can applied a range of shear forces to the cells on the surface of this coverslip to measure the adhesion strength of a population of cells in a robust and sensitive manner. During the experiment, coverslips of engineered bio-adhesive surfaces with adherent cells were mounted on the device, immersed in fluid spin buffer, and spun at constant speed for 5 minutes with constant ramp up and ramp down times. The spinning disk applies a linear range of shear forces that increase with radial distance from the center of the coverslip, generating a sigmoidal detachment profile, shearing the cells from their original position on the coverslip. The hydrodynamic forces present on the surface of the coverslip are well-defined and are prescribed by:

$$\tau = 0.8r\sqrt{\rho\mu\omega 3},$$

where τ is the applied shear stress (force/area), r is the radial position relative to the center of the coverslip, ρ is the density of the solution, μ is the viscosity of the solution, and ω is the speed of rotation. Adherent cells were seeded for 4 or 12 hours on bio-adhesive surfaces coated with different ligand densities to control protein presentation. Coverslips were placed on the spinning platform and submerged in a 2 mM dextrose (Millipore DX0145-1) in PBS (+/+) solution and spun for 5 minutes. After spinning, adherent cells remaining on the coverslip were fixed with cold 3.7% formaldehyde (Sigma F8775), permeabilized with 0.1% Triton X-100 detergent (Millipore TX1568-1), and stained with ethidium homodimer-1 dye (Life Technologies E1169 or Setareh Biotech 7000, 2 mM in 1:4 (v/v) DMSO/H_20) for 20 minutes. Samples were mounted on microscope slides with a #1.5 coverslip and counted using a Nikon TE300 microscope with a LudI motorized stage, a Spot-RT camera, and Image-Pro analysis system and software. The counting macro counts the number of dye-positive cells above a certain fluorescent intensity level at 61 predefined fields of view. The adherent fraction is calculated by normalizing the number of adherent cells in each field of view by the number of adherent cells in the center of the disk, where shear stress applied is negligible, according to the following equation:

$$f = \frac{f_0}{1+ e^{b\,(\tau - \tau_{50})}},$$

where f_0 is the normalized asymptote, b is the slope at the inflection point of the sigmoid, τ is the shear stress applied, and τ_{50} is the shear stress at 50% detachment. We then generated the representative experimental adhesion profile by plotting the adherent fraction as a function of applied shear stress and fitting the previously described sigmoid function to the data. The mean adhesion strength reported was defined as the shear stress at which 50% of cells remain adherent on the coverslip. ll analyses were conducted with MATLAB software.

4.3.8. Statistical Analyses

For continuous data, we used one-way ANOVA with Tukey's tests for multiple comparisons, where necessary (see [225]). GraphPad Prism software (GraphPad, La Jolla, CA) was used to implement analyses.

4.4. Results

4.4.1. Engineered Surfaces for Quantitative Cell Adhesion Analyses

Contemporary analyses of processes involved in cell adhesion complex assembly have many limitations. Current methods analyze protein distributions in fixed or live cells, isolate protein complexes with antibodies through cell extraction protocols, and dissect protein-protein binding with bacterial-expressed proteins *in vitro*. Few, however, allow direct analysis of native protein complexes on cell membranes *in situ.* In order to isolate and amplify the "signal" from cell-cell adhesion complexes, which is small compared to that from cell-ECM complexes, purified cadherin ligands in their correct orientation are required for *in vitro* studies. Additionally, our goal is to generate a model system for an adhesive interface in which one interface is controlled in terms of adhesive ligands and size. To overcome these difficulties, we designed an experimental model system to engineer cell adhesion on a substratum that promotes adhesion specifically through cadherin proteins and not through the ECM. This experimental system precisely controls cellular interactions at the interface of cell-cell adhesive contact, while maintaining high resolution and high-throughput.

We used a mammalian system for the production of cadherin protein domains to ensure that proper post-translation modifications of the protein were made. Constructs of the extracellular domain of VE-cadherin, fused at the C-terminus with the surface protein recognition domain (Fc region) of human immunoglobulin protein and a 6xHis tag (**Figure 4.1)**. The tagged C-terminus domain extracellular domain of VE-cad with its N-terminus domain intact allows for the proper orientation of the protein on a substratum, as proteins will align N-terminus to N-terminus. Constructs were expressed in human embryonic kidney HEK293T/17 SF suspension cell line. Conditioned media was collected, pooled, and purified using a nickel-chelated 6xHis affinity chromatography column. Purification was verified through Western blotting (**Figure 4.2)** under reducing conditions with both cad-5 and GG-7 mouse monoclonal antibodies with reactivity against the extracellular domain of VE-cadherin and the Fc region of human IgG, respectively, imaged with the LI-COR system using the IRDye 680 Goat Anti-Mouse IgG secondary antibody. Protein fractions with highest purity (**Figure 4.2**) were spin-concentrated with centrifugal filters and used for adhesion assays.

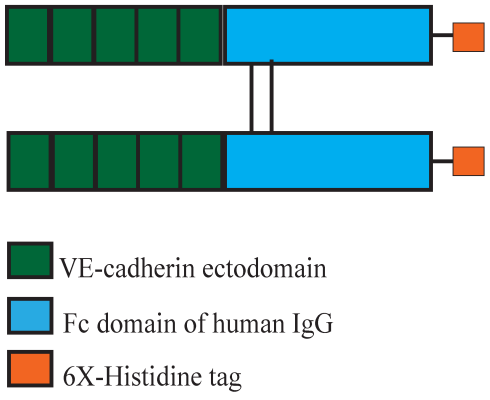

Figure 4. 2: Schematic for recombinant VE-cadherin, comprised of the extracullar region fused ot the Fc domain of human IgG, with 6xHis tag.

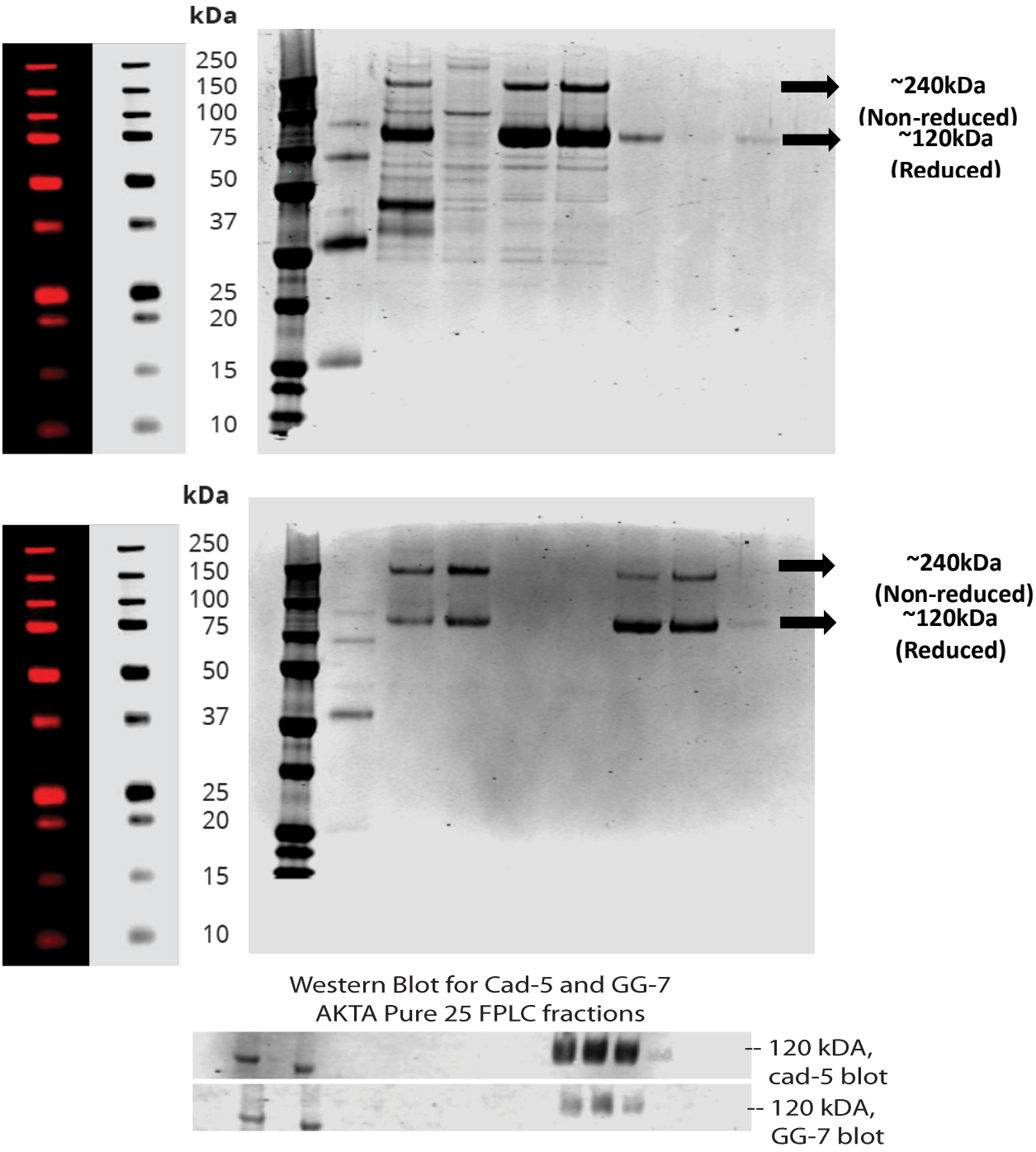

Figure 4. 3: Total protein stains and Western blots for recombinant VE-cadherin under reducing conditions, purified using affinity chromatography. Conditioned Media was collected from HEK-SF suspension cell cultures and was purified with a HisTrap Excel Column. Next, fractions were further purified using a Pierce Nab Protein A Column (SDS-Page and total protein stain results shown on top panel), and then eluates from the Pierce column were centrifuged with an Amicon 100KMWCO filter (SDS-Page and total protein stain results shown in the middle panel). On a different 3-8% Bis-Tris NOVEX gel, Western blots probing for cadherin ectodomains and Fc region of IgG are shown in the last panel.

4.4.2. Tissue Culture Cell Detachment Methods do not Affect Cadherin Receptor Availability/Functionality

We quantified surface level expression of VE-cadherin receptors on human microvascular endothelial cells (HMEC-1s) at 30, 60, and 90 minutes post-cell harvest as a function of four cell detachment methods by flow cytometry to identify methods that would not alter the surface expression levels of VE-cadherin. The four detachment methods tested were 0.05% trypsin-EDTA quenched by media supplemented with fetal bovine serum, 0.05% trypsin-EGTA quenched by media supplemented with fetal bovine serum, Hank's Balanced Saline Solution (w/ calcium and magnesium ions) with either 0.01% trypsin or 0.05% trypsin, quenched by media supplemented with fetal bovine serum and 0.01% trypsin inhibitor. Flow cytometry was quantified using the BV9 antibody against the extracellular domain of VE-cadherin **(Figure 4.3)**. Unstained and isotype control samples were included to verify auto-fluorescence and non-specific binding of the antibody. Quasi-quantitative values for surface level expression were calculated by allowing a 5% overlay on the isotype control plot and reporting the percentage area under each sample curve. Samples were run in duplicate. For all detachment methods, surface level expression of cadherin ligands remained elevated at 30, 60, and 90 minutes post-harvest, indicating that dissociation steps did not significantly alter expression levels. Although higher surface level expression was seen with samples digested without EDTA and EGTA, detachment times for these samples were very long (~15 minutes) and detachment was incomplete for the tissue culure dishes, suggesting that these detachment methods were selecting sub-populations of cells with weaker adhesive signatures. We decided to use 0.05% trypsin-EDTA as the preferred detachment method for all future studies, as this yielded the quickest and most complete cell detachment.

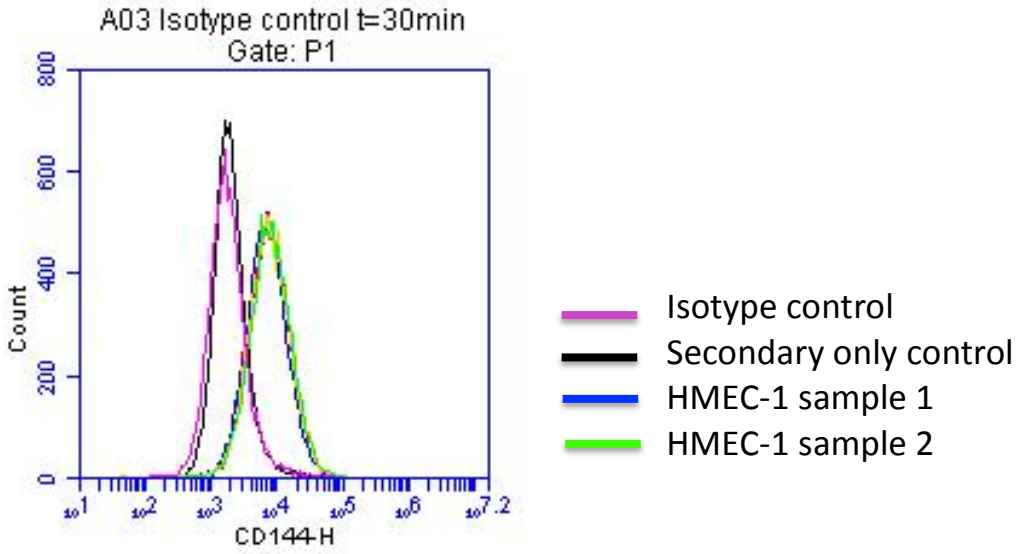

Figure 4. 4: Flow cytometry histograms for CD144 (VE-cadherin) surface expression of human microvascular endothelial cells as a function of 0.05% Trypsin-EDTA detachment method.

4.4.3. Real-time Analysis of Adsorbed Protein Densities Quantified using Surface Plasmon Resonance

We measured the bio-molecular interactions of cadherins with engineered substrates with the Biacore T200 surface plasmon resonance instrument. As the binding of an analyte to a ligand on a sensor chip can be thought of as a two-step reaction event, in which the analyte is transferred out of the bulk solution to the surface of the sensor chip and then binds to the ligand, it is important to consider mass transport limitations in the first step. In the event of partial mass transfer, analyte shortage will occur and will affect binding parameters and confound the interpretation of interaction analyses. This mass transfer conditions depend on the dimensions of the sensor chip flow cell, the flow rate, and the diffusion coefficient of the analyte. The intrinsic reaction rate is flow-independent; thus, varying the flow rate and observing resultant changes in binding parameters is one method to identify a mass transfer limitation.

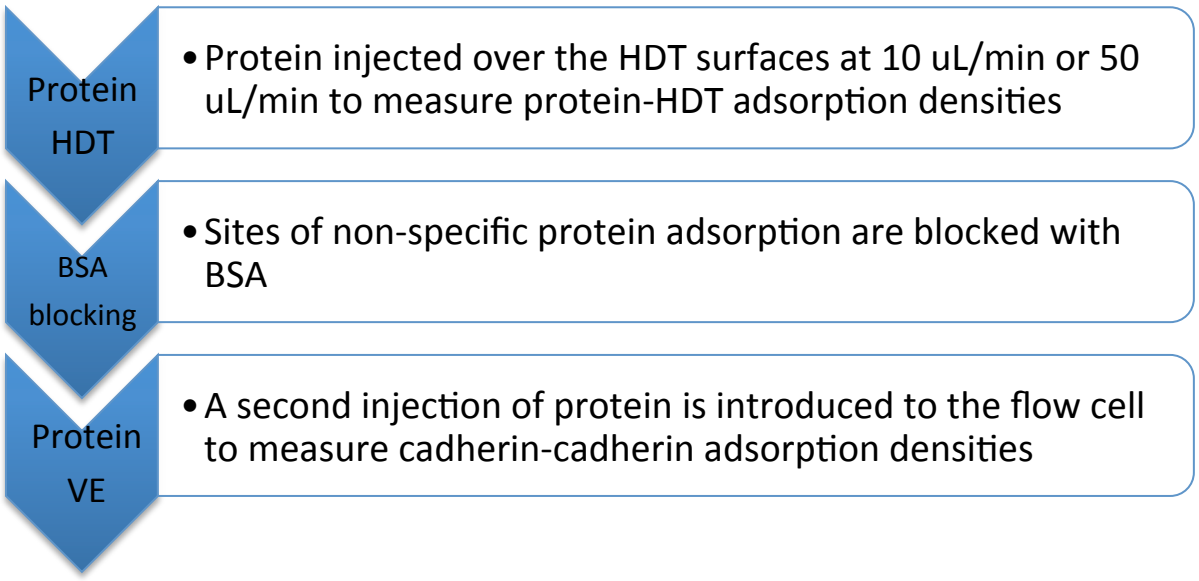

Figure 4. 5: Schematic for mass transport limitations SPR experiment with binding interactions measured at two different flow rates. After incubating with 1.0 mM HDT in ethanol solution, cadherin ligands at prescribed densities are injected into the flow cell and allowed to adsorb on the engineered HDT surface. After initial adsorption of our cadherin ligands to our engineered SAM surface, sites of non-specific protein adsorption to SAM surfaces are blocked with BSA. A final injection round of cadherin ligands at prescribed densities measures a second interaction of adsorption of cadherin protein ligands.

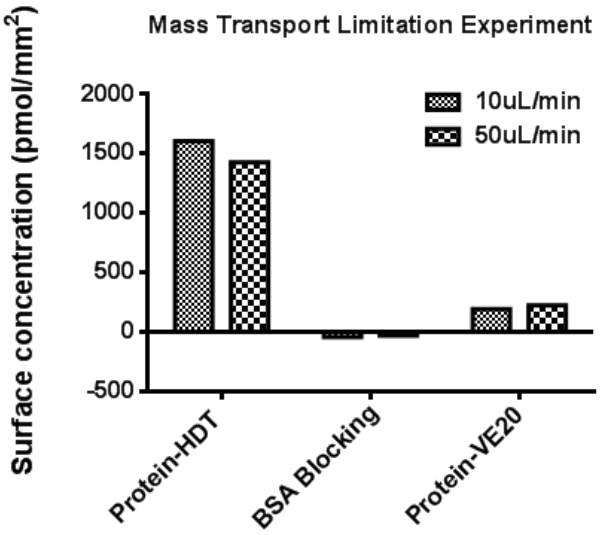

Figure 4. 6: Mass transport limitation SPR experiment with binding interactions measured at two different flow rates. Protein-HDT corresponds to initial adsorption of our cadherin ligands to our engineered SAM surface, BSA blocking corresponds to the subsequent blocking of non-

specific protein adsorption to our surfaces, and Protein-VE20 corresponds to a second interaction of adsorption of cadherin protein ligands.

We monitored the immobilization levels of the analytes of the various steps of our process flow at two different flow rates and observed the changes in immobilization. We did not observe marked differences in immobilization levels **(Figure 4.5)**. Mass transfer models can be verified with Biacore's BiaEvaluation software. We proceeded to measure the bio-molecular interactions at a flow rate of 10 uL/min. In the random attachment configuration, the interaction between the analyte (cadherin ligands) and the sensor surface produces a binding signal with associated surface density values.

For the captured configuration, either protein A or protein G was injected over the sensor surface and allowed to reach saturating surface density values. Cadherin ligands were then injected over the surface under the same conditions as with the passively adsorbed samples. Blank injections, as well as injections in the absence of cations in the flow buffer, were included as control. We then fit hyperbolic curves to the data and interpolated to arrive at concentrations of cadherin ligands, which correspond to equip-molar densities of protein on the sensor chip for the passively adsorbed and captured configurations. These concentrations were then used for all subsequent adhesion assays.

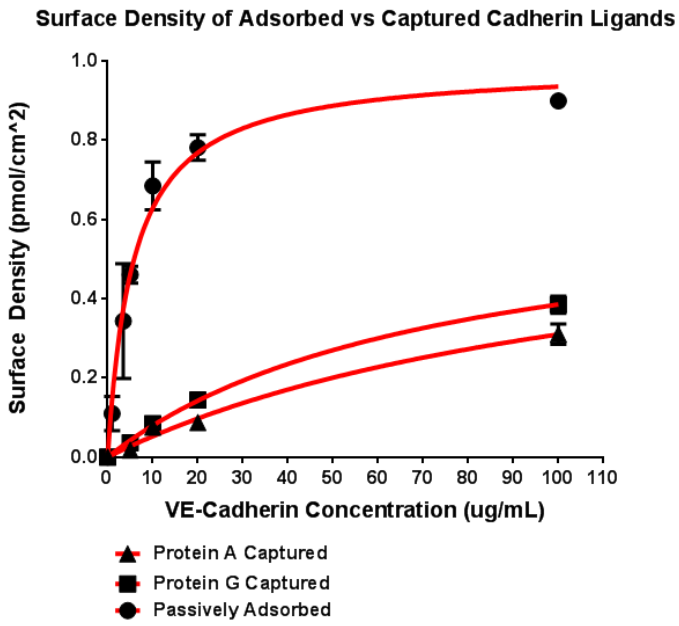

Figure 4. 7: Surface density measurements of passively adsorbed and captured cadherin ligands versus ligand concentration. In the passively adsorbed configuration, the interaction between the analyte (cadherin ligands) and the sensor surface produces a binding signal with associated surface density values. Samples for each test concentration were injected in duplicate. In the captured configuration, protein A or protein G was injected over the sensor surface and allowed to reach saturating surface density values. Cadherin ligands were then injected over the surface at similar concentrations as with the passively adsorbed samples. Blank injections, as well as injections in the absence of cations in the flow buffer, were included as control.

4.4.4. Endothelial Cells Adhere to and Remain Viable on Bio-Adhesive Surfaces

Bio-adhesive surfaces were created as previously described through self-assembled monolayers of alkanethiols on gold-coated glass coverslips [2, 224]. Seminal papers in the field have shown that cell shape is a control switch in cell fate between life and death [226-230]. When grown on small micropatterns, endothelial cells have been shown to undergo apotosis, or programmed cell death. In order to verify that our island array feature size does not elicit an apoptotic response, we used a dual calcein (live) and ethidium homodimer-1 (dead) dye system to detect the viability (through intracellular esterase activity) and cytotoxicity (through plasma

membrane integrity) of cells within a given population (**Figure 4.7**). Human microvascular endothelial (HMEC-1) cells seeded on 20 μm-diameter-sized bio-adhesive arrays remain viable for more than 3 days under sterile culture conditions without evidence of apoptosis, as determined by the live/dead assay. Viability was also tested after adhesion assays (spinning disk assay) in order to verify that the adhesion strength values reported were of interactions within viable cell populations. More importantly, the adhesive structures are localized to and remain constrained on the micropatterned islands.

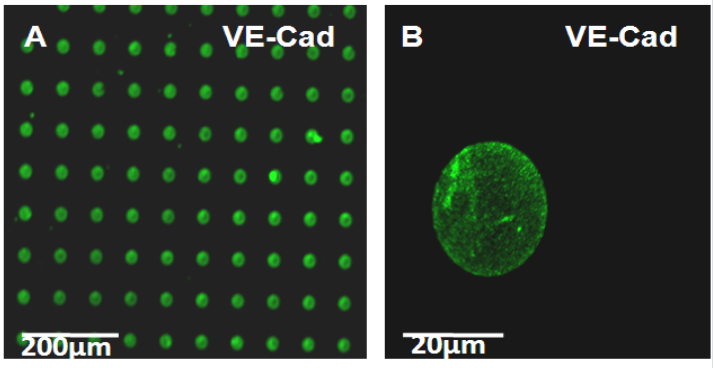

Figure 4. 8: A) Positive stain for vascular endothelial cadherin protein chimera passively adsorbed only onto 20 μm circular patterned bio-adhesive island arrays with a center-to-center distance of 75 μm. B) Magnification shows precise control of adhesive area to features that can support populations of single cells per island for adhesion assays.

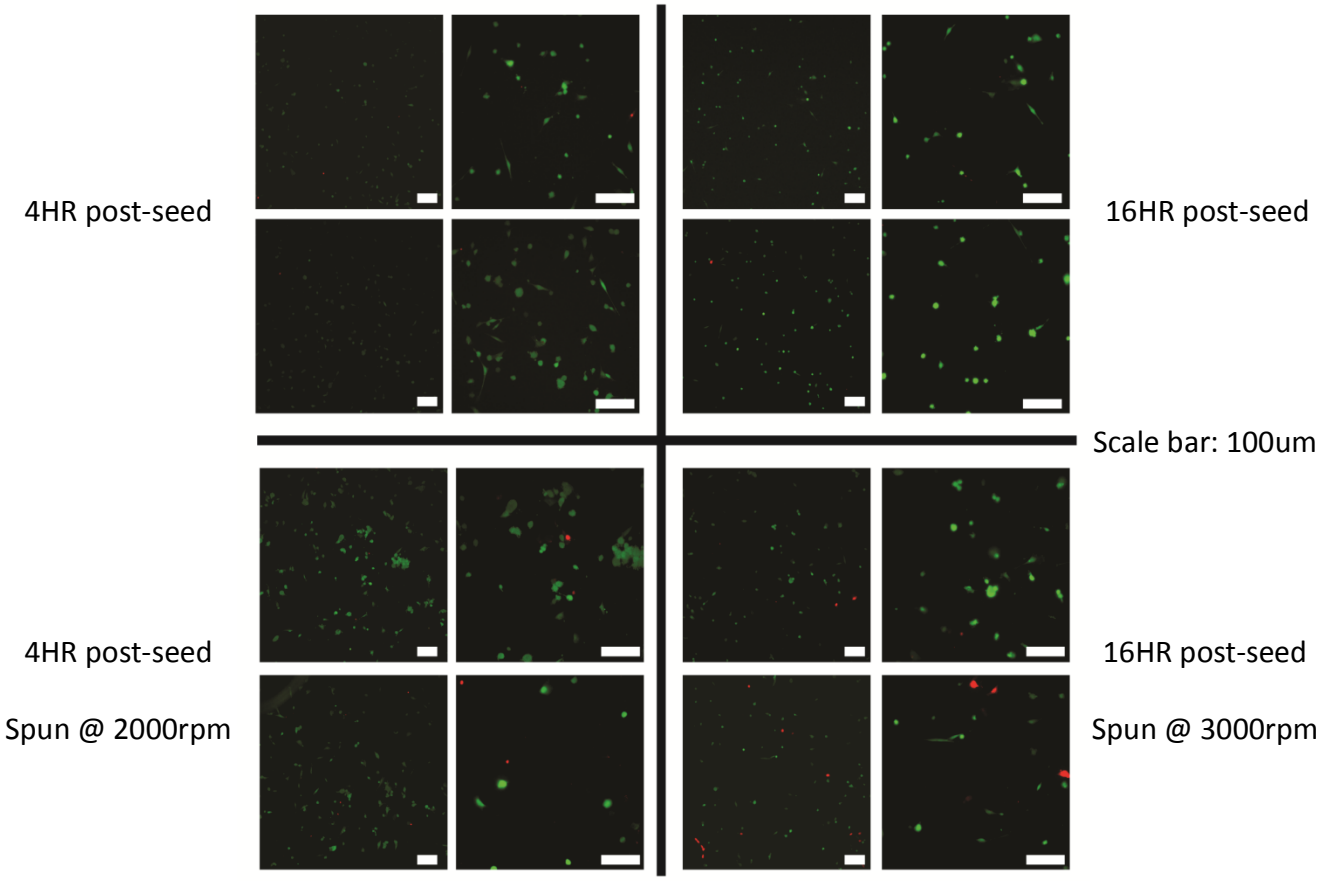

Figure 4. 9: Live/Dead assay of unpatterned human micro-vascular endothelial cells (HMEC-1) on engineered surfaces coated with 20 µg/mL VE-cadherin concentration A) before and B) after adhesion assay experiments.

4.3.5. Cell Adhesion to Cadherin Ligands on Bio-Adhesive Surfaces is Cadherin-Specific

The goal of our experiments was to engineer surfaces that could support the adhesive force generation for cadherin-based cell-cell interactions. We quantified the adhesion strength of human micro-vascular endothelial cells (HMEC-1) adhered to protein ligands.

Cell adhesion strength values were measured using the spinning disk device as previously described [174]. For each adhesion profile, we fit the detachment profile of the fraction of adherent cells as a function of applied shear stress to a sigmoid function and report the adhesion

strength as the shear stress for which 50% of the cell population on the coverslip remain adherent **(Figure 4.10).**

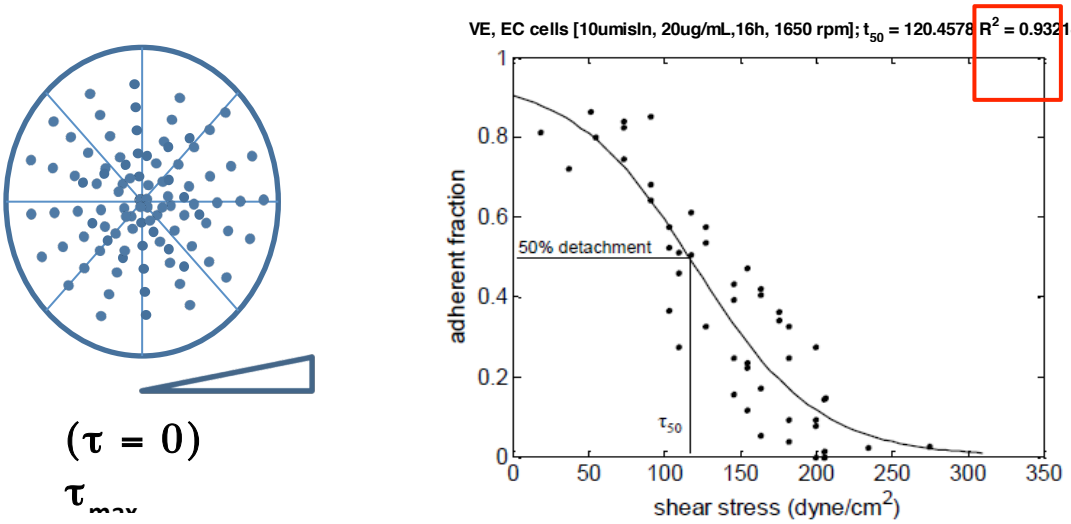

Figure 4. 10: Schematic showing representative fields of view analyzed by the counting macro. The resultant plot is fit to a sigmoid, yielding adhesion strength values.

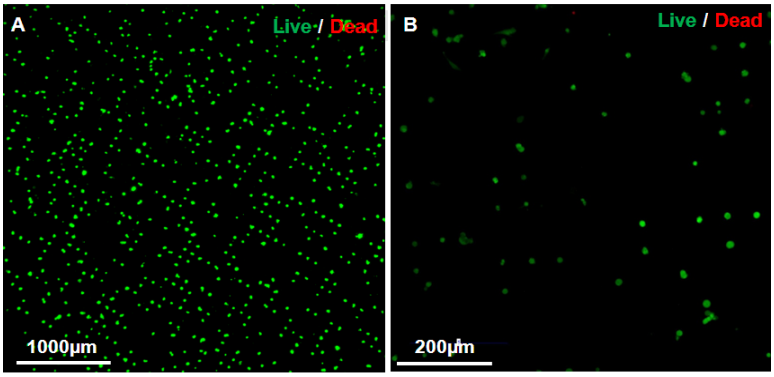

Figure 4. 11: Live/Dead assay of human micro-vascular endothelial cells (HMEC-1) on 10 μm bio-adhesive island arrays coated with 40 μg/mL VE-cadherin concentration A) before and B) after adhesion assay experiments. Single cells remain constrained on each adhesive island and remain viable. The geometrical constraints imposed on these single cells do not induce apoptosis (programmed cell death).

To ascertain that cell adhesion strength values being measured were mediated solely through cadherin interactions between our defined ligands on the surface and HMEC-1 cells, we

used blocking antibodies against cadherin, as well as added 4 mM EGTA to culture media to eliminate adhesive strength to the bio-adhesive surfaces (data not shown). For the blocking assay experiment, HMEC-1 cells were washed with PBS and harvested with trypsin. Cells were rinsed and centrifuged down with fresh media to ensure greater efficacy of the blocking antibody. Cells were then incubated with high concentration (25 μg/mL) of anti-cadherin-5 antibody for 30 minutes prior to cell seeding on prepared substrates with periodic and gentle agitation to uniformly mix the cell solution. Antibody-incubated HMEC-1s were then seeded at uniform cell densities on substrates passively adsorbed with high concentration of VE-cadherin:Fc ligand (20 μg/mL) for 4 hours. At the same time, untreated HMEC-1 cells were seeded onto substrates with high concentration (20 μg/mL) of cadherin ligand. Subsequent adhesion strength analysis showed that mean adhesion strength values for both groups were statistically significant from each other ($p < 0.05$, t-test).

Adhesion data for antibody-incubated cells seeded on 20 μg/mL-coated islands showed non-zero values of adhesion strength (**Figure 4.12**), indicating that these cells retain some adhesion activity and that there might be recycling of cadherin receptors, as adhesion strength values recover after 12 hours of antibody-incubation. Collectively, these data indicate that the development and strengthening of adhesive forces in this engineered system is mediated by cadherin-specific binding interactions to pre-adsorbed VE-cadherin:Fc on pattern arrays and excludes significant contributions from other adhesive receptors or extracellular ligands. 4 mM EGTA blocking experiments of calcium-dependent cadherin interactions yielded negligible adhesion strength values for all groups (data not shown).

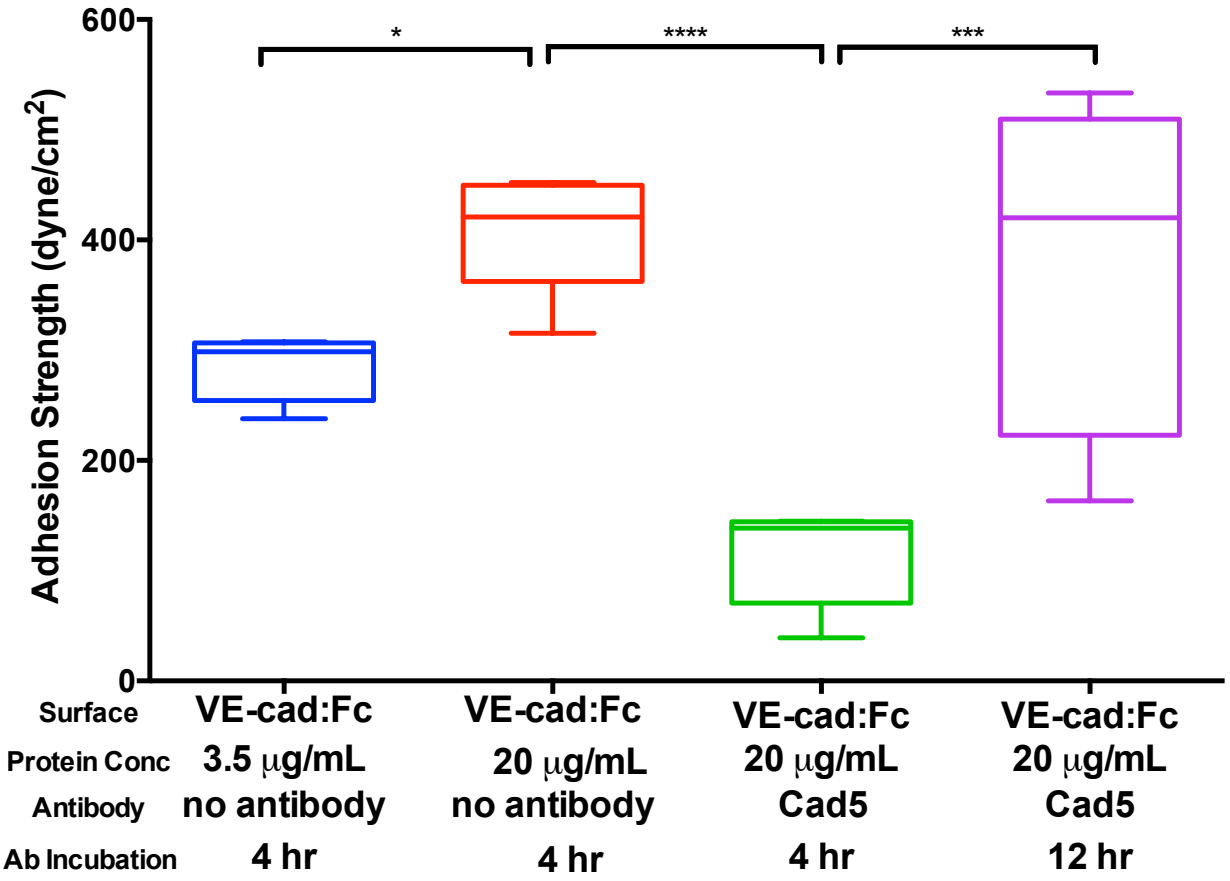

Figure 4. 12: Blocking assay experiment against cadherin-mediated cell adhesion with functional blocking antibody cadherin-5, or Cad-5, clone 75, incubated at 25ug/mL at short times (4 hours) and long times (12 hours) for human microvascular endothelial cells (HMEC-1) seeded on surfaces coated with 20 ug/mL of VE-cadherin:Fc protein. Adhesion strength values for untreated samples at 3.5 ug/mL and 20 ug/mL concentrations of VE-cadherin:Fc protein are included. Adhesion strength values were significantly higher for the untreated 20 ug/mL samples than for the 3.5 ug/mL samples ($p < 0.05$, t-test). Adhesion strength values for samples incubated with a functional blocking antibody were statistically lower than for untreated samples at the same time-point and protein concentration ($p < 0.05$, t-test). Over time, the decrease observed in adhesion strength values because of functional blocking is lost, as the adhesion strength values for HMEC-1s seeded on surfaces coated with 20 ug/mL of protein at 12 hours is significantly higher than cells seeded on the same protein concentration at earlier time points (4 hours).

4.4.6. Mean Adhesion Strength Values Increase with Increasing Cadherin Ligand Concentration until Reaching Saturation Values

We then tested the dependence of adhesion strength on cadherin ligand density at 12 hours. Briefly, cells were seeded onto 10 μm patterned arrays of passively adsorbed cadherin ligands of varying concentration under serum conditions. The surface densities we measured were between 0 – 1.0 pmol/cm^2 VE-cad:Fc. Cells remained unperturbed under sterile cell culture conditions for 16 hours and were spun at different speeds to yield adequate adhesion profiles. Compiled mean adhesion data were very strongly correlated ($R^2 = 0.91$) with our hyperbolic fit function. These results indicate that steady-state adhesion strength was strongly dependent on cadherin ligand density, which is consistent with a simple model in which receptor-ligand bond numbers (and therefore adhesion strength) increase with increasing ligand density until reaching saturation values. The use of micro-patterned substrates maintained similar cell morphologies between experimental groups, restricted the size (total surface area) and position of cadherin-specific adhesive contacts, and allowed for the analysis of adhesion strength independent of the effects of cell spreading. Overall, these preliminary studies show that our system allows us to measure adhesive forces independently from cell shape or ligand density changes. Our experimental model system addresses the technical difficulties inherent to the direct analysis of native protein complexes on cell membranes. We express and purify recombinant cadherin islands with high purity and efficiency. Through the combined technologies of chemical lithography and self-assembled monolayer alkanethiol chemistries, we are able to precisely control cellular interactions at the interface of adhesion with high resolution and high throughput. We use a hydrodynamic assay to quantify adhesive strength as a function of ligand concentration on the surface of the substratum and show that this interaction is cadherin-specific. Together,

these results prove that this engineered system yields reliable and sensitive measurements of cadherin-mediated adhesion strength. Our system is an improvement over other systems in that it presents purified VE-cadherin ligands with precise control over the spatial arrangement of cadherin ligands and it reduces the complexity of two cells binding in the adhesive interface to that of cells binding to purified cadherin ligands presented on an engineered surface.

4.4.7. Screening of Chinese Hamster Ovary Cells Show Desired Production Levels for VE-Cadherin-Expressing and Wild-Type Cells

We quantified surface level expression of VE-cadherin receptors on wild-type Chinese Hamster Ovary cells (CHO cells) and Chinese Hamster Ovary Cells stably-expressing VE-cadherin (CHO-VE cells), both received as a gift from Dr. Andrew Kowalczyk of Emory University. As CHO cells do not express endogenous levels of cadherin proteins, they have been used traditionally for many gain of function experiments, wherein cadherin proteins have been transfected into the cells in order to test for adhesive potential [231-233]. To verify the expression of cadherin proteins of these CHO cells, we conducted flow cytometry experiments using the BV9 antibody against the extracellular domain of VE-cadherin **(Figure 4.13)**. Unstained and isotype control samples were included to verify auto-fluorescence and non-specific binding of the antibody. Quasi-quantitative values for surface level expression were calculated by allowing a 5% overlay on the isotype control plot and reporting the percentage area under each sample curve. Samples were run in duplicate.

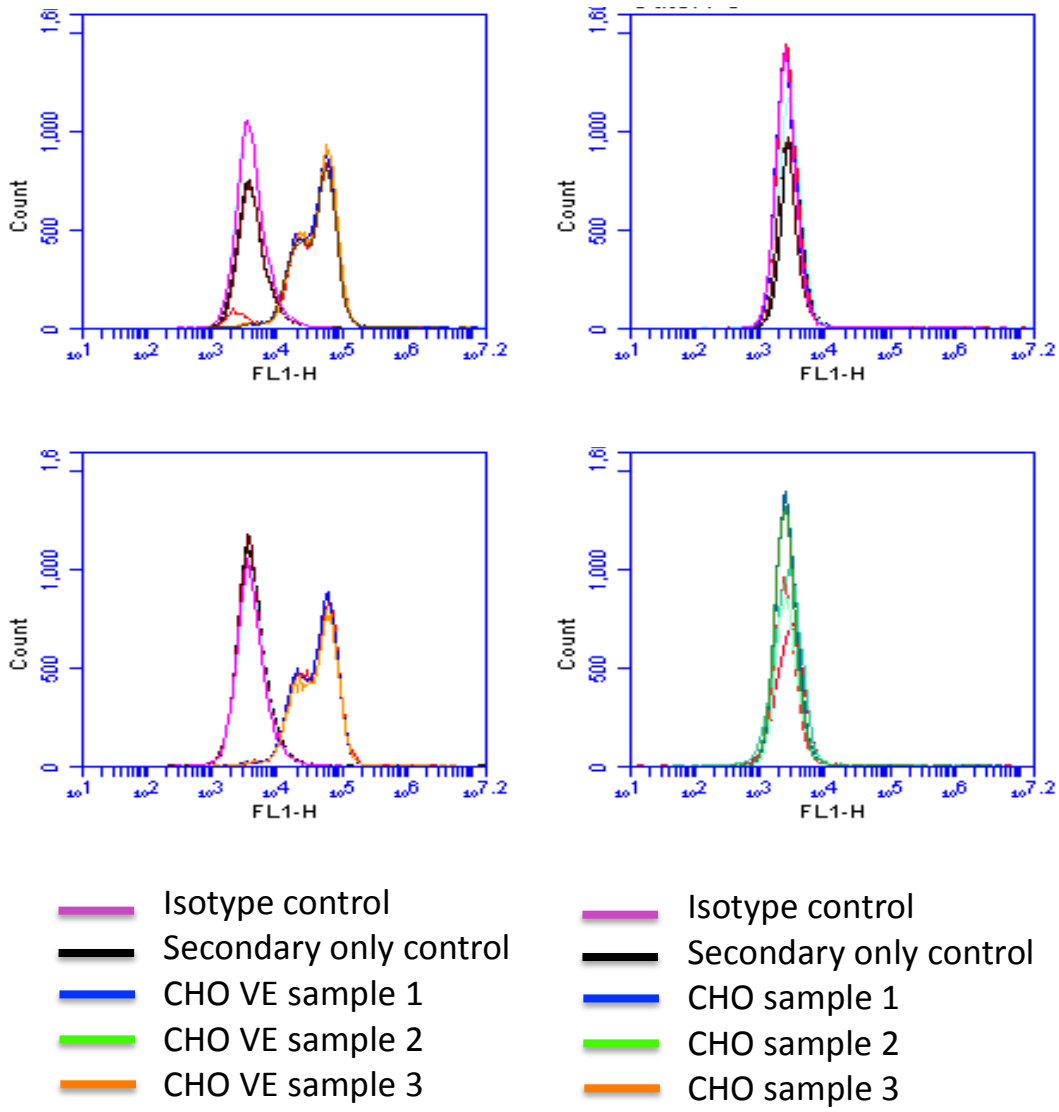

Figure 4. 13: Flow cytometry histograms for CD144 (vascular endothelial cadherin) surface expression of VE-expressing (CHO VE, left panel) and wild-type Chinese Hamster Ovary (CHO, right panel) cells immediately after staining for CD144 (top panel) and 120 minutes after staining for CD144 (bottom panel).

For VE-cadherin-expressing CHO cells, surface level expression of cadherin ligands was high as compared to isotype controls, validating VE-cadherin expression levels for subsequent experiments. In contrast, expression levels for wild-type CHO cells were similar to both isotype and untreated controls. Flow cytometry experiments were conducted before force measurements

to validate expression levels based on passage number (expression levels for VE-expressing CHO cells decreased after passage 20).

4.4.8. Adhesion Strength Analyses of Wild-Type and VE-Expressing CHO Cells on Engineered Surfaces

We then conducted quantitative analyses of adhesion strength of wild-type CHO and VE-expressing CHO (CHO VE) cells on surfaces coated with 20 μg/mL purified VE-cadherin:Fc ligands at 4 hours and 16 hours after protein adsorption. Theses surfaces were blocked with 1% (wv) 65 ° C-heat-denatured BSA to prevent non-specific adsorption of proteins. Unexpectedly, there were no statistical differences between the mean adhesion strength of the two groups (CHO vs CHO-VE cells) at 4 hours. Similarly, at 14 hours, there were no statistical differences between wild-type CHO cells and VE-expressing CHO cells. There was a statistical difference between wild-type CHO cells spun at 4 hours vs. 14 hours, as well as between VE-expressing CHO cells at 4 hours vs. 14 hours, indicating an increase in mean adhesion strength over time (**Figure 4.14**).

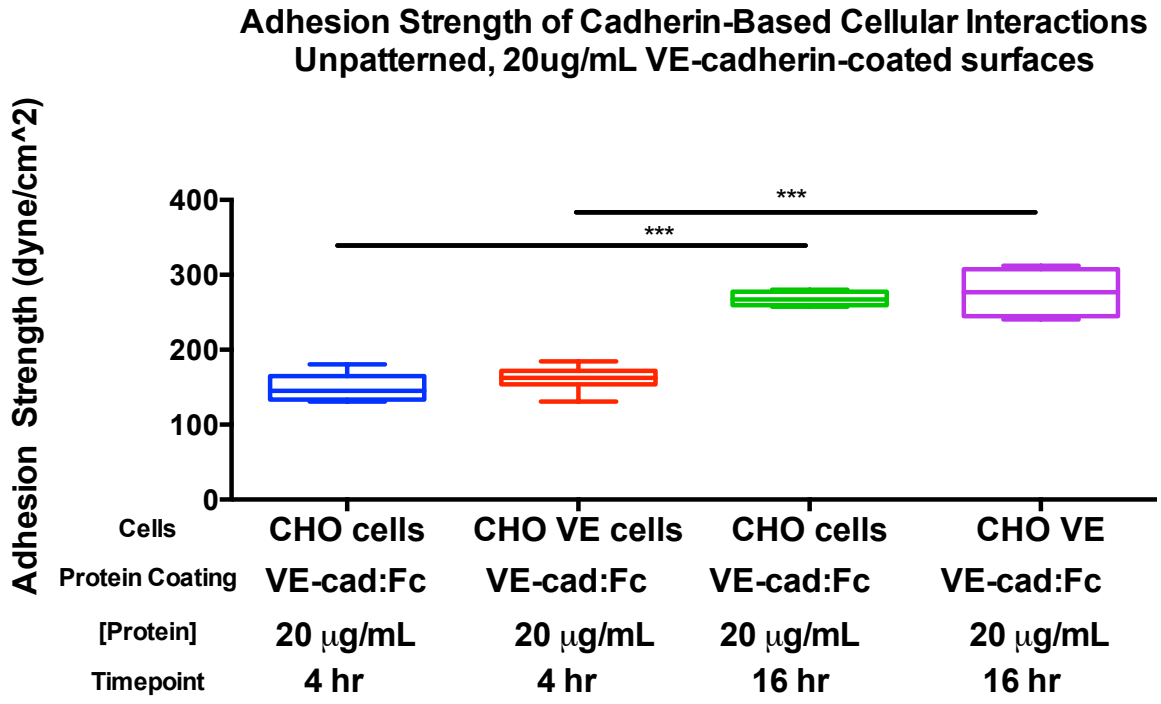

Figure 4. 14: Adhesion strength analysis of VE-cadherin-expressing and wild-type CHO cells interacting with cadherin ligands on engineered surfaces at early and late times. Cells were seeded on unpatterned coverslips coated with purified VE-cadherin:Fc ligands at concentration of 20 μg/mL and allowed to adhere for 4 hours or 16 hours before quantitative analysis using the spinning disk. Box-whisker plot (mean, 10^{th}, 25^{th}, 75^{th}, and 90^{th} percentile) for adhesion strength (> 5 coverslips per condition). The mean adhesion strength of CHO cells at 16 hours was found to be statistically different (Tukey test; ***$p < 0.0001$). The mean adhesion strength of VE-expressing CHO cells at 14 hours was found to be statistically different (Tukey test; ***$p < 0.0001$).

In order to verify the sensitivity of our system to detect mean adhesion strength at different protein concentrations, as well as to verify that the lack of differences in mean adhesion strength we observed between wild-type and VE-expressing CHO cells was not because we were measuring below the adhesion strength threshold of the system, we engineered surfaces presenting purified VE-cadherin ligands at both 5 μg/mL and 20 μg/mL. Cells were allowed to adhere for 4 hours in order to test if there were differences in mean adhesion strength between wild-type CHO and VE-expressing CHO cells at early time points (**Figure 4.15**).

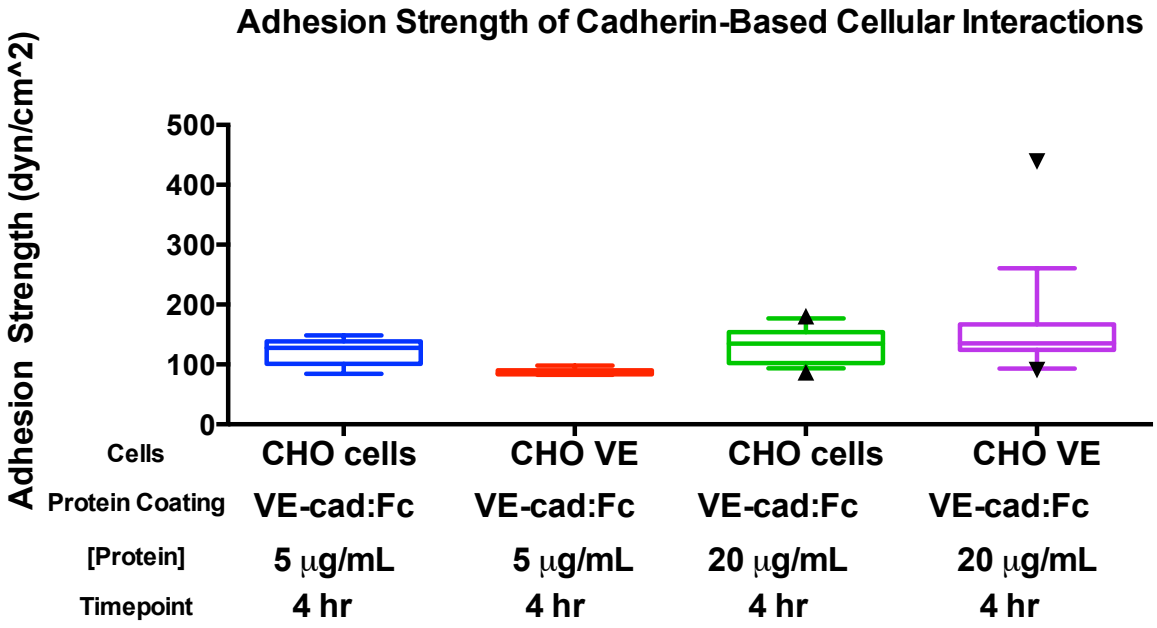

Figure 4. 15: Adhesion strength analysis of VE-cadherin-expressing and wild-type CHO cells interacting with cadherin ligands on engineered surfaces at early times on surfaces of different concentrations of adsorbed protein. Cells were seeded on unpatterned coverslips coated with purified VE-cadherin:Fc ligands at concentration of either 5 μg/mL or 20 μg/mL and allowed to adhere for 4 hours before quantitative analysis using the spinning disk. Box-whisker plot (mean, 10^{th}, 25^{th}, 75^{th}, and 90^{th} percentile) for adhesion strength (> 7 coverslips per condition). No mean adhesion strength pairwise comparison (CHO vs. CHO VE cells at 5 μg/mL or 20 μg/mL; CHO vs CHO cells at 5 μg/mL and 20 μg/mL) was found to be statistically different (Tukey test; $p > 0.05$).

Based on our initial adhesion strength analyses, we found a consistent trend of increasing mean adhesion strength as a function of time, for both wild-type and VE-expressing CHO cells. However, mean adhesion strength of VE-cadherin-expressing versus wild-type CHO cells **(Figure 4.16** and **Figure 4.17)** show no statistical difference at either time point (4 hours or 16 hours) or for protein concentration for engineered surfaces coated with different concentrations of purified VE-cadherin ligand coatings (5 μg/mL or 20 μg/mL). This result is surprising, as we would expect differences in adhesive force generation between our wild-type and our VE-expressing cells. Indeed, we would expect lower levels of mean adhesion strength of wild-type

CHO cells adhering to our purified cadherin ligands. We explored multiple explanations for these results.

One explanation for the lack of significant differences in mean adhesion strength between the same cells seeded on similar surfaces coated at different concentrations of purified VE-cadherin ligand coatings (5 μg/mL or 20 μg/mL) or the different cells seeded at the same protein concentration is that there was insufficient blocking of non-specific protein adsorption at the adhesive interface. In order to eliminate this possibility, we investigated using different blocking buffer reagents to abrogate residual protein adsorption/deposition on the surface of our coverslips. In addition to the 1% (w/v) 65˚C-heat-denatured BSA, we examined 100 μg/mL human IgG, 1% (w/v) casein, and a commercial Pierce blocking buffer (data not shown) to block non-specific adsorption of proteins on the engineered surfaces, based on literature searches [234]. We repeated our previous experiments for assessing adhesion strength as a function of time, protein concentration, and blocking buffer reagent. The goal of this experiment was to find a blocking buffer candidate that eliminated non-specific protein adsorption, as evidenced by highest mean adhesion strength and to use the best candidate for subsequent adhesion analyses of cadherin-coated surfaces. For this experiment, we used fibronectin as our control protein because we wanted to rule out that the purity of our vascular endothelial cadherin was not a factor in the lack of differences in mean adhesion strength that we observed in prior experiments. In spreading assay experiments (not shown), we verify that both wild-type and VE-expressing CHO cells spread well on fibronectin-coated surfaces, so we decided to use VE-expressing CHO cells for this preliminary experiment. By using fibronectin protein at high concentration (20 μg/mL) and including surfaces with no adsorbed fibronectin, we wanted to understand how well our reagents blocked these engineered surfaces over time (4 hours and 14 hours). The results for the

overall experiment (**Figure 4.16**), the surfaces with no pre-adsorbed fibronectin (**Figure 4.17**), and the surfaces with adsorbed fibronectin (**Figure 4.18**) followed by the different blocking conditions are presented.

Overall, we found that for VE-expressing CHO cells at each blocking buffer and time point combination, mean adhesion strength for fibronectin-coated surfaces was consistently higher than surfaces with no pre-adsorbed fibronectin, as expected, for all blocking conditions and time points (**Figure 5.4**). On surfaces with no pre-adsorbed fibronectin, we observed a significant difference in mean adhesion strength between surfaces blocked with casein and surfaces blocked with HumanIgG (**Figure 4.14**). No other pairwise comparison in the experiement was found to be statistically significant, whether it was between surfaces blocked with different blocking reagents for the same protein concentration and time point, or for surfaces blocked with different blocking reagents for different time points (**Figure 5.15, Figure 4.16, Figure 4.17**).

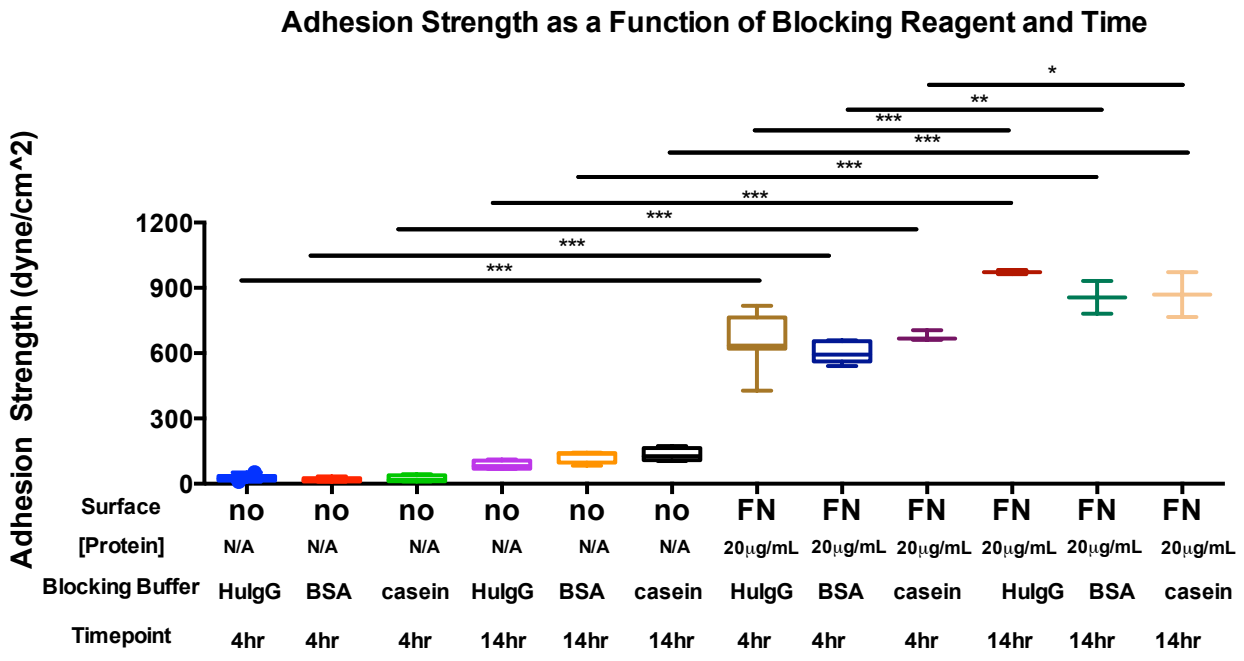

Figure 4. 16: Adhesion strength analyses for VE-cadherin-expressing CHO cells on fibronectin-coated surfaces and surfaces with no pre-adsorbed fibronectin, blocked with various blocking reagents and seeded at early (4 hours) and late times (14 hours). Cells were either seeded on unpatterned coverslips that were uncoated with protein or coated with fibronectin (FN) ligands at concentration of 20 µg/mL, with VE-expressing CHO cells allowed to adhere for 4 hours or 14 hours before quantitative analyses using the spinning disk. After incubation with or without FN, cells were blocked with either 100 µg/mL Human IgG, 1% (w/v) 65˚C-heat-denatured BSA, or 1% (w/v) casein to prevent non-specific adsorption of proteins on the engineered surfaces. Box-whisker plot (mean, 10^{th}, 25^{th}, 75^{th}, and 90^{th} percentile) for adhesion strength (> 3 coverslips per condition). The mean adhesion strength of VE-expressing CHO on surfaces coated with no fibronectin were statistically higher than cells seeded on uncoated surfaces for all blocking conditions (Human IgG, BSA, and casein) and time points (4 hours and14 hours) (Tukey test; ***p < 0.0001). The mean adhesion strength of VE-expressing CHO cells for fibronectin-coated surfaces is statistically different for HumanIgG-blocked surfaces at 4 vs. 14 hours (Tukey test; ***p < 0.0001), for BSA-blocked surfaces at 4 vs. 14 hours (Tukey test; **p = .0005), and for casein-blocked surfaces at 4 vs. 14 hours (Tukey test; *p = .0435).

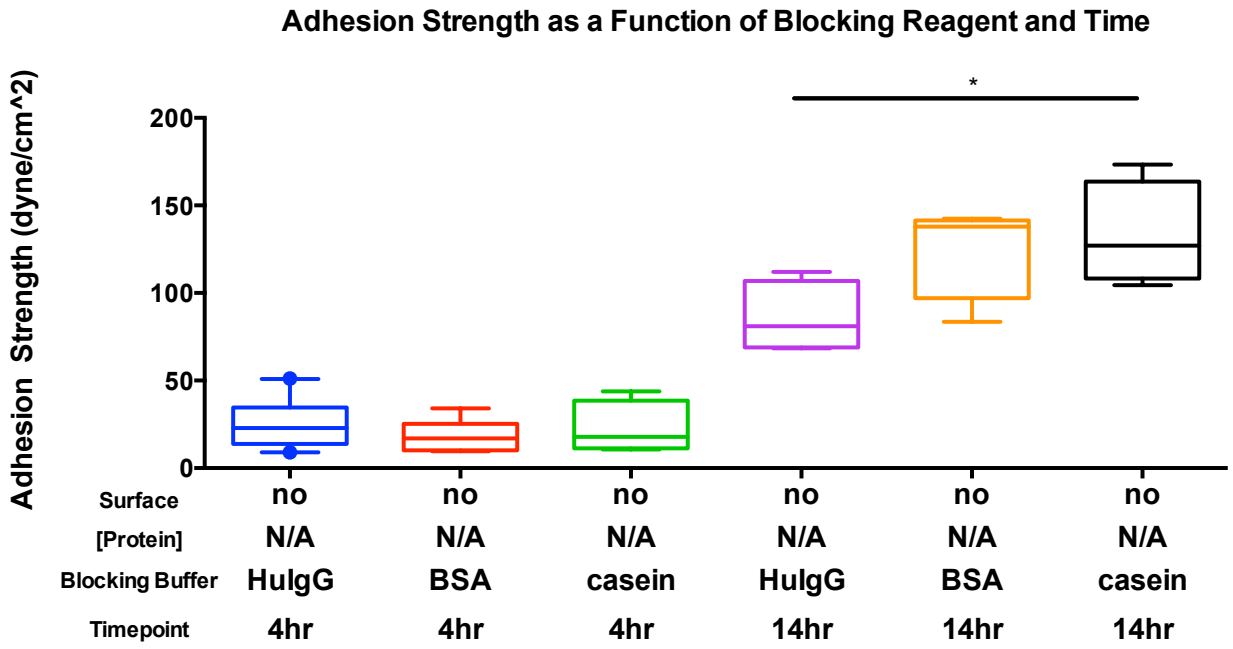

Figure 4. 17: Adhesion strength analyses for VE-cadherin-expressing CHO cells on surfaces with no pre-adsorbed fibronectin, blocked with various blocking reagents and seeded at early (4 hours) and late times (14 hours). Cells were seeded on unpatterned coverslips that were uncoated with protein, with VE-expressing CHO cells allowed to adhere for 4 hours or 14 hours before quantitative analyses using the spinning disk. Before cell seeding, surfaces were blocked with either 100 µg/mL Human IgG, 1% (w/v) 65˚C-heat-denatured BSA, or 1% (w/v) casein to prevent non-specific adsorption of proteins on the engineered surfaces. Box-whisker plot (mean,

10th, 25th, 75th, and 90th percentile) for adhesion strength (> 3 coverslips per condition). The mean adhesion strength of VE-expressing CHO cells for uncoated surfaces is statistically different for HumanIgG-blocked vs. casein-blocked surfaces at. 14 hours (Tukey test; *p < = 0.0143)

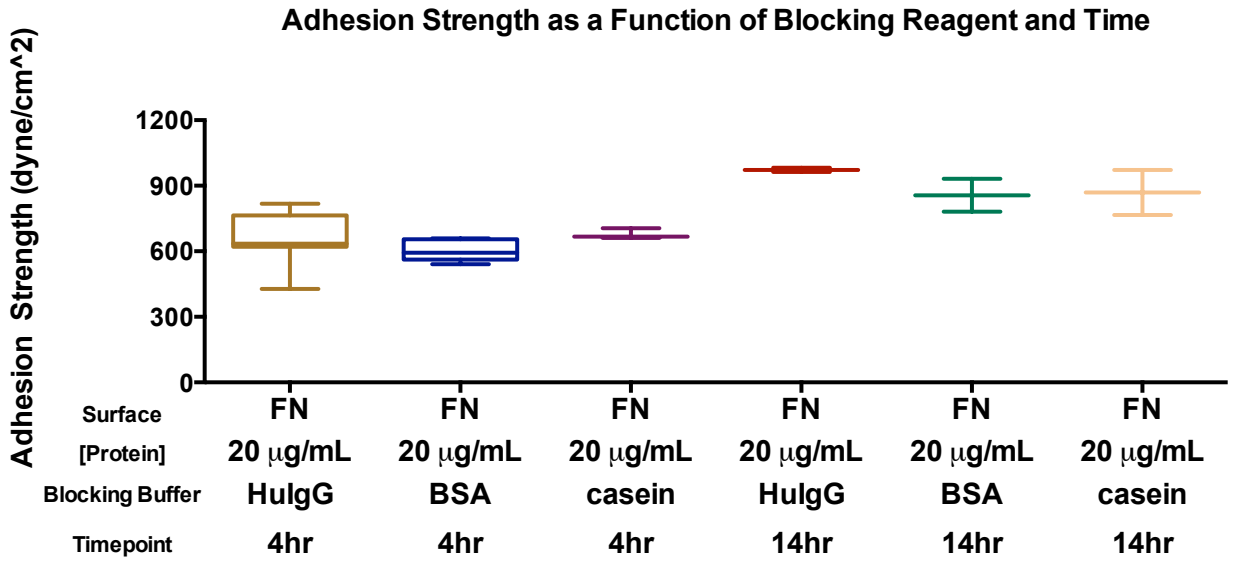

Figure 4. 18: Adhesion strength analyses for VE-cadherin-expressing CHO cells on fibronectin-coated surfaces, blocked with various blocking reagents and seeded at early (4 hours) and late times (14 hours). Cells were seeded on unpatterned coverslips that were coated with fibronectin (FN) ligands at concentration of 20 μg/mL, with VE-expressing CHO cells allowed to adhere for 4 hours or 14 hours before quantitative analysis using the spinning disk. After incubation with FN, cells were blocked with either 100 μg/mL Human IgG, 1% (w/v) 65˚C-heat-denatured BSA, and 1% (w/v) casein to block non-specific adsorption of proteins on the engineered surfaces. Box-whisker plot (mean, 10th, 25th, 75th, and 90th percentile) for adhesion strength (> 3 coverslips per condition). The mean adhesion strength of CHO cells for fibronectin-coated surfaces at 4 or 14 hours was not found to be statistically different between surfaces blocked by different blocking buffer reagents (Tukey test; $p > 0.05$).

Follow-up experiments were conducted to address three different possibilities to explain the apparent lack of differences between wild-type CHO and VE-expressing CHO cells on our engineered surfaces, namely: 1) the sensitivity and measurement threshold of our system; 2) the possibility of non-specific protein binding/adsorption; and 3) the strength of the specific interaction of our cells to our purified cadherin ligands. To test each of these claims, we tested a lower protein concentration, we assayed adhesion strength for surfaces blocked with different

blocking reagents, and we used a different protein altogether that we had shown to support cell spreading (data not shown). From these results, we observed that blocking with HumanIgG presented a surface that had the lowest adhesion strength in the absence of adsorbed VE-cadherin or fibronectin as well as the highest adhesion strength when our engineered surfaces were coated with VE-cadherin or fibronectin ligands. We then decided to use HumanIgG as our preferred blocking buffer reagent.

In order to test the whether the adhesion stregnth we were measuring using our engineered surfaces was cadherin-specific, we conducted a cell spreading assay as well as quantitative adhesion analyses for wild-type and VE-expressing CHO cells on surfaces uncoated with protein or coated with our purified cadherin ligands (20 μg/mL), incubated with or without 4mM EGTA. We chose EGTA for calcium chelation because it is more selective than EDTA in capturing calcium [235, 236]. For the *in vitro* cell spreading, engineered surfaces were prepared as usual, coated with 20 μg/mL purified VE-cadherin ligands, blocked with 100 μg/mL human IgG, and seeded with 150 cells/mm^2 of each cell type. Wild-type and VE-expressing CHO cells were allowed to adhere to our uncoated protein and purified cadherin-coated surfaces for 14 hours, after which some samples were incubated with 4 mM EGTA for 30 minutes. Cells were then imaged for spreading using phase contrast microscopy. Immediately after, cells treated with inhibitor and control cells were spun with the spinning disk for 5 minutes.

Representative phase contrast images were taken for the wild-type and VE-expressing CHO cell lines for four different conditions (no VE-cadherin:Fc ligand coating, VE-cadherin:Fc ligand coating, VE-cadherin:Fc ligand coating, prior to 30-minute incubation with 4mM EGTA but before spinning disk analysis, and VE-cadherin:Fc ligand coating, after a 30-minute incubation with 4mM EGTA but before spinning disk analysis). These images show that both

wild-type and VE-expressing cells spread on the purified VE-cadherin:Fc ligand, while there is little spreading on the on the uncoated (control) surfaces (**Figure 4.19**). More importantly, this cell spread area is calcium-dependent, as 30-minute 4 mM EGTA incubation eliminates spreading. There appear no differences in spreading between the two cell types.

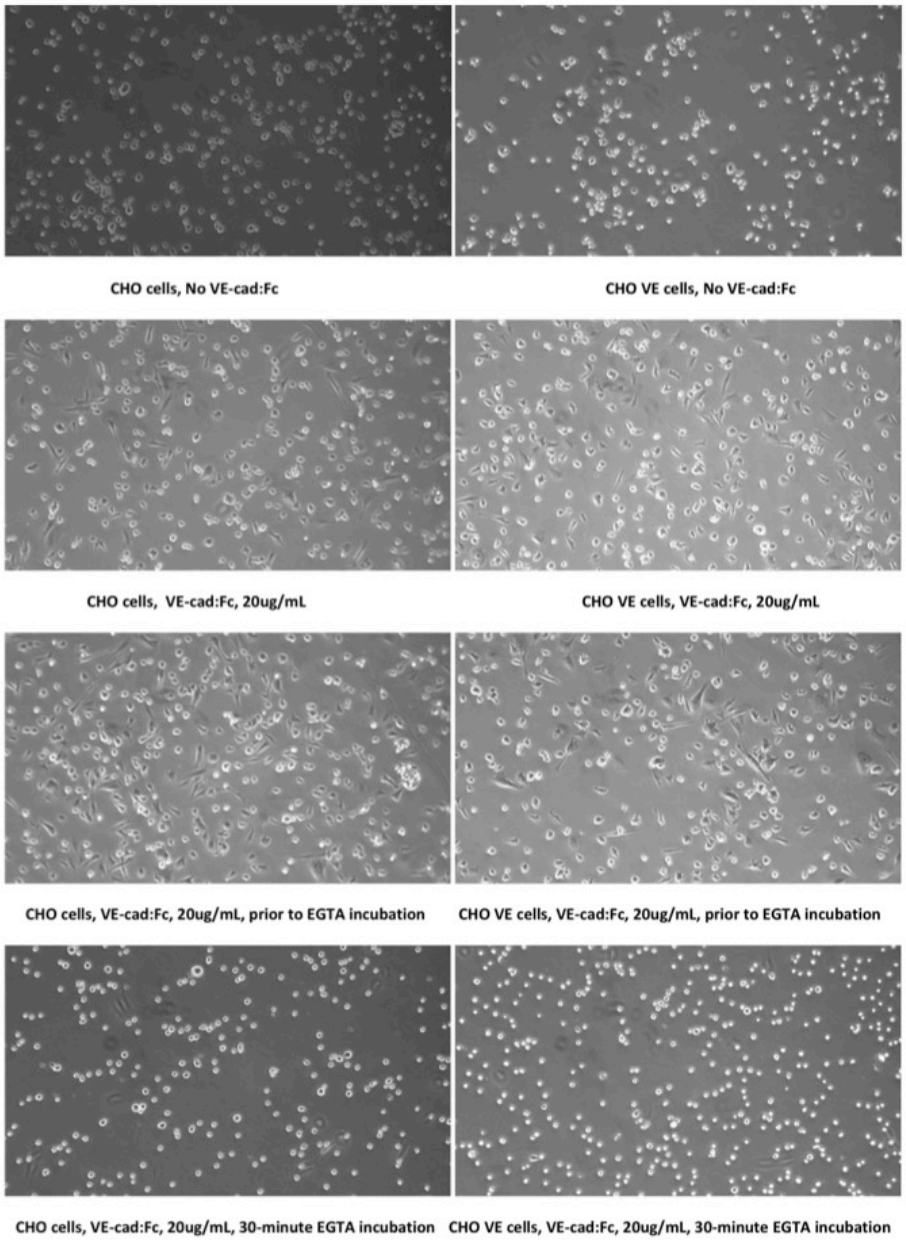

Figure 4. 19: Cell spread area assay for VE-cadherin-expressing and wild-type CHO cells on vascular endothelial cadherin-coated surfaces and surfaces with no pre-adsorbed vascular endothelial cadherin, blocked with 100 μg/mL humanIgG and seeded at late times (14 hours).

Cells were seeded on unpatterned coverslips that were either uncoated or coated with VE-cadherin ligands at a concentration of 20 μg/mL, with both groups of cells allowed to adhere for 14 hours before quantitative analysis using the spinning disk. Before spinning analyses, coverslips were either incubated with 4 mM EGTA or left untreated.

Adhesion strength analyses of our wild-type and VE-expressng CHO cells mirror the cell spread area data. We observe high mean adhesion strength values for both cell lines on our purified cadherin-coated surfaces, low adhesion strength on the control surfaces (surfaces that remained uncoated with protein), and increases in adhesion strength being eliminated by incubtion in 4 mM EGTA for 30 minutes, indicating that adhesion is calcium-dependent. However, we observe higher differences in mean adhesion strength between our wild-type and VE-expressing CHO cell lines, with our wild-type CHO cells showing greater mean adhesion strength on both uncoated and cadherin-coated surfaces with no EGTA incubation. Upon EGTA incubation, these differences are eliminated (**Figure 4.20**).

One explanation for this surprising result was that these wild-type CHO cells were expressing another cadherin protein, other than VE-cadherin, responsible for the adhesion strength data we observed. Because our intial flow cytometry data confirmed drastically different expression levels for surface levels of VE-cadherin (CD144) for both the wild-type and VE-expressing CHO cells, we explored whether these wild-type cells endogenously express other cadherin proteins that could mediate and generate heterotypic adhesive forces. To verify the expression levels of VE-cadherin (CD144), E-cadherin (CD324) and N-cadherin (CD325), we conducted flow cytometry experiments on several passages of our wild-type and VE-expressing CHO cells to see if there were differences in expression levels of cadherin proteins that could be mediating adhesion (data not shown). We observed no differences in expression levels of

cadherin proteins, especially in these wild-type CHO cells that could explain the *in vitro* cell spread area data or the adhesion strength data.

Secondly, these wild-type and VE-expressing cells express an adhesive protein such as fibronectin, generating adhesive forces through cell-ECM adhesions in addition to through cell-cell contact. Further studies including flow cytometry experiments and quantitave analyses of cells incubated with functional blocking antibodies are necessary to rule out this reason.

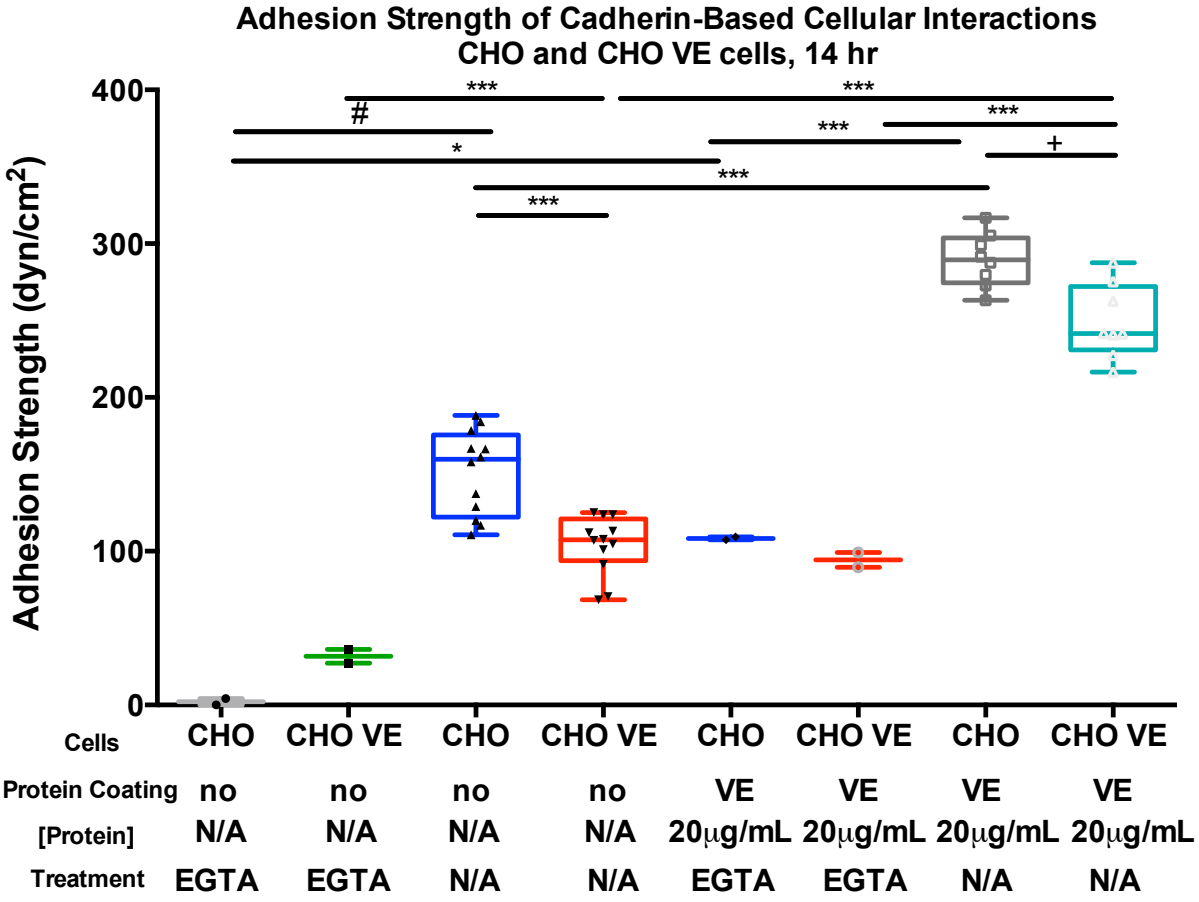

Figure 4. 20: Adhesion strength analyses for VE-cadherin-expressing and wild-type CHO cells on vascular endothelial cadherin-coated surfaces and surfaces with no pre-adsorbed vascular endothelial cadherin, blocked with 100 μg/mL HumanIgG and seeded at late times (14 hours). Cells were seeded on unpatterned coverslips that were either uncoated or coated with VE-cadherin ligands at a concentration of 20 μg/mL, with both groups of cells allowed to adhere for 14 hours before quantitative analysis using the spinning disk. Before spinning analyses, coverslips were either incubated with 4 mM EGTA or left untreated. Box-whisker plot (mean,

10^{th}, 25^{th}, 75^{th}, and 90^{th} percentile) for adhesion strength (> 3 coverslips per condition). The mean adhesion strength of CHO cells at 14 hours on uncoated samples was found to be statistically different than those treated with 4mM EGTA (Tukey test; #$p < 0.0001$). The mean adhesion strength of VE-expressing CHO cells at 14 hours was found to be statistically different (Tukey test; ***$p < 0.0001$).

4.4.9. Traction Force Analyses of Wild-Type and VE-Expressing CHO cells on Engineered Surfaces

We decided to pursue studies investing another force measurement, that of cellular traction forces. We utilized micro-fabricated post-array-detectors (mPADs) of different stiffnessness values (data not shown) with printed (data not shown), passively adsorbed (data not shown), or tethered purified vascular-endothelial cadherin ligands. Briefly, Sylgard 184 PDMS was used to make elastomeric micropost arrays through replica molding. Cast on top of silicon masters with templates of defined post height, post diameter and post spacing, cured PDMS was peeled, silanized, and supercritically dried for use. We seeded our wild-type and VE-expressing cells on top of posts of different stiffnesses with effective moduli between 5 – 15 kPa (data not shown). Based on how well the cells spread on each mPAD array, we utilized mPADs of effective modulus of 9 kPA for all experiments. We testing the following metrics using our mPADs: total traction force, traction force per post occupied by the cell, total spread cell area, and aspect ratio of the cells on top of the posts (**Figure 4.29**).

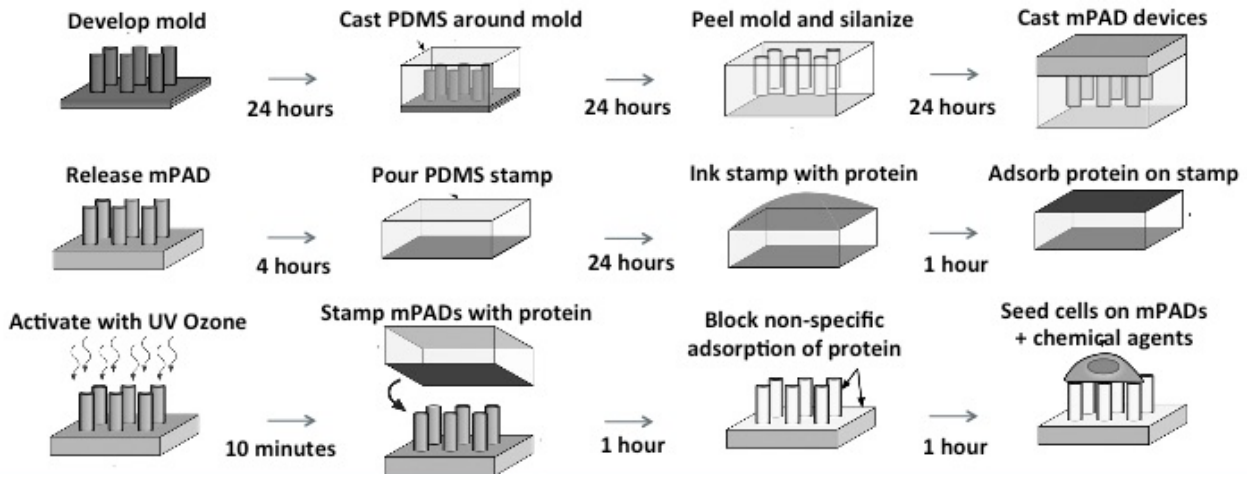

Figure 4. 21: Process flow for quantitative analyses using the micro-fabricated post detector arrays. Altogether, one complete experiment cycle lasts at least 120 hours.

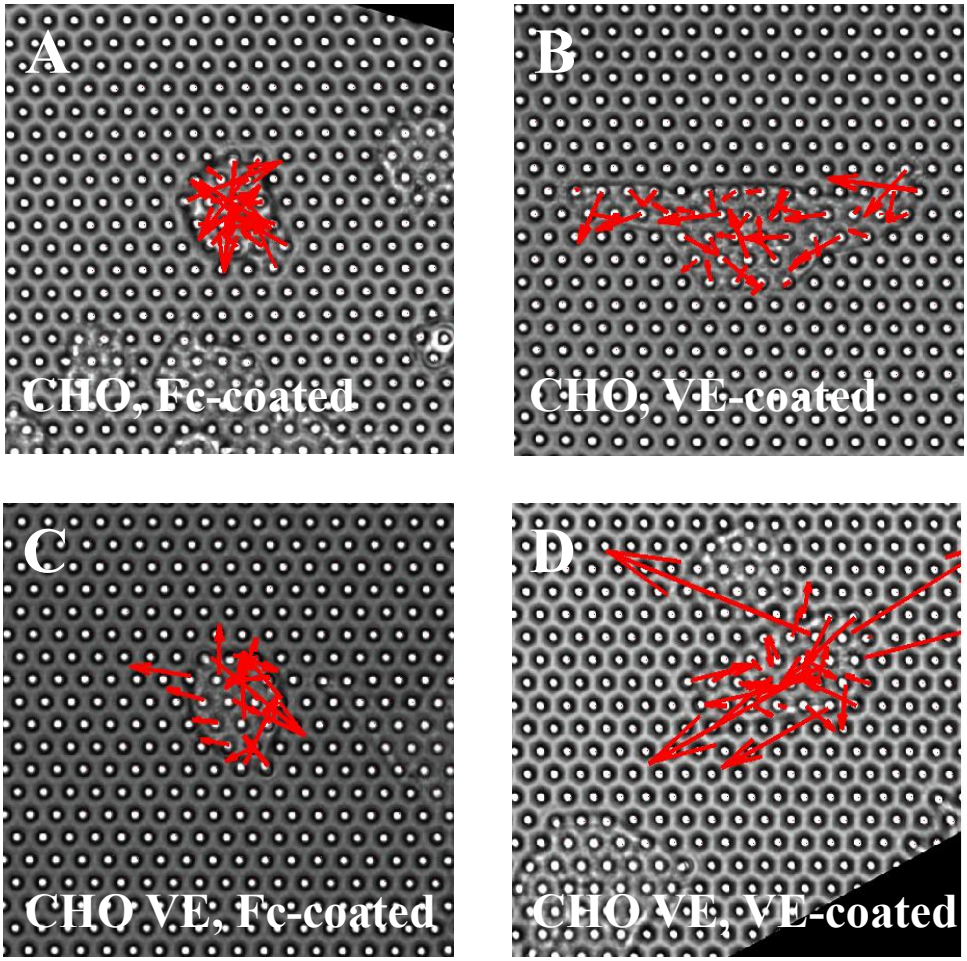

Figure 4. 22: Force vector map of wild-type CHO cells (A and C) and VE-expressing cells (B and D) on Human Fc fragment (or Fc-coated) surfaces (A and B) and vascular endothelial

cadherin-coated surfaces (C and D), blocked with glycine, pluronics F-127, and 1% (w/v) 65°C heat-denatured BSA, and seeded at late times (12 hours). Cells were seeded on micro-fabricated post array detectors that were coated with VE-cadherin:Fc ligands or with Fc fragment at a concentration of 50 μg/mL, with both groups of cells allowed to adhere for 12 hours before quantitative analysis of post deflections using the confocal microscopy and MATLAB analysis, as well as cell morphology using MATLAB and ImageJ.

We seeded cells at 200,000 cells per sample in each experimental condition, keeping seeding densities constant in the presence of 10% serum (data not shown), 0.1% serum (data not shown), and in the absence of serum. We found that serum-starvation (serum-free cell seeding) for 12 hours helped limit non-specific cell attachment, adhesion and spreading. For all conditions that were seeded under serum-free conditions, serum addition occurred at the 11 hour time-point for 1 hour before confocal microscopy image analysis proceeded, making the experimental time point 12 hours. The Fc fragment of human IgG was used as a control protein against which VE-cadherin:Fc was compared. We measured post deflections by taking confocal microscopy images of the top and bottom planes of the post-aray detectors. We aligned the images in MATLAB and quantify force vector maps of traction forces generated by these cells. We utilized the Kruskal-Wallis test to compare the distribution of the traction forces of groups of VE-cadherin-expressing CHO cells and wild-type CHO cells (**Figure 4.23**).

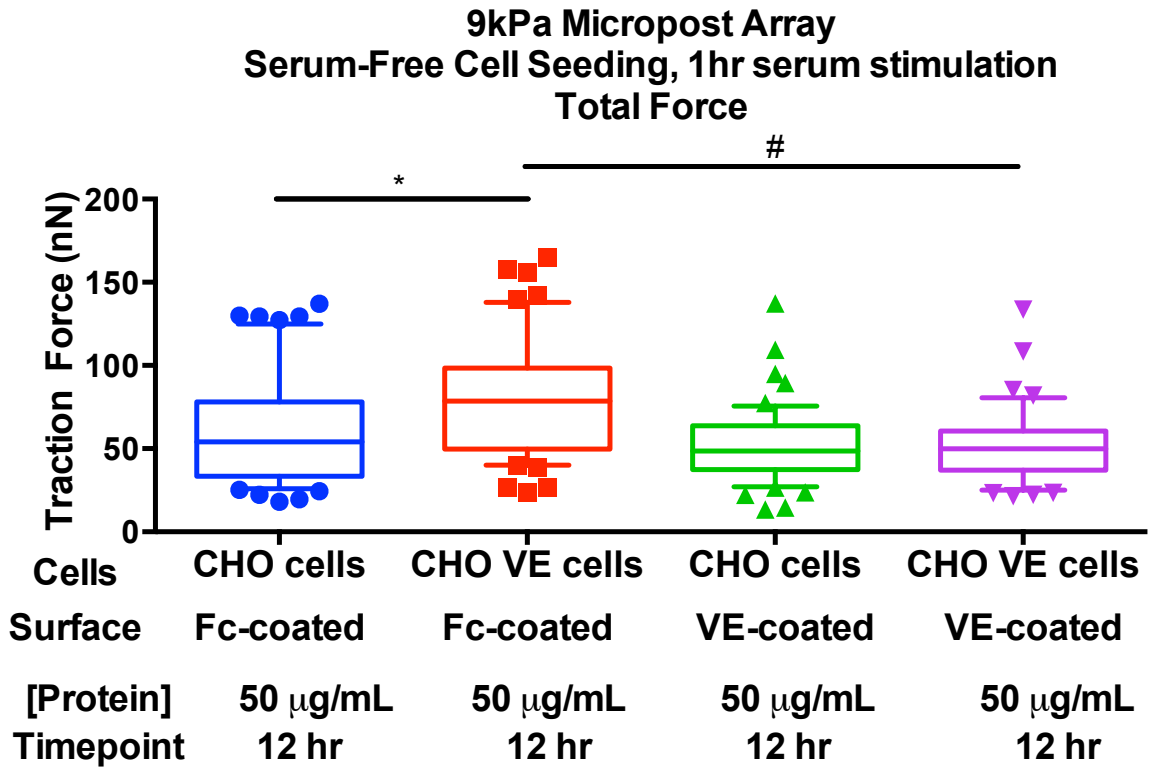

Figure 4. 23: Traction force analyses for VE-cadherin-expressing and wild-type CHO cells on vascular endothelial cadherin-coated surfaces and Human Fc fragment (or Fc-coated) surfaces, blocked with glycine, pluronics F-127, and 1% (w/v) 65°C heat-denatured BSA, and seeded at late times (12 hours). Cells were seeded on micro-fabricated post array detectors that were coated with VE-cadherin:Fc ligands or with Fc fragment at a concentration of 50 μg/mL, with both groups of cells allowed to adhere for 12 hours before quantitative analysis of post deflections using the confocal microscopy and MATLAB analysis. Box-whisker plot (mean, 10^{th}, 25^{th}, 75^{th}, and 90^{th} percentile) for traction force (> 25 cells per condition).

Upon comparison of the distribution of groups for wild-type CHO and VE-expressing CHO cells on human Fc fragment-coated mPADs and VE-cadherin:Fc-coated mPADs, we found that the total traction force for wild-type CHO cells on Fc-coated mPADs was different than VE-expressing cells, also on Fc-coated mPADs. We also observed differences in traction forces for VE-expressing cells, for surfaces that were Fc- vs. VE-cad:Fc-coated, with the traction forces generated by VE-expressing cells on Fc-coated surfaces higher than those generated on VE-coated surfaces. This is a surprising result, as we would expect VE-expressing cells to generate

more traction forces on surface that present purified cadherin ligands (**Figure 4.24**). Furthermore, one would expect no difference in traction forces between wild-type and VE-expressing CHO cells on control surfaces (Fc-coated surfaces), yet VE-expressing cells show higher traction forces over wild-type cells (**Figure 4.23**).

Upon force per post assessment, which is the total traction force normalized by the number of micro-pillar posts occupied by the cell, apparent differences between all groups disappear (**Figure 4.24**). This implies differences in cell spread area, or total cell area occupied by the cells, between the groups.

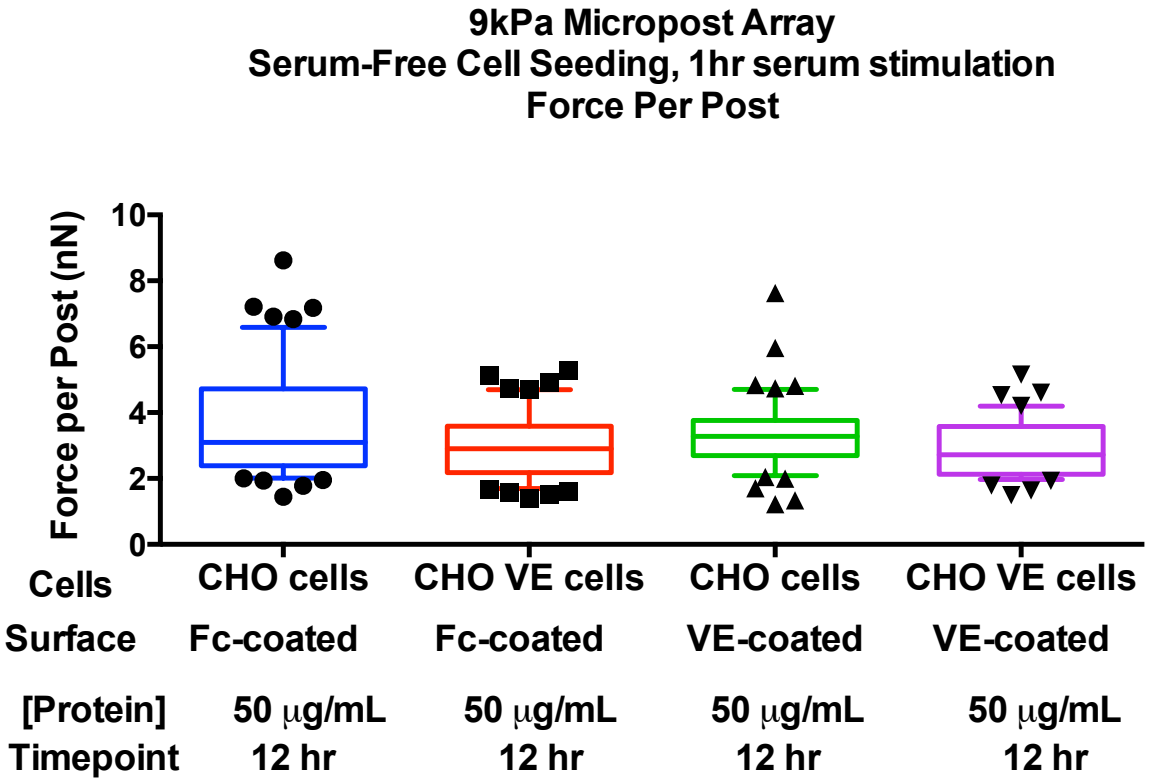

Figure 4. 24: Force per post analyses for VE-cadherin-expressing and wild-type CHO cells on vascular endothelial cadherin-coated surfaces and Human Fc fragment (or Fc-coated) surfaces, blocked with glycine, pluronics F-127, and 1% (w/v) 65°C heat-denatured BSA, and seeded at late times (12 hours). Cells were seeded on micro-fabricated post array detectors that were coated with VE-cadherin:Fc ligands or with Fc fragment at a concentration of 50 μg/mL, with both groups of cells allowed to adhere for 12 hours before quantitative analysis of post deflections using the confocal microscopy and MATLAB analysis. Box-whisker plot (mean, 10^{th}, 25^{th}, 75^{th}, and 90^{th} percentile) for traction force (> 25 cells per condition).

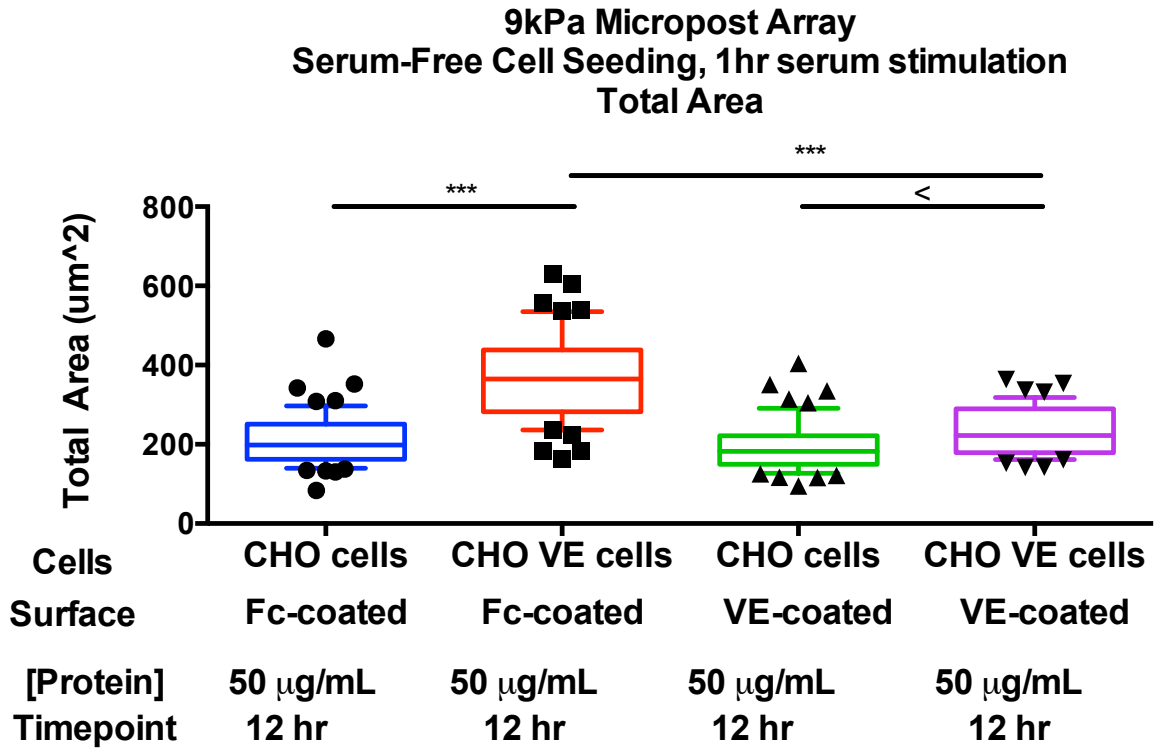

Figure 4. 25: Spread area for VE-cadherin-expressing and wild-type CHO cells on vascular endothelial cadherin-coated surfaces and Human Fc fragment (or Fc-coated) surfaces, blocked with glycine, pluronics F-127, and 1% (w/v) 65°C heat-denatured BSA, and seeded at late times (12 hours). Cells were seeded on micro-fabricated post array detectors that were coated with VE-cadherin:Fc ligands or with Fc fragment at a concentration of 50 μg/mL, with both groups of cells allowed to adhere for 12 hours before quantitative analysis of spread area using the confocal microscopy and ImageJ analysis for cell morphology. Box-whisker plot (mean, 10^{th}, 25^{th}, 75^{th}, and 90^{th} percentile) for traction force (> 25 cells per condition).

Total area results show differences between wild-type CHO and VE-expressing CHO cells on Fc-coated samples, on VE-cad:Fc-coated samples, as well as for VE-expressing cells on Fc-coated vs. VE-cad:Fc-coated samples. VE-expressing cells were more spread on purified VE-cad:Fc-coated surfaces than wild-type cells, but were not as spread as VE-expressing cells on Fc-coated surfaces. This, too, was surprising, as one would expect greater spreading between VE-expressing cells and surfaces that present purified cadherin ligands as opposed to a control surface (Fc-coated surfaces). On control surfaces, we would expect no differences between the

wild-type CHO and VE-expressing cells, but we observe higher spreading for our VE-expressing cells on control surfaces (**Figure 4.25**)

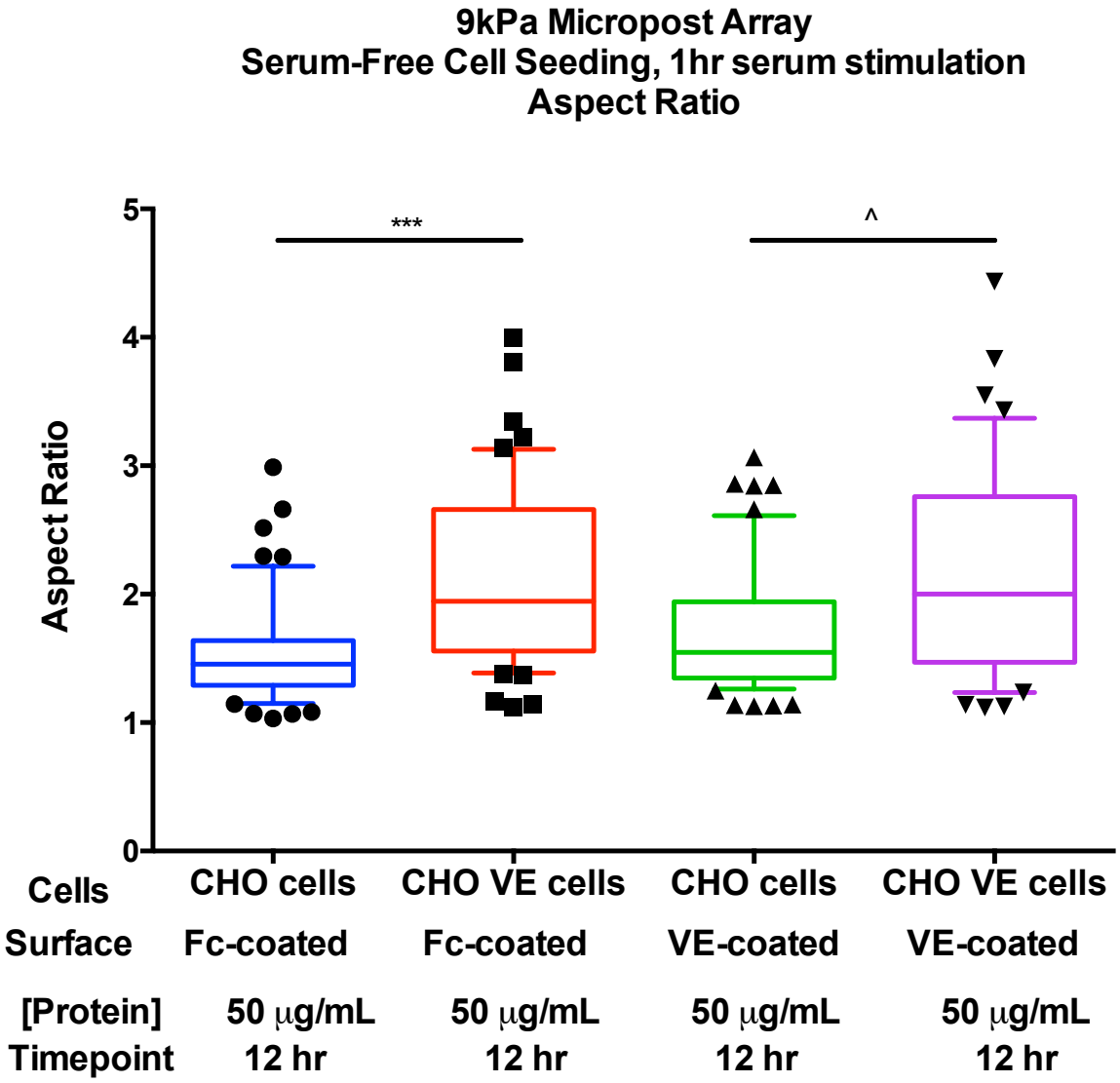

Figure 4. 26: Aspect ratio analyses for VE-cadherin-expressing and wild-type CHO cells on vascular endothelial cadherin-coated surfaces and Human Fc fragment (or Fc-coated) surfaces, blocked with glycine, pluronics F-127, and 1% (w/v) 65°C heat-denatured BSA, and seeded at late times (12 hours). Cells were seeded on micro-fabricated post array detectors that were coated with VE-cadherin:Fc ligands or with Fc fragment at a concentration of 50 μg/mL, with both groups of cells allowed to adhere for 12 hours before quantitative analysis of post deflections using the confocal microscopy and ImageJ analysis for cell morphology. Box-whisker plot (mean, 10^{th}, 25^{th}, 75^{th}, and 90^{th} percentile) for traction force (> 25 cells per condition).

We measure the aspect ratio of each cell to gain an understanding of its morphology on our engineered surfaces. The aspect ratio is a direct measurement of cell elongation, that is a ratio of the approximated dimensions of the cell. This morphology is a result of a competition between internal traction forces, the cell's elasticity, and the force from adhesion-induced spreading. Although the aspect ratio in some cells is highly correlated to cell polarity and to a crosstalk between actin networks and microtubule networks, we can only report the aspect ratio for these wild-type and VE-expressing CHO cells as the elongation of the cell as a measure of cellular response between the balance between traction forces generated and adhesion-induced spreading, as we did not measure cytoskeletal alignment [237-239]. There are statistical differences between VE-expressing CHO cells and wild-type CHO cells for each type of surface upon aspect ratio assessment (**Figure 4.26**).

We also measured traction force per unit area, in order to normalize traction forces over the differences in spread area we observed. Once normalized by the area, there were no statistical differences in traction forces observed between any of the groups, whether for wild-type CHO cells or VE-expressing CHO cells on either of our engineered surfaces.

4.4.9. Conclusions

Several possibilities exist to explain the surprising results we saw for cell spread area and traction forces. One could be that the CHO cells are secreting matrix proteins, whose deposition is allowing for increases in traction forces and cell spread area.

Another explanation could be that our engineered surfaces were insufficiently blocked against non-specific adsorption of protein. This explanation is unlikely, as we sequentially blocked with multiple different blocking reagents within each experiment (0.2% Pluronics F-127, 1% (w/v) 65°C heat-denatured BSA, and glycine as additional control). We also hypothesized that VE-expressing CHO cells could have reached a traction force maximum before the 12-hour time point, so we conducted traction force experiments at early time points (4 hours, data not shown) to eliminate this possibility and observed similar results. Because we hypothesized tht these cells may be re-modeling their underlying extra-cellular matrix despite our blocking treatment of the surface to limit non-specific protein deposition, we began to look for alternate cells with which to conduct our analyses. To examine whether the choice of cell type was a determining factor in the lack of differences in our metrics (total traction force, force per post, aspect ratio, total area, force per area) between our control group (human Fc fragment-coated surfaces) and our experimental group (VE-cadherin:Fc-coated surfaces), we repeated these experiments at early (6 hours) and late (12 hours) time-points post-seeding with human umbilical vein endothelial cells (HUVECs), GFP-expressing human umbilical vein endothelial cells (HUVEC-GFPs, data not shown), and human micro-vascular endothelial cells (HMEC-1s, data not shown).

CHAPTER V: VASCULAR ENDOTHELIAL CADHERIN-DEPENDENT CHANGES IN ADHESIVE FORCE UPON EXPOSURE TO TUMOR NECROSIS FACTOR-ALPHA, INHIBITION OF CALCIUM, AND INHIBITION OF RHO KINASE ACTIVITY

5.1. Summary

We investigated the traction forces of human umbilical vein endothelial cells seeded on engineered post-array detectors presenting VE-cadherin early (6 hours) and late (12 hours) times. We investigated traction forces based on treatment by TNF-α, an inducer of endothelial cell elongation and alignment as well as endothelial permeability, Y-27632, a Rho kinase inhibitor, and EGTA, a calcium-binding inhibitor. We found no differences in traction force upon TNF-α treatment and decreases in traction force upon Y-27632 treatment. As junctions have been shown to be tightly regulated by endothelial permeability, and in turn affected by chemical signals such as TNF-α, we sought to investigate the VE-cadherin-dependent changes in adhesive force upon endothelial cell stimulation by these chemical signals. Future studies with longer durations of TNF-α treatment are necessary to completely explore VE-cadherin dependent changes in traction forces.

5.2. Introduction

The stability of endothelial cell-cell junctions preserves the barrier function in vascular tissue. Junctions that are dysregulated are often indicators of pathologies such as vascular leakage, tumor-associated angiogenesis, and inflammation [78, 240, 241]. Growth factors that

promote angiogenesis and endothelial permeability, including vascular endothelial growth factor (VEGF) and tumor necrosis factor (TNF-α), remodel cell-cell junctions by mediating the phosphorylation and endocytosis of the VE-cadherin complex. Additionally, endothelial junctions are also remodeled by actin cytoskeleton dynamics, in that actomyosin contraction promotes angiogenic sprouting and trans-endothelial migration. VEGF and TNF-α are also implicated in actomyosin contractility, activating RhoA. Thus, actomyosin-based tension at junctions contributes to their remodeling. In the absence of hormones, junctions have been reported to reinforce themselves proportionally to increasing force [182]. Therefore, an interplay between chemical signals and cytoskeletal forces exists to control endothelial junctional remodeling.

More specifically, endothelial hormones induce the formation of so-called focal adherens junctions, VE-cadherin-marked cell-cell junctions that have vinculin and are contacted by radial F-actin bundles [242]. At these junctions that are actively being remodeled, VE-cadherin localizes perpendicularly to the rear of the migrating cells that also pull on the corresponding junction of non-migrating cells and attaches to radial actin bundles of both cells. Stable adherens junctions, in contrast, have parallel actin bundles that have no overlap with VE-cadherin [242].

As the remodeling of endothelial junctions has been shown to be tightly regulated by endothelial permeability, and in turn is affected by chemical signals such as VEGF and TNF-α, we sought to investigate the VE-cadherin-dependent changes in adhesive force upon endothelial cell stimulation by TNF-α. The increase in the endothelial expression of adhesion molecules (including selectin and vascular adhesion molecules) can be induced by TNF-α [243, 244]. According to a recent study, TNF-α induces alignment of endothelial cells and their elongation, which in turn induces the formation of focal adherens junctions [242]. As our cells are seeded on

engineered substrates and are unconstrained in their area, we hypothesize that incubation of human umbilical vein endothelial cells with TNF-α will lead to an increase in traction force because of an increase in actomyosin contractility. We will include inhibitors for Rho kinase activity as well as calcium activity to test whether actomyosin contractility and calcium binding affect the generation and stability of traction forces at cadherin-based cell-cell contacts.

5.3. Materials and Methods

5.3.1. mPAD Fabrication

Micro-fabricated post-array detectors were created from silicon masters provided by Dr. Jianping Fu's lab from the University of Michigan [245, 246]. The elastomeric micro-post arrays were fabricated using Sylgard 184 PDMS and curing agent (Dow-Corning) via replica molding. PDMS pre-polymer was cast atop mPAD silicon masters, cured at 110˚C for 1 hour, peeled off, oxidized with oxygen plasma (Plasma-Preen; Terra Universal), and silanized with (tridecafluoro-1,1,2,2,- tetrahydrooctyl)-1-trichlorosilane (Sigma-Aldrich) vapor under vacuum for 16 hours. For the fabrication of the mPAD device used for experiments, 10:1 PDMS pre-polymer/curing agent mixture was cast on the template, degassed under vacuum for 30 minutes, and cured at 110˚C for 20 hours and peeled off the template. Collapse of the mPADs induced by the peeling process was reversed by sonication in 100% ethanol (Decon Labs), followed by super-critical drying in liquid CO_2 using a critical point dryer (Samdri-PVT-3D, Tousimis). Excess PDMS was scraped off the device to ready it for use.

5.3.2. Protein Coating

Early experiments with our mPAD platform were performed by printing the protein, that is, by transferring the protein onto the surface of the elastomeric array using another elastomer. Briefly, we poured stamps (20:1 PDMS: curing agent) by casting well-mixed and degassed PDMS pre-polymer mixture on silanized silicon wafers. After curing, stamps were cut to size and were coated in saturating concentration of protein, whether it was fibronectin (50 μg/mL in DPBS) or our purified VE-cadherin (50 μg/mL in DPBS) or for 1 hr. Afterwards, these stamps were immersed in distilled water and dried under a stream of N_2. These stamps were then inverted onto the plasma treated mPADs surface for around 10 seconds. Oxygen plasma treatment occurred at 100 mW/cm^2 for 3 seconds (Plasma-Preen, Terra Universal). These substrates with stamp were then sequentially washed in 100% ethanol, and three times in 70% ethanol, three times in water, and in PBS, after which they were blocked with 0.2% Pluronics F-127, 1% (w/v) 65˚C-heat denatured BSA, rinsed with PBS and prepared for cell seeding.

For the experiments using the wild-type and VE-expressing CHO cells, we use a silane-NHS-PEG tethering procedure to tether the proteins to the surface of the mPADs. Briefly, 1 μg/mL silane-PEG-NHS (3400 MW, Nanocs) was dissolved in 200-proof ethanol by agitating for at least 20 minutes at room temperature to allow thorough mixture. The day prior, we poured stamps (20:1 PDMS: curing agent) by casting well-mixed and degassed PDMS pre-polymer mixture on silanized silicon wafers. After curing, stamps were cut to size and while silane-PEG-NHS was dissolving, we UV-ozone-treated stamps for 90 seconds to hydrolyze the surface. We then added 5% 10mM acetic acid (pH 4.5 in DI water) to the silane-PEG-NHS solution to hydrolyze the reaction for exactly 2 minutes. We then coated the flat stamps with excess solution

of the hydrolyzed silane-PEG-NHS, drying with a stream of filtered N_2. We then inverted the stamp onto our mPAD devices, after activating the surfaces for 3 seconds with a plasma etcher. Oxygen plasma treatment occurred at 100 mW/cm^2 for 3 seconds (Plasma-Preen, Terra Universal). We printed the silane-PEG-NHS onto the surface of the stamp for 10 seconds, flicking off the stamp gently. We then placed the mPADs under vacuum in the dark for 30 minutes to facilitate proper silane tethering onto the mPAD surface.

After washing with 70% ethanol and PBS, we blocked sites that were not properly silane-tethered with .2% Pluronics F-127 (Sigma) for 30 minutes at pH7.4 to maintain the slow hydrolysis rate of NHS. After washing off the Pluronics F-127, we incubated protein, whether it was fibronectin (50 μg/mL) or our purified VE-cadherin (50 μg/mL) or our human Fc Fragment (Jackson Laboratories), all dissolved in 50 mM HEPES solution at pH 8, and incubated for at least 3 hours at room temperature to allow proper tethering.

After protein incubation, a series of blocking steps were taken to block sites of non-specific protein adsorption, including quenching with Tris-HCl (in 50 mM HEPES buffer, pH 8, 30 minutes), passivating with 0.2% Pluronics F-127 (30 minutes), passivating with 1% (w/v) 65˚ C-heat denatured BSA (30 minutes) , rinsed with PBS and prepared for cell seeding.

For the last set of studies, we coated the surfaces of the elastomeric post-array detectors with protein by UV ozone-treated our mPAD devices for at least 10 minutes. After immersing the mPADs in sequential washes of 100% ethanol, 70% ethanol in DPBS, water, and PBS, devices were immersed in Vybrant DiD or DiI lipophilic tracers (LifeTechnologies), which allow for the proper visualizations of the posts, acquisition of accurate measurements of micro-post deflections, and proper analyses. After rinsing thoroughly in water, mPADs were coated with

protein for at least 1 hour at room temperature before blocking with .2% Pluronics F-127 (30 minutes) and passivating with 1% (w/v) 65˚C-heat denatured BSA (30 minutes), rinsing with PBS and prepared for cell seeding.

5.3.3. Cell Culture and Reagents

Wild-type CHO and VE-expressing CHO cells were received from Dr. Andrew P. Kowalczyk from Emory University through an MTA agreement. Both cells were grown in Kaighn's modification of Ham's F-12 medium (F-12K, ATCC 30-2004), supplemented with 10% fetal bovine serum and 1% antibiotic solution (MediaTech 30-004-CI). The VE-expressing CHO cell line is stable in 1mg/mL G-418 (Corning 30-234-CR). To passage the cells, we wash them twice with DPBS without divalent cations and dislodge the cells with 0.5% Trypsin-EDTA. The wild-type CHO cells were split at a ratio of 1:3 and the VE-expressing cell line no more than 1:3 or 1:4 to avoid the possibility of inadvertently enriching for the non-VE-cad-expressing cells (the VE-cad expression rate of VE-expressing cells is about 90%, data not shown).

Human umbilical vein endothelial cells (HUVECs, Lonza) were grown on tissue culture plates coated in 0.1% Gelatin (Millipore ES-006-B) using EBM-2 Media (Lonza cc-3156), supplemented with bullet kit components (Lonza cc-2517). All adherent cells were detached in the presence of warm 0.05% Trypsin-EDTA (Life Technologies 25300-054).

5.3.4. Confocal Microscopy

For our live-cell microscopy of our cells during traction force analyses, we transferred our mPAD devices to an aluminum coverslip holder (Attoflour Cell Chamber; Invitrogen) and

placed it in a sealed incubator chamber that regulates temperature, humidity, and CO_2 (Live Cell; Pathology Devices). Confocal images were taken with a Nikon-C2+ Laser Scanning Confocal connected to a Nikon Ti- Eclipse Inverted Microscope using a high magnification objective (CFI Plan Apochromat TIRF 60x oil, N.A. 1.45; Nikon). Post images were captured using the 561 or 640 nm channel (for DiI- or DiD- stained posts, respectively).

5.3.5. Analysis and Statistics

Images of post-deflections were saved in .nd2 format and imported into Fiji (ImageJ, NIH) using the “”ND to Image6D” plugin. These images were split into their respective channels. By utilizing an mPAD analysis suite GUI in MATLAB, received as a gift from the Christopher Chen Lab at Boston University, we identified specific regions of interest by placing a ROI box around an isolated cell. The software then aligns top and bottom images of the stained post arrays together and automatically extracts the post deflections, calculating and exporting the aforementioned analysis metrics (total traction force and force per post) to Excel. Displacement was converted to force by multiplying values with the stiffness of the mPADs device. We then utilized ImageJ to calculate the total cell spread area, aspect ratio, and by extension, force per area of the cell. Final data output was graphed in GraphPad Prism 6 (Graphpad Software, CA). Statistical analyses were also conducted in GraphPad Prism.

5.4. Results

5.4.1. Traction Force Analyses of Human Umbilical Vein Endothelial Cells on Engineered Surfaces

Similar to our previous studies using Chinese Hamster Ovary cells, we seeded human umbilical vein endothelial cells (HUVECs) on micro-fabricated post-array-detectors (mPADs) of different stiffness values (data not shown) with printed (data not shown) and passively adsorbed (data not shown) purified vascular-endothelial cadherin ligands. Briefly, Sylgard 184 PDMS was used to make elastomeric micropost arrays through replica molding. Cast on top of silicon masters with templates of defined post height, post diameter and post spacing, PDMS cured overnight at 110°C was peeled, silanized, and supercritically dried for use. We seeded HUVECs on top of posts of different stiffnesses with effective moduli between 5 – 15 kPa (data not shown), and based on how well the cells spread on each mPAD array, we decided to utilize mPADs of effective modulus of 9 kPA for all experiments, similar to the CHO cell experiments. We testing the following metrics using our mPADs: total traction force, traction force per post occupied by the cell, total spread cell area, aspect ratio of the cells on top of the posts, and force per total spread cell area (**Figure 5.1**).

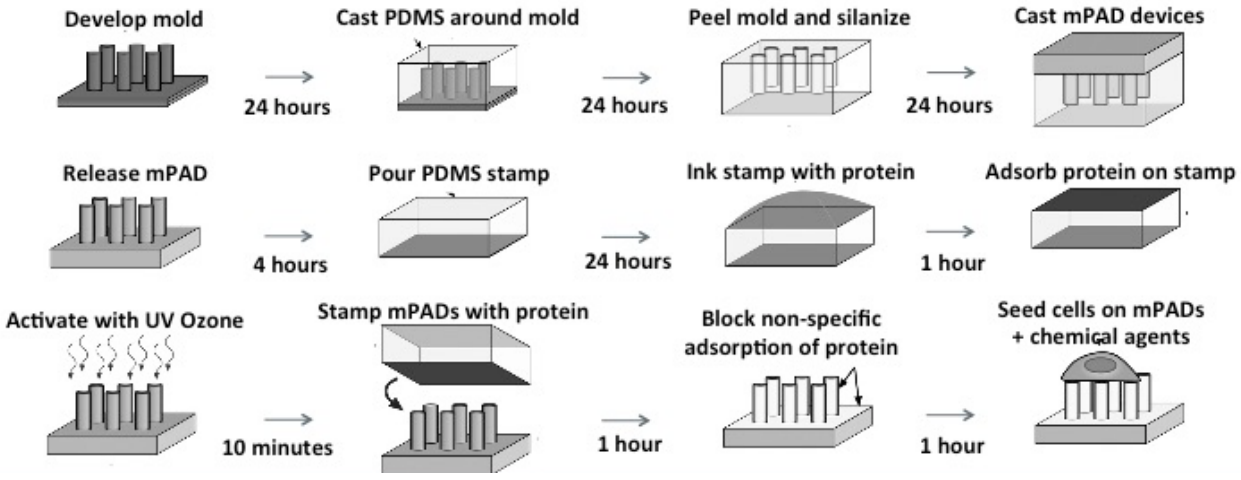

Figure 5. 1: Process flow for quantitative analyses using the micro-fabricated post detector arrays, seeded with HUVECs. Cell seeding took place every 2 hours (per sample) and analyses began at either 6 hours or 12 hours. Altogether, one complete experiment cycle lasts at least 120 hours.

For the traction force analyses, we assessed traction forces for HUVECs on VE-cadherin:Fc-coated and control Fc-coated mPADs. We also include mPADs coated with the antibody, BV9, whose epitope maps to the cadherin extracellular domain between ectodomain 3 (EC3) and ectodomain 4 (EC4) [76]. We included this group to understand whether the force response is different than for the VE-cadherin:Fc-coated surfaces. We expected lower traction forces for this protein-control group because the functional blocking antibody will prevent cadherin complex binding partners from binding and generating strong traction forces. For traction force data, traction forces for HUVECs at 6 hours and 12 hours were statistically significant as compared to our control surface (human Fc fragment-coated) and antibody control (BV9-coated). We hypothesized that purified cadherin ligands presented on our engineered mPAD surfaces would generate greater traction forces as compared to control surfaces, and this hypothesis was confirmed at both early and late time points (**Figure 5.2A**).

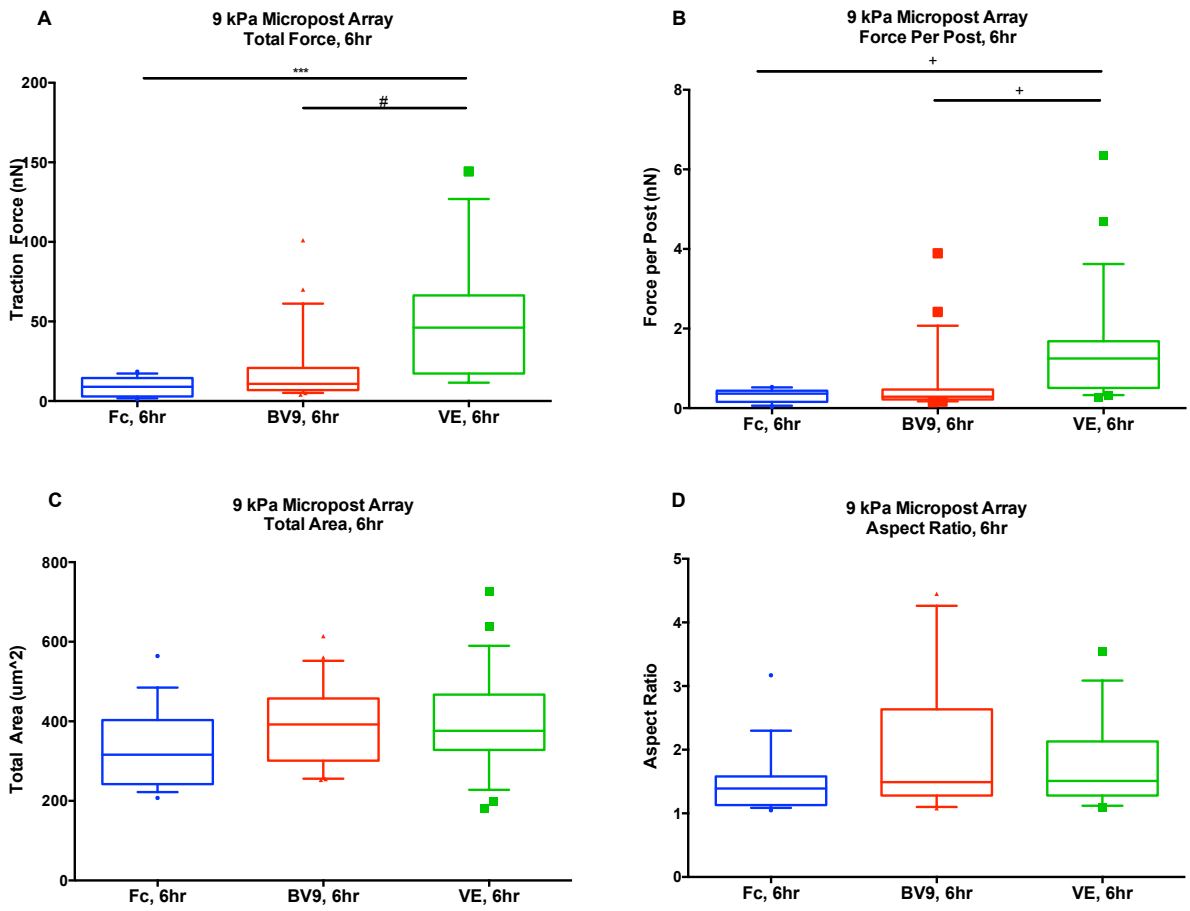

Figure 5. 2: Micro-fabricated post-array detector analyses for human umbilical vein endothelial cells (HUVECs) on vascular endothelial cadherin-coated surfaces and human Fc fragment (or Fc-coated) surfaces, blocked with 0.2% Pluronics F-127, and 1% (w/v) 65°C heat-denatured BSA, and seeded at early times (6 hours). Cells were seeded on micro-fabricated post array detectors that were coated with VE-cadherin:Fc ligands or with Fc fragment at a concentration of 50 µg/mL, with both groups of cells allowed to adhere for 6 hours before quantitative analysis of post deflections using the confocal microscopy and MATLAB analysis. A) Box-whisker plot (mean, 10^{th}, 25^{th}, 75^{th}, and 90^{th} percentile) for traction force (> 25 cells per condition). B) Box-whisker plot (mean, 10^{th}, 25^{th}, 75^{th}, and 90^{th} percentile) for force per post occupied by the cell (> 25 cells per condition). C) Box-whisker plot (mean, 10^{th}, 25^{th}, 75^{th}, and 90^{th} percentile) for total area occupied by the cell (> 25 cells per condition). D) Box-whisker plot (mean, 10^{th}, 25^{th}, 75^{th}, and 90^{th} percentile) for cell aspect ratio (> 25 cells per condition).

Similarly, we saw statistical differences in the traction force, as normalized to the number of posts the cells occupied, or force per post. We saw higher force per post metrics for HUVECs on VE-cadherin:Fc-coated surfaces as compared to our control and antibody-coated surfaces

(**Figure 5.2B** and **Figure 5.3B**). For cell spread area, we did not see any statistical differences in total spread cell area between Fc-coated, BV9-coated, or VE-cadherin:Fc surfaces, indicating that at early times (6 hours), cells were equally spread amongst the groups (**Figure 5.2C** and **(Figure 5.3C**).

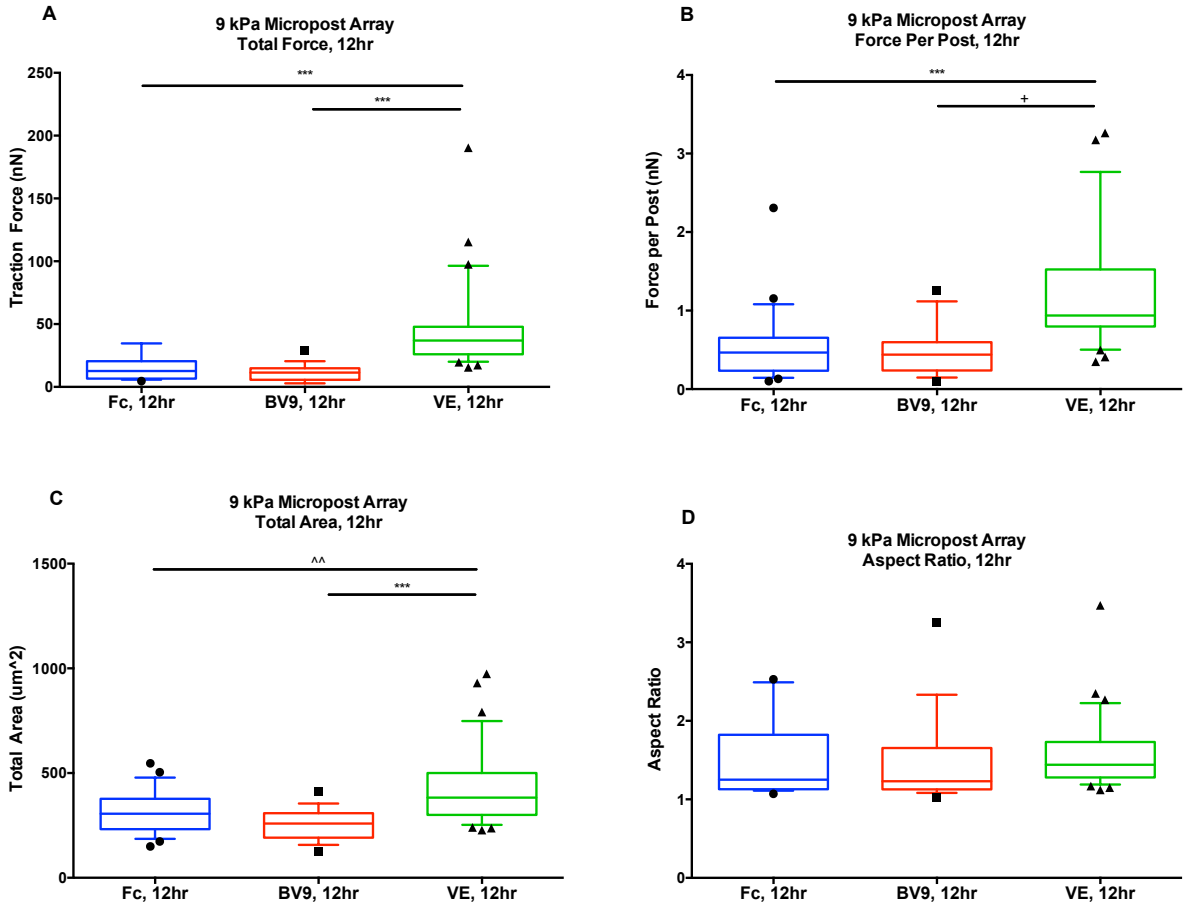

Figure 5. 3: Micro-fabricated post-array detector analyses for human umbilical vein endothelial cells (HUVECs) on vascular endothelial cadherin-coated surfaces and human Fc fragment (or Fc-coated) surfaces, blocked with 0.2% Pluronics F-127, and 1% (w/v) 65°C heat-denatured BSA, and seeded at late times (12 hours). Cells were seeded on micro-fabricated post array detectors that were coated with VE-cadherin:Fc ligands or with Fc fragment at a concentration of 50 µg/mL, with both groups of cells allowed to adhere for 12 hours before quantitative analysis of post deflections using the confocal microscopy and MATLAB analysis. A) – D) Box-whisker plot (mean, 10^{th}, 25^{th}, 75^{th}, and 90^{th} percentile) for traction force (> 25 cells per condition).

At later time points, however, we saw a statistical difference in spread area between our VE-cadherin:Fc surface and our antibody-coated surfaces. Interestingly, at 6 hours, BV9-coated surfaces supported greater cell spread area, indicating that cells became less spread on antibody-coated surfaces over time, a trend that is reversed for HUVECs on purified cadherin-coated surfaces. One hypothesis is that when seeded on antibody coated surfaces, HUVECs spread initially but upon hitting a threshold in the amount of traction force generated, cells stop spreading. The total spread area for HUVECs on Fc-coated surfaces remains constant over time, while HUVECs on VE-cadherin:Fc surfaces become more spread over time, supporting our hypothesis.

We observed no differences in aspect ratio amongst the groups for neither early nor late times (**Figure 5.2D** and **Figure 5.3D**).

Taken together, these results show that micro-fabricated post array detectors are a robust platform for investigating the cadherin-based cell-cell adhesive force of HUVECs on engineered surfaces, given the inclusion of proper controls. We used Fc-coated surfaces as control, as our recombinant protein has Fc region of human IgG fused to the extracellular domain of VE-cadherin. We also include BV9 as an additional control surface. For subsequent experiments, we present data only for HUVECs seeded on Fc-coated control surfaces and cadherin-coated surfaces.

These results are also different from the results we obtained using the wild-type CHO and VE-expressing CHO cells.

5.4.2. Immunofluorescence of Alpha-Catenin and Vinculin on HUVECs on Micro-Fabricated Post Array Detectors

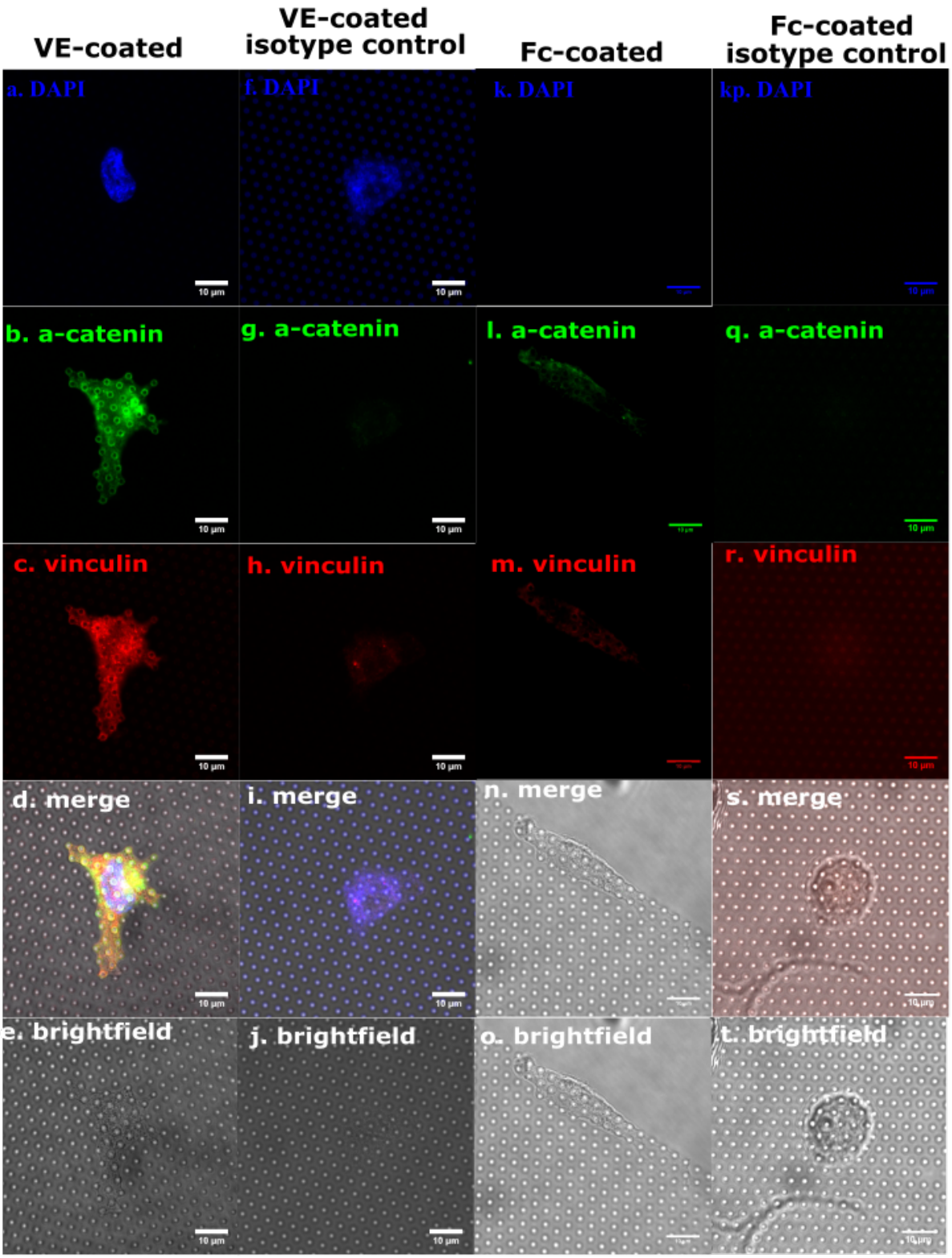

Figure 5. 5: Immunofluorescence images of human umbilical vein endothelial cells (HUVECs) on VE-cadherin-coated surfaces on micro-fabricated post-array detector analyses, blocked with 0.2% Pluronics F-127 and 1% (w/v) 65°C heat-denatured BSA, and seeded at late times (12 hours). Cells were fixed with 4% paraformaldehyde for 10 minutes, permeabilized with 0.5% Triton-X 100 for 5 minutes, blocked with 2 % (v/v) BSA for 1 hour before incubation with primary antibodies for vinculin and α-catenin. Images are of (from top to bottom): DAPI (A and F), α-catenin (B and G), vinculin (C and H), merged (D and I), and transmitted light (E and J) images. The panels are of (from left to right): staining for HUVEC cells seeded on VE-cadherin-coated surfaces, HUVECs cells seeded on VE-cadherin-coated surfaces incubated with isotype control antibodies for vinculin and α-catenin, staining for HUVEC cells seeded on Fc-coated surfaces, and HUVECs cells seeded on Fc-coated surfaces incubated with isotype control antibodies for vinculin and α-catenin.

In order to prove that our surfaces supported the immune-localization of cadherin-associated adhesion complexes in HUVECs, we immuno-stained for the recruitment of vinculin and α-catenin. We observed increased accumulation of these markers for our cells on mPADs as compared to stains of isotype controls. We show similar lack of staining for immune-stained HUVECs on Fc-coated mPADs (data not shown). Overall, the enrichment of these markers showed the recruitment of cadherin complex proteins at the surfaces of the mPADs.

We also calculated the area fraction of the posts occupied by our protein stains. We observed negligible signals for vinculin or α-catenin on Fc-coated islands. Occupancy of vinculin and α-catenin on VE-coated mPADs, however were high (> 70% in both cases). This shows improved enrichment and recruitment of cadherin complex proteins to the mPADs. These data further validate this platform as a robust tool for investigating cadherin-based adhesive force.

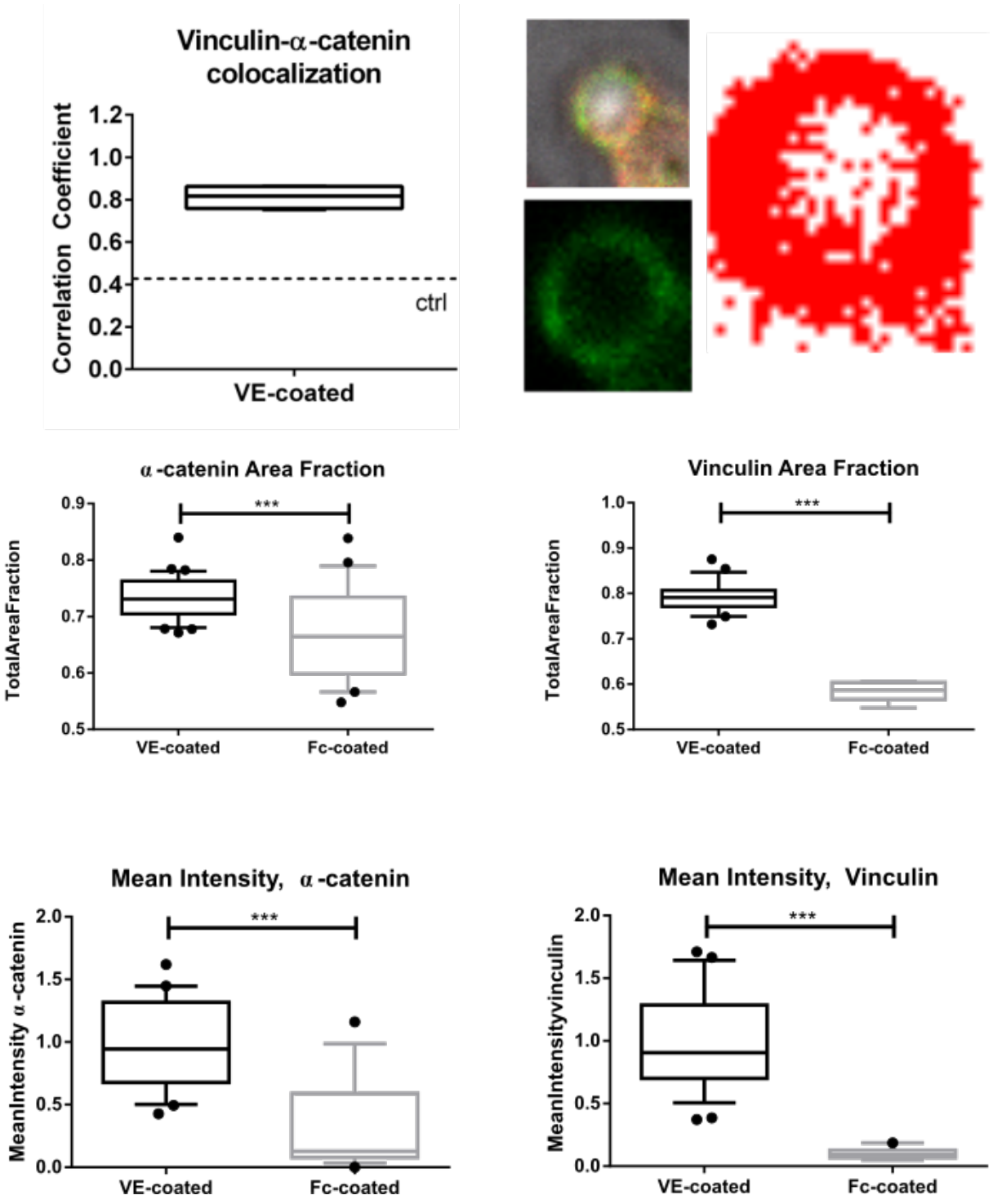

Figure 5.6: Analyses of immunofluorescence for HUVEC cells seeded on either Fc or VE-coated mPADs show greater enrichment of cadherin complex proteins to VE-cadherin-coated mPADs than for Fc mPADs. Colocalization of vinculin with α-catenin as quantified by Pearson's *r*. Thick line, median (n = 4-5 cells); box, interquartile range; whiskers, full range. The median for cells on VE-cadherin surfaces incubated with isotype control (r = .43) is drawn. Total area fractions were of vinculin and α-catenin were calculated by taking intensity thresholds of

either channel to eliminate background staining (calculated fraction in red) and normalizing areas occupied by vinculin or α-catenin staining to areas on top of the posts. t-test, $p < 0.0001$ ($N > 25$).

5.4.3. Stimulation with TNF-α and Perturbations of Calcium Binding and Rho-Kinases

Based on our previous results, we were confident in our system in its sensitivity to delineate differences in cadherin-based traction forces for our experimental and control groups. To further investigate cadherin function using our system, we perturbed the adhesive contact by modulating calcium binding, Rho-kinase activity, as well as activated the endothelial cell to evaluate cadherin-dependent changes in adhesive force. In order to modulate calcium binding, we seeded the HUVECs seeded for ~12 hours, after which we treated with 4mM EGTA, a specific chelator of calcium ions. In order to eliminate Rho-kinase activity, we used 10mM Y-27632, a specific inhibitor of Rho-kinase activity for 30 minutes. We stimulated the endothelial cell by incubating with 10ng/mL TNF-α for 30 minutes. We hypothesized that disruption of calcium binding, or performing the so-called calcium-switch assay, would result in decreases in traction forces. We also expected that disrupting Rho-kinase activity would result in decreases in traction forces and of spread area, as the Rho-associated protein kinase ROCK, a major effector of RhoA, has been implicated in many studies as a key regulator of cadherin function in several cell lines. We expect increases in traction forces as a result of endothelial cell stimulation upon TNF-α incubation. We repeated our previous experiments detailed in the previous section, but include these inhibitors/activators for HUVECs on both Fc-coated and VE-cadherin:Fc-coated surfaces. For subsequent experiments, since we had the greatest traction forces at later time points, we conducted all future experiments at the 12-hour time point.

For the traction force, we observed that at 12 hours, perturbing Rho kinase activity (incubation with Y-27632) abrogated traction force generation for HUVECs seeded on VE-cadherin:Fc-coated surfaces (**Figure 5.6**). This result is expected, as it confirms accepted knowledge in the field that ROCK is integral for cadherin-based adhesive strengthening. There was no statistical difference in traction force found for Y-27632-treated HUVECs seeded on Fc-coated surfaces as compared to control (**Figure 5.5**).

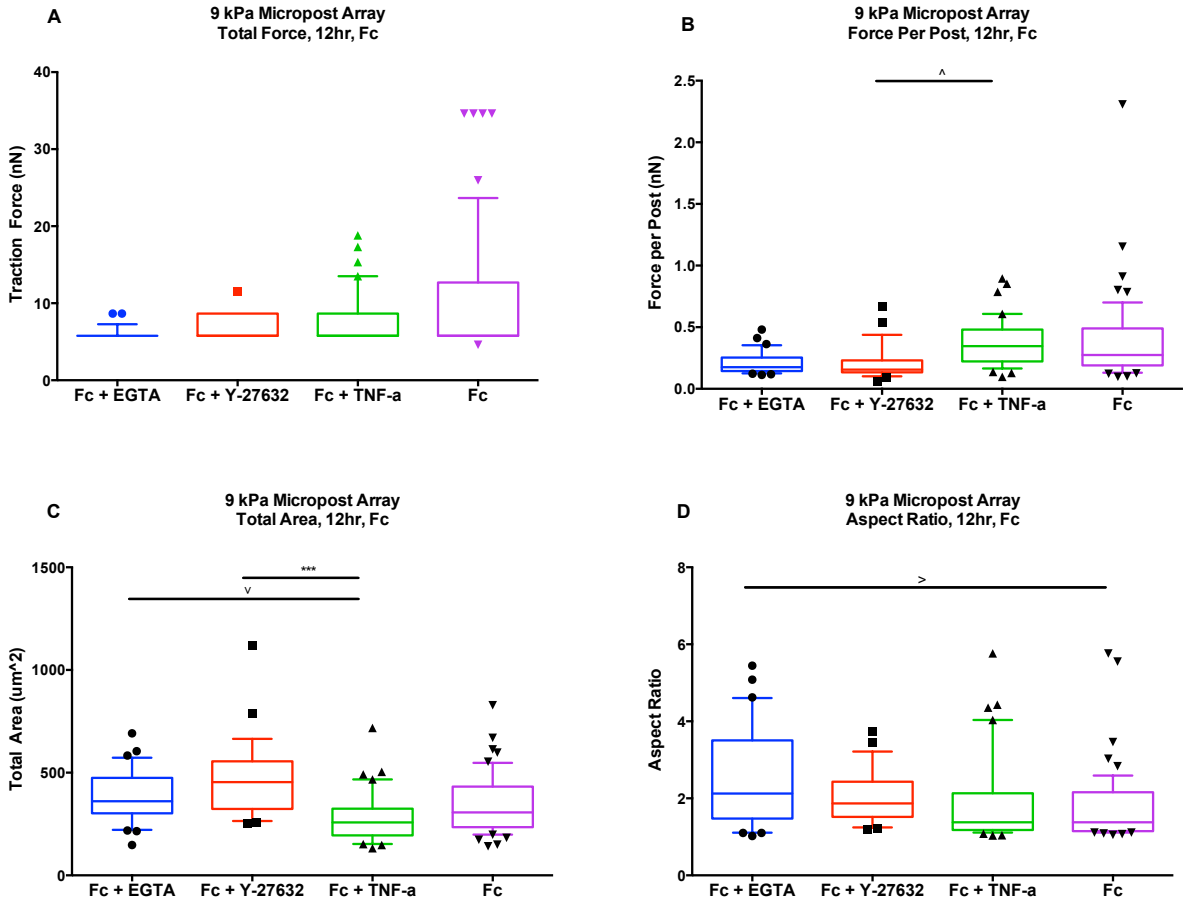

Figure 5. 5: Micro-fabricated post-array detector analyses for human umbilical vein endothelial cells (HUVECs) on human Fc fragment (or Fc-coated) surfaces, blocked with 0.2% Pluronics F-127, and 1% (w/v) 65°C heat-denatured BSA, and seeded at late times (12 hours). Cells were seeded on micro-fabricated post array detectors that were coated with VE-cadherin:Fc ligands or with Fc fragment at a concentration of 50 µg/mL, with both groups of cells allowed to adhere for 12 hours. At the 12th hour, cell were treated for 30 minutes with either 4mM EGTA (to elimate calcium binding), 10mM Y-27632 (to eliminate Rho kinase activity), or 10 ng/mL TNF-α (to induce endothelial cell stimulation) before quantitative analysis of post deflections using the

confocal microscopy and MATLAB analysis. A) – D) Box-whisker plot (mean, 10th, 25th, 75th, and 90th percentile) for traction force (> 25 cells per condition).

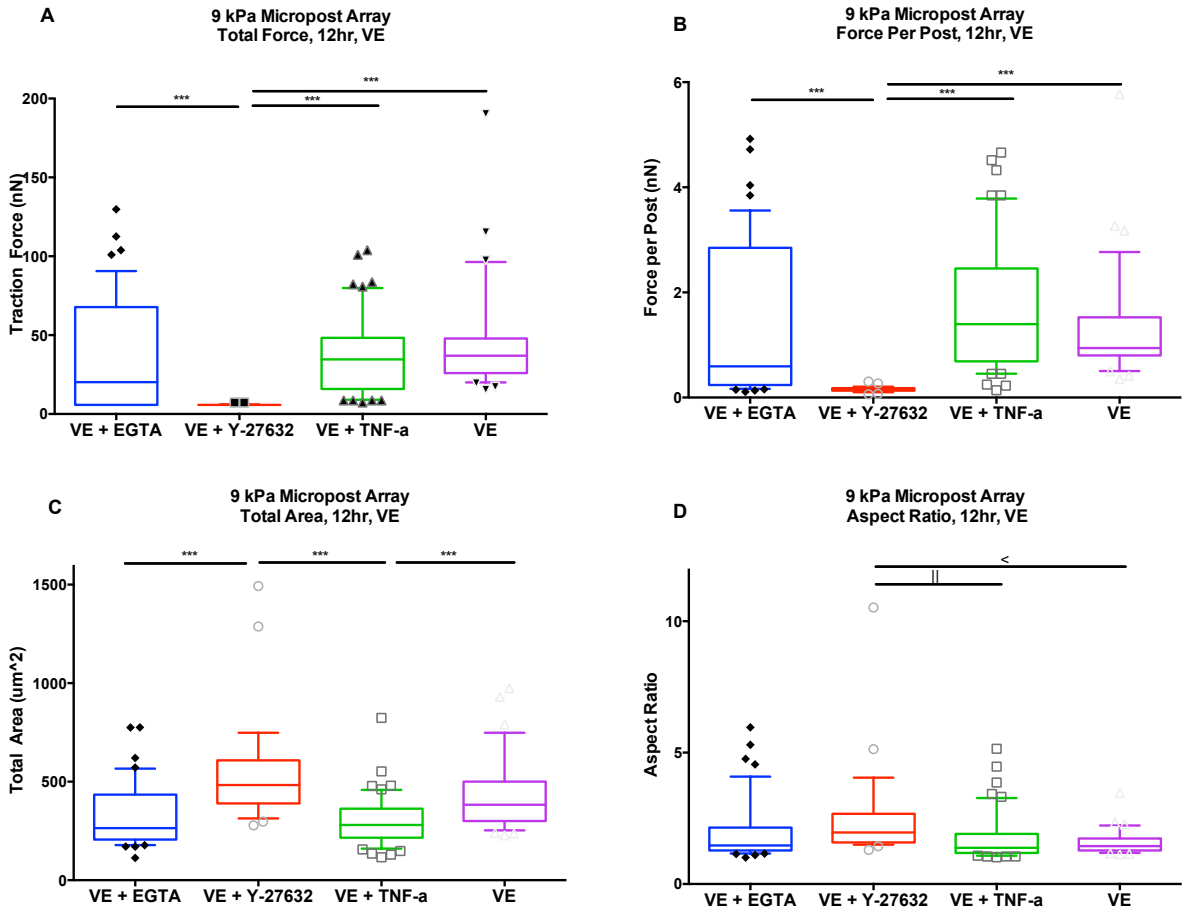

Figure 5. 6: Micro-fabricated post-array detector analyses for human umbilical vein endothelial cells (HUVECs) on human Fc fragment (or Fc-coated) surfaces, blocked with 0.2% Pluronics F-127, and 1% (w/v) 65°C heat-denatured BSA, and seeded at late times (12 hours). Cells were seeded on micro-fabricated post array detectors that were coated with VE-cadherin:Fc ligands or with Fc fragment at a concentration of 50 µg/mL, with both groups of cells allowed to adhere for 12 hours. At the 12th hour, cell were treated for 30 minutes with either 4mM EGTA (to elimate calcium binding), 10mM Y-27632 (to eliminate Rho kinase activity), or 10 ng/mL TNF-α (to induce endothelial cell stimulation) before quantitative analysis of post deflections using the confocal microscopy and MATLAB analysis. A) – D) Box-whisker plot (mean, 10th, 25th, 75th, and 90th percentile) for traction force (> 25 cells per condition).

5.5. Conclusion

Huveneers et al report the existence of focal adherens junctions, in which VE-cadherin-marked cell-cell junctions have vinculin and are contacted by radial F-actin bundles [242]. At these junctions that are actively being remodeled, VE-cadherin localizes perpendicularly to the rear of the migrating cells that also pull on the corresponding junction of non-migrating cells. Furthermore, VE-cadherin attaches to the radial actin bundles of both cells. As junctions have been shown to be tightly regulated by endothelial permeability, and in turn affected by chemical signals such as TNF, we sought to investigate the VE-cadherin-dependent changes in adhesive force by stimulating endothelial cells with TNF, an inducer of endothelial cell elongation and alignment. We investigated traction forces based on treatment by TNF, Y-27632, a Rho kinase inhibitor, and EGTA, a calcium-binding inhibitor. We found no differences in traction force upon TNF treatment and decreases in traction force upon Y-27632 treatment. We recognize that the interplay between TNF-induced endothelial permeability and TNF-induced actomyosin contractility (and subsequent formation of the focal adherens junction) lends itself to a complexity of cell signaling cross-talk. We expect that over time, traction forces due to TNF treatment will decrease as cells complete their junctional remodeling to increase vascular permeability. Future studies with longer durations of TNF treatment are necessary to completely explore VE-cadherin-ependent changes in traction forces.

CHAPTER VI: SUMMARY AND FUTURE DIRECTIONS

Cell adhesion is a critical determinant of tissue architecture and tissue organization. Cadherin proteins mediate cell-cell adhesion in a calcium-dependent manner. The functional roles for cadherin proteins early in development and in adults, as well as the multiple disease phenotypes resulting from cadherin dysregulation underscore the importance of cadherin proteins. Quantitative assessment of cadherin interaction structure, interaction dynamics, and force is not yet completely understood because of lack of experimental platforms to study cadherin proteins as well as their often-conflicting roles in a tissue-specific manner. Adhesive force measurements promise to meet this challenge of elucidating how cadherin complex assembly and function progresses in a spatiotemporal manner in human health and disease.

Specifically, cadherin adhesion can be thought of as a two-step process in which initial binding occurs and subsequent force generation occurs. Cadherin proteins form many bonds with different functions and bind catenin proteins, which help stabilize the cadherin complex and connect it to the cytoskeletal network. Consensus for quantitative force measurement data for cadherin proteins has been slow in coming. Indeed, the utility of a cohesive model for how cadherin mechanotransduction occurs is limited to a synthesis of data across robust experimental platforms.

The goal of this thesis was to engineer adhesive surfaces that support cadherin-based adhesive force. We engineered two different types of surfaces that present isolated and purified VE-cadherin ligands, namely, self-assembled monolayers of alkanethiols on gold surfaces as well as micro-fabricated post-array detectors. Adhesive force generation is important for regulating tissue function and tissue architecture.

To investigate the influence of ligand density and contact time on adhesion strength, we engineered surfaces passively adsorbed with VE-cadherin. We then evaluated adhesion strength values based on these variables. Perturbation of cadherin binding using functional blocking antibodies or calcium chelators abrogated adhesion strength. We then measured intracellular traction forces for VE-cadherin-expressing Chinese Hamster Ovary (CHO) cells and compared these force measurements against wild-type CHO cells. Adhesion strength values for these two populations were not statistically different, despite verification of endogenous cadherin levels by quantitative flow cytometry. mPAD analyses of traction forces for VE-cadherin-expressing Chinese Hamster Ovary (CHO) cells and wild-type CHO cells also show unexpected results. The rationale for choosing these cells was that we could express VE-cadherin in a system that does not normally express cadherin proteins. We explored several possibilities for these results, including the existence of endogenous cadherins or other adhesion molecules that could confound results and incorporated several blocking agents to eliminate the non-specific adsorption of proteins on our engineered surfaces. Another explanation is that as these cells do not normally express cadherins, they may be missing important intracellular components that may affect adhesion dynamics. Ultimately, we decided to investigate the traction forces of human umbilical vein endothelial cells (HUVECs) at early (6 hours) and late times (12 hours) in response to their interaction with our purified cadherin ligands as compared to human Fc-fragment-coated surfaces. We saw consistent increases in traction force between traction force and force per post measurement of HUVECs on our VE-cadherin-coated surfaces as compared to Fc-coated surfaces at early and late times, with additional increases in spread area observed between the two surfaces at 12 hours. When we treat with Y-27632, a Rho kinase inhibitor, traction forces are eliminated, corroborating other studies that implicate ROCK and other Rho

kinases in the formation and stability of adherens junctions. Treatment with TNF showed increases in traction forces, although the duration of treatment (30 minutes) was short compared to other times reported (24 hours) for the full effect of TNF stimulation of endothelial cells. Longer treatment is necessary to fully investigate the effects of TNF on cadherin-dependent traction forces.

The novelty of this work is that it is, to our knowledge, the first type of its kind to detail differences in traction forces for cadherin-specific interactions on surfaces coated with cadherin proteins and not ECM proteins like fibronectin [247]. Previous studies using mPADs typically used fibronectin proteins to coat the surfaces of the mPAD, utilizing NIH 3T3 fibroblasts to conduct traction force measurements [189, 190, 248-252]. Experiments using endothelial cells have used confluent monolayers of HUVECs, also seeded on high concentration of fibronectin proteins to evaluate "cadherin-based" adhesive forces. To date, only one paper utilized cadherin proteins to decorate the surface before cell seeding, but the authors cited concerns about coating density, cell crawling between posts and beneath the top of posts, as well as multi-cellular cell masses [253]. Unlike previous work, we use purified cadherin proteins to mediate cell-ligand adhesion. Moreover, our cells are well spread, and induce higher levels of traction forces (mean traction forces ~ 50 nN as compared to 15 nN) than Ganz's paper. It must be noted that the Ganz paper utilized N-cadherin ligands with C2 cells and not VE-cadherin with HUVECs, so traction force comparisons are limited in scope. We also use extensive controls, and we include Fc-coated surfaces as comparison, showing that Fc-coated surfaces have lower traction forces at both early (6 hours) and late (12 hours) times. Although we see no differences in aspect ratio for untreated cells and see increased aspect ratio for Y-27632-treated cells, recent work from the Pruitt and Nelson labs spatially controlled the patterning of cell pairs on collagen-coated

polyacrylamide gels and measured cell-cell and cell-ECM traction forces as a function of the aspect ratio of the cell [254]. The goal of the Nelson and Pruitt lab team was to investigate whether cell spread area and shape regulate the force balance in pairs of cells and what effect this had on E-cadherin load bearing. By enforcing cell spread area (and ECM protein deposition) through micro-patterning and modulating aspect ratio, they were able to observe that total force and strain energies correlated strongly with cell spread area, as expected. However, E-cadherin tension remained constant independent of cell spread area, total traction force, or force balance, implying that junctions regulate their length and regulate E-cadherin density as force balance is varied. It would be intriguing to constrain cadherin distribution and to measure concomitant increases in the distribution of traction forces or post deflections and correlate those to enrichment of cadherin complex proteins at the distal ends of the cell. Mertz et al conducted an experiment for differing numbers of cells on thin films coated with fibronectin seeded with wild-type primary keratinocytes and found the localization of traction stresses to the periphery for strong E-cadherin-ased adhesions [255].

This work is significant because it provides two validated and complimentary platforms for studying cadherin-based adhesion phenomena corresponding to larger force regimes (as compared to micromanipulation experiments) and longer times (as compared to timescales of minutes). Future studies should incorporate long-term treatment of hormones that mediate endothelial cell permeability, actomyosin contractility, and focal adherens junction formation while measuring traction forces in real-time, in order to elucidate the temporal and cadherin-dependent changes in force and cell morphology. Of note, these platforms could be used to study cellular trafficking events and how trafficking dynamics affect traction force and adhesive strength generation. Recent reviews have elucidated clear regulatory pathways delineating

cadherin trafficking, including endocytic pathways, degradation, and recycling [197, 256]. Reagents such as cells and protein mutants and specific chemical regulators of endocytic pathways can be used to modulate cadherin trafficking and see how that affects adhesive forces in real-time [257-262]. For future studies with mPADs, additional specificity for cadherin-based adhesive force generation could be added by using fluorophore-conjugated VE-cadherin proteins or tension sensors. Furthermore, tension-sensing studies could be another complimentary approach to the measurement of cadherin-mediated force dynamics. Additional studies include studying 3D-adhesive force studies (using hydrogels or bead-embedded matrices), or magnetic twisting cytometry to probe how active force loading modulates cadherin-based adhesion.

REFERENCES

1. Leckband, D., *Beyond structure: mechanism and dynamics of intercellular adhesion.* Biochemical Society Transactions, 2008. **36**: p. 213-220.
2. Gallant, N.D., K.E. Michael, and A.J. Garcia, *Cell adhesion strengthening: contributions of adhesive area, integrin binding, and focal adhesion assembly.* Mol Biol Cell, 2005. **16**(9): p. 4329-40.
3. Kowalczyk, A.P., et al., *Structure and function of desmosomal transmembrane core and plaque molecules.* Biophys Chem, 1994. **50**(1-2): p. 97-112.
4. Vincent, P.A., et al., *VE-cadherin: adhesion at arm's length.* Am J Physiol Cell Physiol, 2004. **286**(5): p. C987-97.
5. Delva, E., D.K. Tucker, and A.P. Kowalczyk, *The desmosome.* Cold Spring Harb Perspect Biol, 2009. **1**(2): p. a002543.
6. Delva, E. and A.P. Kowalczyk, *Regulation of cadherin trafficking.* Traffic, 2009. **10**(3): p. 259-67.
7. Lotz, M.M., et al., *Cell adhesion to fibronectin and tenascin: quantitative measurements of initial binding and subsequent strengthening response.* J Cell Biol, 1989. **109**(4 Pt 1): p. 1795-805.
8. Bershadsky, A.D., N.Q. Balaban, and B. Geiger, *Adhesion-dependent cell mechanosensitivity.* Annu Rev Cell Dev Biol, 2003. **19**: p. 677-95.
9. Yamada, S., et al., *Deconstructing the cadherin-catenin-actin complex.* Cell, 2005. **123**(5): p. 889-901.
10. Takeichi, M., *Morphogenetic roles of classic cadherins.* Curr Opin Cell Biol, 1995. **7**(5): p. 619-27.
11. Gumbiner, B.M. and K.M. Yamada, *Cell-to-cell contact and extracellular matrix.* Curr Opin Cell Biol, 1995. **7**(5): p. 615-8.
12. Discher, D.E., P. Janmey, and Y.L. Wang, *Tissue cells feel and respond to the stiffness of their substrate.* Science, 2005. **310**(5751): p. 1139-43.
13. Vogel, V. and M. Sheetz, *Local force and geometry sensing regulate cell functions.* Nat Rev Mol Cell Biol, 2006. **7**(4): p. 265-75.
14. Lecuit, T., *Adhesion remodeling underlying tissue morphogenesis.* Trends Cell Biol, 2005. **15**(1): p. 34-42.
15. Kumar, S. and V.M. Weaver, *Mechanics, malignancy, and metastasis: the force journey of a tumor cell.* Cancer Metastasis Rev, 2009. **28**(1-2): p. 113-27.
16. Zaidel-Bar, R., et al., *Functional atlas of the integrin adhesome.* Nat Cell Biol, 2007. **9**(8): p. 858-67.
17. Dubash, A.D., et al., *Chapter 1. Focal adhesions: new angles on an old structure.* Int Rev Cell Mol Biol, 2009. **277**: p. 1-65.
18. Izzard, C.S. and L.R. Lochner, *Formation of cell-to-substrate contacts during fibroblast motility: an interference-reflexion study.* J Cell Sci, 1980. **42**: p. 81-116.
19. Zaidel-Bar, R., et al., *Hierarchical assembly of cell-matrix adhesion complexes.* Biochem Soc Trans, 2004. **32**(Pt3): p. 416-20.
20. Zaidel-Bar, R. and B. Geiger, *The switchable integrin adhesome.* J Cell Sci, 2010. **123**(Pt 9): p. 1385-8.

21. Dumbauld, D.W., et al., *Contractility modulates cell adhesion strengthening through focal adhesion kinase and assembly of vinculin-containing focal adhesions.* J Cell Physiol, 2010. **223**(3): p. 746-756.
22. Prakasam, A.K., V. Maruthamuthu, and D.E. Leckband, *Similarities between heterophilic and homophilic cadherin adhesion.* Proceedings of the National Academy of Sciences of the United States of America, 2006. **103**(42): p. 15434-15439.
23. Chu, Y.S., et al., *Force measurements in E-cadherin-mediated cell doublets reveal rapid adhesion strengthened by actin cytoskeleton remodeling through Rac and Cdc42.* J Cell Biol, 2004. **167**(6): p. 1183-94.
24. Caplan, M.J., P. Seo-Mayer, and L. Zhang, *Epithelial junctions and polarity: complexes and kinases.* Curr Opin Nephrol Hypertens, 2008. **17**(5): p. 506-12.
25. Giepmans, B.N. and S.C. van Ijzendoorn, *Epithelial cell-cell junctions and plasma membrane domains.* Biochim Biophys Acta, 2009. **1788**(4): p. 820-31.
26. Yap, A.S., C.M. Niessen, and B.M. Gumbiner, *The juxtamembrane region of the cadherin cytoplasmic tail supports lateral clustering, adhesive strengthening, and interaction with p120ctn.* J Cell Biol, 1998. **141**(3): p. 779-89.
27. Halbleib, J.M. and W.J. Nelson, *Cadherins in development: cell adhesion, sorting, and tissue morphogenesis.* Genes Dev, 2006. **20**(23): p. 3199-214.
28. Takeichi, M., *Cadherins: key molecules for selective cell-cell adhesion.* IARC Sci Publ, 1988(92): p. 76-9.
29. Steinberg, M.S. and S.F. Gilbert, *Townes and Holtfreter (1955): directed movements and selective adhesion of embryonic amphibian cells.* J Exp Zool A Comp Exp Biol, 2004. **301**(9): p. 701-6.
30. Steinberg, M.S. and P.M. McNutt, *Cadherins and their connections: adhesion junctions have broader functions.* Curr Opin Cell Biol, 1999. **11**(5): p. 554-60.
31. Steinberg, M.S. and M. Takeichi, *Experimental Specification of Cell Sorting, Tissue Spreading, and Specific Spatial Patterning by Quantitative Differences in Cadherin Expression.* Proceedings of the National Academy of Sciences of the United States of America, 1994. **91**(1): p. 206-209.
32. Bacac, M. and I. Stamenkovic, *Metastatic cancer cell.* Annu Rev Pathol, 2008. **3**: p. 221-47.
33. Huber, O., *Structure and function of desmosomal proteins and their role in development and disease.* Cell Mol Life Sci, 2003. **60**(9): p. 1872-90.
34. McKoy, G., et al., *Identification of a deletion in plakoglobin in arrhythmogenic right ventricular cardiomyopathy with palmoplantar keratoderma and woolly hair (Naxos disease).* Lancet, 2000. **355**(9221): p. 2119-2124.
35. Huang, H., et al., *Disparate effects of different mutations in plakoglobin on cell mechanical behavior.* Cell Motil Cytoskeleton, 2008. **65**(12): p. 964-78.
36. Lai-Cheong, J.E., K. Arita, and J.A. McGrath, *Genetic diseases of junctions.* Journal of Investigative Dermatology, 2007. **127**(12): p. 2713-2725.
37. Venkiteswaran, K., et al., *Regulation of endothelial barrier function and growth by VE-cadherin, plakoglobin, and beta-catenin.* American Journal of Physiology-Cell Physiology, 2002. **283**(3): p. C811-C821.
38. Xiao, K., et al., *Role of p120-catenin in cadherin trafficking.* Biochimica Et Biophysica Acta-Molecular Cell Research, 2007. **1773**(1): p. 8-16.

39. Guo, W. and F.G. Giancotti, *Integrin signalling during tumour progression.* Nat Rev Mol Cell Biol, 2004. **5**(10): p. 816-26.
40. Powell, K., *The sticky business of discovering cadherins.* The Journal of Cell Biology, 2005. **170**(4): p. 514.
41. Takeichi, M., *Functional correlation between cell adhesive properties and some cell surface proteins.* J Cell Biol, 1977. **75**(2 Pt 1): p. 464-74.
42. Matsuyoshi, N., et al., *Cadherin-mediated cell-cell adhesion is perturbed by v-src tyrosine phosphorylation in metastatic fibroblasts.* J Cell Biol, 1992. **118**(3): p. 703-14.
43. Hatta, K., et al., *Cloning and expression of cDNA encoding a neural calcium-dependent cell adhesion molecule: its identity in the cadherin gene family.* J Cell Biol, 1988. **106**(3): p. 873-81.
44. Hirano, S., et al., *Calcium-dependent cell-cell adhesion molecules (cadherins): subclass specificities and possible involvement of actin bundles.* J Cell Biol, 1987. **105**(6 Pt 1): p. 2501-10.
45. Cavey, M. and T. Lecuit, *Molecular Bases of Cell-Cell Junctions Stability and Dynamics.* Cold Spring Harbor Perspectives in Biology, 2009. **1**(5): p. -.
46. Amagai, M., et al., *Delayed assembly of desmosomes in keratinocytes with disrupted classic-cadherin-mediated cell adhesion by a dominant negative mutant.* J Invest Dermatol, 1995. **104**(1): p. 27-32.
47. Leckband, D., et al., *Molecular forces in cadherin adhesion: Forces mediating the assembly of cell-cell adherens junctions.* Abstracts of Papers of the American Chemical Society, 1998. **216**: p. U264-U264.
48. Nollet, F., P. Kools, and F. van Roy, *Phylogenetic analysis of the cadherin superfamily allows identification of six major subfamilies besides several solitary members.* J Mol Biol, 2000. **299**(3): p. 551-72.
49. El-Amraoui, A. and C. Petit, *Cadherin defects in inherited human diseases.* Prog Mol Biol Transl Sci, 2013. **116**: p. 361-84.
50. Pokutta, S., et al., *Conformational changes of the recombinant extracellular domain of E-cadherin upon calcium binding.* Eur J Biochem, 1994. **223**(3): p. 1019-26.
51. Koch, A.W., et al., *Calcium binding and homoassociation of E-cadherin domains.* Biochemistry, 1997. **36**(25): p. 7697-705.
52. Larue, L., et al., *E-cadherin null mutant embryos fail to form a trophectoderm epithelium.* Proc Natl Acad Sci U S A, 1994. **91**(17): p. 8263-7.
53. Butz, S. and L. Larue, *Expression of catenins during mouse embryonic development and in adult tissues.* Cell Adhes Commun, 1995. **3**(4): p. 337-52.
54. Larue, L., et al., *A role for cadherins in tissue formation.* Development, 1996. **122**(10): p. 3185-94.
55. Urushihara, H. and M. Takeichi, *Cell-cell adhesion molecule: identification of a glycoprotein relevant to the Ca2+-independent aggregation of Chinese hamster fibroblasts.* Cell, 1980. **20**(2): p. 363-71.
56. Takeichi, M., *The cadherins: cell-cell adhesion molecules controlling animal morphogenesis.* Development, 1988. **102**(4): p. 639-55.
57. Fidler, L.M., et al., *Abnormal connexin43 in arrhythmogenic right ventricular cardiomyopathy caused by plakophilin-2 mutations.* Journal of Cellular and Molecular Medicine, 2009. **13**(10): p. 4219-4228.

58. Asimaki, A., et al., *A novel dominant mutation in plakoglobin causes Arrhythmogenic right ventricular cardiomyopathy.* American Journal of Human Genetics, 2007. **81**(5): p. 964-973.
59. Stemmler, M.P., *Cadherins in development and cancer.* Mol Biosyst, 2008. **4**(8): p. 835-50.
60. Boda-Heggemann, J., A. Regnier-Vigouroux, and W.W. Franke, *Beyond vessels: occurrence and regional clustering of vascular endothelial (VE-)cadherin-containing junctions in non-endothelial cells.* Cell and Tissue Research, 2009. **335**(1): p. 49-65.
61. Reinhold, W.C., et al., *Multifactorial regulation of E-cadherin expression: an integrative study.* Mol Cancer Ther, 2010. **9**(1): p. 1-16.
62. Suzuki, S., K. Sano, and H. Tanihara, *Diversity of the cadherin family: evidence for eight new cadherins in nervous tissue.* Cell Regul, 1991. **2**(4): p. 261-70.
63. Vestweber, D., *Cadherins in tissue architecture and disease.* J Mol Med (Berl), 2015. **93**(1): p. 5-11.
64. Vestweber, D., *VE-cadherin: the major endothelial adhesion molecule controlling cellular junctions and blood vessel formation.* Arterioscler Thromb Vasc Biol, 2008. **28**(2): p. 223-32.
65. Lampugnani, M.G., et al., *A novel endothelial-specific membrane protein is a marker of cell-cell contacts.* J Cell Biol, 1992. **118**(6): p. 1511-22.
66. Breviario, F., et al., *Functional properties of human vascular endothelial cadherin (7B4/cadherin-5), an endothelium-specific cadherin.* Arterioscler Thromb Vasc Biol, 1995. **15**(8): p. 1229-39.
67. Breier, G., et al., *Molecular cloning and expression of murine vascular endothelial-cadherin in early stage development of cardiovascular system.* Blood, 1996. **87**(2): p. 630-41.
68. Huber, P., et al., *Genomic structure and chromosomal mapping of the mouse VE-cadherin gene (Cdh5).* Genomics, 1996. **32**(1): p. 21-8.
69. Dancer, A., et al., *Expression of thymidine kinase driven by an endothelial-specific promoter inhibits tumor growth of Lewis lung carcinoma cells in transgenic mice.* Gene Ther, 2003. **10**(14): p. 1170-8.
70. Gory-Faure, S., et al., *Role of vascular endothelial-cadherin in vascular morphogenesis.* Development, 1999. **126**(10): p. 2093-102.
71. Gory, S., et al., *The vascular endothelial-cadherin promoter directs endothelial-specific expression in transgenic mice.* Blood, 1999. **93**(1): p. 184-92.
72. Hisatsune, H., et al., *High level of endothelial cell-specific gene expression by a combination of the 5′ flanking region and the 5′ half of the first intron of the VE-cadherin gene.* Blood, 2005. **105**(12): p. 4657-63.
73. Gotsch, U., et al., *VE-cadherin antibody accelerates neutrophil recruitment in vivo.* J Cell Sci, 1997. **110 (Pt 5)**: p. 583-8.
74. Matsuyoshi, N., et al., *In vivo evidence of the critical role of cadherin-5 in murine vascular integrity.* Proc Assoc Am Physicians, 1997. **109**(4): p. 362-71.
75. Gulino, D., et al., *Alteration of endothelial cell monolayer integrity triggers resynthesis of vascular endothelium cadherin.* J Biol Chem, 1998. **273**(45): p. 29786-93.
76. Corada, M., et al., *Monoclonal antibodies directed to different regions of vascular endothelial cadherin extracellular domain affect adhesion and clustering of the protein and modulate endothelial permeability.* Blood, 2001. **97**(6): p. 1679-84.

77. Corada, M., et al., *Vascular endothelial-cadherin is an important determinant of microvascular integrity in vivo.* Proc Natl Acad Sci U S A, 1999. **96**(17): p. 9815-20.
78. Dejana, E., F. Orsenigo, and M.G. Lampugnani, *The role of adherens junctions and VE-cadherin in the control of vascular permeability.* Journal of Cell Science, 2008. **121**(13): p. 2115-2122.
79. Dejana, E., E. Tournier-Lasserve, and B.M. Weinstein, *The control of vascular integrity by endothelial cell junctions: molecular basis and pathological implications.* Dev Cell, 2009. **16**(2): p. 209-21.
80. Gray, K.A., et al., *Genenames.org: the HGNC resources in 2015.* Nucleic Acids Res, 2015. **43**(Database issue): p. D1079-85.
81. *HGCN Database, HUGO Gene Nomenclature Committee (HGNC), EMBL Outstationi - Hinxton, Euorpean Bioinformatics Institute, Wellcome Trust Genome Campus, Hinxton Cambridgeshire, CB10 1SD, UK* http://www.genenames.org. 2015.
82. Redies, C., N. Hertel, and C.A. Hubner, *Cadherins and neuropsychiatric disorders.* Brain Res, 2012. **1470**: p. 130-44.
83. El-Amraoui, A. and C. Petit, *Cadherins as targets for genetic diseases.* Cold Spring Harb Perspect Biol, 2010. **2**(1): p. a003095.
84. Takeichi, M., *Control of synaptic junction dynamics: Roles of the cadherin-catenin complex.* Journal of Neurochemistry, 2005. **94**: p. 1-1.
85. Takeichi, M., *Cadherin-controlled synaptic connections.* Neuroscience Research, 2006. **55**: p. S4-S4.
86. Tanabe, K., et al., *Cadherin is required for dendritic morphogenesis and synaptic terminal organization of retinal horizontal cells.* Development, 2006. **133**(20): p. 4085-4096.
87. Togashi, H. and M. Takeichi, *The roles of adhesion systems in inter-neuronal synapse formation.* Seikagaku, 2006. **78**(7): p. 615-621.
88. Kadowaki, M., et al., *N-cadherin mediates cortical organization in the mouse brain.* Developmental Biology, 2007. **304**(1): p. 22-33.
89. Suzuki, S.C., et al., *Cadherin-8 is required for the first relay synapses to receive functional inputs from primary sensory afferents for cold sensation.* Journal of Neuroscience, 2007. **27**(13): p. 3466-3476.
90. Takeichi, M., *The cadherin superfamily in neuronal connections and interactions.* Nature Reviews Neuroscience, 2007. **8**(1): p. 11-20.
91. Suzuki, S.C. and M. Takeichi, *Cadherins in neuronal morphogenesis and function.* Development Growth & Differentiation, 2008. **50**: p. S119-S130.
92. Sild, M., R.P. Chatelain, and E.S. Ruthazer, *Improved method for the quantification of motility in glia and other morphologically complex cells.* Neural Plast, 2013. **2013**: p. 853727.
93. Sild, M. and E.S. Ruthazer, *Radial glia: progenitor, pathway, and partner.* Neuroscientist, 2011. **17**(3): p. 288-302.
94. Hirano, S., S.T. Suzuki, and C. Redies, *The cadherin superfamily in neural development: diversity, function and interaction with other molecules.* Front Biosci, 2003. **8**: p. d306-55.
95. Hirano, S. and M. Takeichi, *Differential Expression of Alpha-N-Catenin and N-Cadherin during Early Development of Chicken Embryos.* International Journal of Developmental Biology, 1994. **38**(2): p. 379-384.

96. Hertel, N., C. Redies, and L. Medina, *Cadherin expression delineates the divisions of the postnatal and adult mouse amygdala.* J Comp Neurol, 2012. **520**(17): p. 3982-4012.
97. Krishna, K.K., N. Hertel, and C. Redies, *Cadherin expression in the somatosensory cortex: evidence for a combinatorial molecular code at the single-cell level.* Neuroscience, 2011. **175**: p. 37-48.
98. Hertel, N. and C. Redies, *Absence of layer-specific cadherin expression profiles in the neocortex of the reeler mutant mouse.* Cereb Cortex, 2011. **21**(5): p. 1105-17.
99. Krishna, K. and C. Redies, *Expression of cadherin superfamily genes in brain vascular development.* J Cereb Blood Flow Metab, 2009. **29**(2): p. 224-9.
100. Neudert, F., K.K. Nuernberger, and C. Redies, *Comparative analysis of cadherin expression and connectivity patterns in the cerebellar system of ferret and mouse.* J Comp Neurol, 2008. **511**(6): p. 736-52.
101. Neudert, F. and C. Redies, *Neural circuits revealed by axon tracing and mapping cadherin expression in the embryonic chicken cerebellum.* J Comp Neurol, 2008. **509**(3): p. 283-301.
102. Treubert-Zimmermann, U., D. Heyers, and C. Redies, *Targeting axons to specific fiber tracts in vivo by altering cadherin expression.* J Neurosci, 2002. **22**(17): p. 7617-26.
103. Korematsu, K. and C. Redies, *Restricted expression of cadherin-8 in segmental and functional subdivisions of the embryonic mouse brain.* Dev Dyn, 1997. **208**(2): p. 178-89.
104. Redies, C., K. Engelhart, and M. Takeichi, *Differential Expression of N-Cadherin and R-Cadherin in Functional Neuronal Systems and Other Structures of the Developing Chicken Brain.* Journal of Comparative Neurology, 1993. **333**(3): p. 398-416.
105. Redies, C. and M. Takeichi, *N- and R-cadherin expression in the optic nerve of the chicken embryo.* Glia, 1993. **8**(3): p. 161-71.
106. Arikkath, J., *N-cadherin: stabilizing synapses.* J Cell Biol, 2010. **189**(3): p. 397-8.
107. Arikkath, J., et al., *Delta-catenin regulates spine and synapse morphogenesis and function in hippocampal neurons during development.* J Neurosci, 2009. **29**(17): p. 5435-42.
108. Arikkath, J., *Regulation of dendrite and spine morphogenesis and plasticity by catenins.* Mol Neurobiol, 2009. **40**(1): p. 46-54.
109. Arikkath, J. and L.F. Reichardt, *Cadherins and catenins at synapses: roles in synaptogenesis and synaptic plasticity.* Trends Neurosci, 2008. **31**(9): p. 487-94.
110. Uhl, G.R., et al., *Genome-wide association for methamphetamine dependence.* Archives of General Psychiatry, 2008. **65**(3): p. 345-355.
111. Djabali, K., et al., *Evidence for extensive locus heterogeneity in Naxos disease.* Journal of Investigative Dermatology, 2002. **118**(3): p. 557-560.
112. Sahly, I., et al., *Localization of Usher 1 proteins to the photoreceptor calyceal processes, which are absent from mice.* J Cell Biol, 2012. **199**(2): p. 381-99.
113. van Roy, F., *Beyond E-cadherin: roles of other cadherin superfamily members in cancer.* Nat Rev Cancer, 2014. **14**(2): p. 121-34.
114. van Roy, F. and G. Berx, *The cell-cell adhesion molecule E-cadherin.* Cell Mol Life Sci, 2008. **65**(23): p. 3756-88.
115. Inge, L.J., et al., *Soluble E-cadherin promotes cell survival by activating epidermal growth factor receptor.* Exp Cell Res, 2011. **317**(6): p. 838-48.
116. Jeanes, A., C.J. Gottardi, and A.S. Yap, *Cadherins and cancer: how does cadherin dysfunction promote tumor progression?* Oncogene, 2008. **27**(55): p. 6920-9.

117. Berx, G. and F. van Roy, *Involvement of members of the cadherin superfamily in cancer.* Cold Spring Harb Perspect Biol, 2009. **1**(6): p. a003129.
118. Paredes, J., et al., *Epithelial E- and P-cadherins: role and clinical significance in cancer.* Biochim Biophys Acta, 2012. **1826**(2): p. 297-311.
119. De Craene, B. and G. Berx, *Regulatory networks defining EMT during cancer initiation and progression.* Nat Rev Cancer, 2013. **13**(2): p. 97-110.
120. Thiery, J.P. and C.T. Lim, *Tumor dissemination: an EMT affair.* Cancer Cell, 2013. **23**(3): p. 272-3.
121. Thiery, J.P., et al., *Epithelial-mesenchymal transitions in development and disease.* Cell, 2009. **139**(5): p. 871-90.
122. Lammens, T., et al., *N-cadherin in neuroblastoma disease: expression and clinical significance.* PLoS One, 2012. **7**(2): p. e31206.
123. Sanchez-Heras, E., et al., *The fibroblast growth factor receptor acid box is essential for interactions with N-cadherin and all of the major isoforms of neural cell adhesion molecule.* J Biol Chem, 2006. **281**(46): p. 35208-16.
124. Hazan, R.B., et al., *Cadherin switch in tumor progression.* Ann N Y Acad Sci, 2004. **1014**: p. 155-63.
125. Suyama, K., et al., *A signaling pathway leading to metastasis is controlled by N-cadherin and the FGF receptor.* Cancer Cell, 2002. **2**(4): p. 301-14.
126. Kotb, A.M., A. Hierholzer, and R. Kemler, *Replacement of E-cadherin by N-cadherin in the mammary gland leads to fibrocystic changes and tumor formation.* Breast Cancer Res, 2011. **13**(5): p. R104.
127. Libusova, L., et al., *N-cadherin can structurally substitute for E-cadherin during intestinal development but leads to polyp formation.* Development, 2010. **137**(14): p. 2297-305.
128. Derksen, P.W., et al., *Mammary-specific inactivation of E-cadherin and p53 impairs functional gland development and leads to pleomorphic invasive lobular carcinoma in mice.* Dis Model Mech, 2011. **4**(3): p. 347-58.
129. Derksen, P.W., et al., *Somatic inactivation of E-cadherin and p53 in mice leads to metastatic lobular mammary carcinoma through induction of anoikis resistance and angiogenesis.* Cancer Cell, 2006. **10**(5): p. 437-49.
130. Werling, A.M., et al., *Homo- and heterotypic cell-cell contacts in Merkel cells and Merkel cell carcinomas: heterogeneity and indications for cadherin switching.* Histopathology, 2011. **58**(2): p. 286-303.
131. Van Marck, V., et al., *P-cadherin promotes cell-cell adhesion and counteracts invasion in human melanoma.* Cancer Res, 2005. **65**(19): p. 8774-83.
132. Wheelock, M.J., et al., *Cadherin switching.* J Cell Sci, 2008. **121**(Pt 6): p. 727-35.
133. Bryan, R.T. and C. Tselepis, *Cadherin switching and bladder cancer.* J Urol, 2010. **184**(2): p. 423-31.
134. Van Marck, V., et al., *P-cadherin in adhesion and invasion: opposite roles in colon and bladder carcinoma.* Int J Cancer, 2011. **128**(5): p. 1031-44.
135. Ribeiro, A.S., et al., *Extracellular cleavage and shedding of P-cadherin: a mechanism underlying the invasive behaviour of breast cancer cells.* Oncogene, 2010. **29**(3): p. 392-402.

136. Paredes, J., et al., *Breast carcinomas that co-express E- and P-cadherin are associated with p120-catenin cytoplasmic localisation and poor patient survival.* J Clin Pathol, 2008. **61**(7): p. 856-62.
137. Cheung, L.W., et al., *P-cadherin cooperates with insulin-like growth factor-1 receptor to promote metastatic signaling of gonadotropin-releasing hormone in ovarian cancer via p120 catenin.* Oncogene, 2011. **30**(26): p. 2964-74.
138. Kucharczak, J., et al., *R-Cadherin expression inhibits myogenesis and induces myoblast transformation via Rac1 GTPase.* Cancer Res, 2008. **68**(16): p. 6559-68.
139. Agiostratidou, G., et al., *Loss of retinal cadherin facilitates mammary tumor progression and metastasis.* Cancer Res, 2009. **69**(12): p. 5030-8.
140. Shapiro, L. and W.I. Weis, *Structure and biochemistry of cadherins and catenins.* Cold Spring Harb Perspect Biol, 2009. **1**(3): p. a003053.
141. Zhang, Y., et al., *Resolving cadherin interactions and binding cooperativity at the single-molecule level.* Proc Natl Acad Sci U S A, 2009. **106**(1): p. 109-14.
142. Meng, W.X. and M. Takeichi, *Adherens Junction: Molecular Architecture and Regulation.* Cold Spring Harbor Perspectives in Biology, 2009. **1**(6): p. -.
143. Niessen, C.M., D. Leckband, and A.S. Yap, *Tissue organization by cadherin adhesion molecules: dynamic molecular and cellular mechanisms of morphogenetic regulation.* Physiol Rev, 2011. **91**(2): p. 691-731.
144. Petrova, Y.I., M.M. Spano, and B.M. Gumbiner, *Conformational epitopes at cadherin calcium-binding sites and p120-catenin phosphorylation regulate cell adhesion.* Mol Biol Cell, 2012. **23**(11): p. 2092-108.
145. Buckley, C.D., et al., *Cell adhesion. The minimal cadherin-catenin complex binds to actin filaments under force.* Science, 2014. **346**(6209): p. 1254211.
146. Pokutta, S., et al., *Structural and thermodynamic characterization of cadherin.beta-catenin.alpha-catenin complex formation.* J Biol Chem, 2014. **289**(19): p. 13589-601.
147. Hansen, S.D., et al., *alphaE-catenin actin-binding domain alters actin filament conformation and regulates binding of nucleation and disassembly factors.* Mol Biol Cell, 2013. **24**(23): p. 3710-20.
148. Miller, P.W., et al., *Danio rerio alphaE-catenin is a monomeric F-actin binding protein with distinct properties from Mus musculus alphaE-catenin.* J Biol Chem, 2013. **288**(31): p. 22324-32.
149. Rimm, D.L., et al., *Alpha 1(E)-catenin is an actin-binding and -bundling protein mediating the attachment of F-actin to the membrane adhesion complex.* Proc Natl Acad Sci U S A, 1995. **92**(19): p. 8813-7.
150. Borghi, N., et al., *E-cadherin is under constitutive actomyosin-generated tension that is increased at cell-cell contacts upon externally applied stretch.* Proc Natl Acad Sci U S A, 2012. **109**(31): p. 12568-73.
151. Drees, F., et al., *Alpha-catenin is a molecular switch that binds E-cadherin-beta-catenin and regulates actin-filament assembly.* Cell, 2005. **123**(5): p. 903-15.
152. Choi, H.J., et al., *alphaE-catenin is an autoinhibited molecule that coactivates vinculin.* Proc Natl Acad Sci U S A, 2012. **109**(22): p. 8576-81.
153. Yonemura, S., et al., *alpha-Catenin as a tension transducer that induces adherens junction development.* Nat Cell Biol, 2010. **12**(6): p. 533-42.
154. Leckband, D.E. and J. de Rooij, *Cadherin adhesion and mechanotransduction.* Annu Rev Cell Dev Biol, 2014. **30**: p. 291-315.

155. Leckband, D.E., et al., *Mechanotransduction at cadherin-mediated adhesions.* Curr Opin Cell Biol, 2011. **23**(5): p. 523-30.
156. Leckband, D. and A. Prakasam, *Mechanism and dynamics of cadherin adhesion.* Annu Rev Biomed Eng, 2006. **8**: p. 259-87.
157. Prakasam, A., et al., *Calcium site mutations in cadherin: impact on adhesion and evidence of cooperativity.* Biochemistry, 2006. **45**(22): p. 6930-9.
158. Prakasam, A.K., V. Maruthamuthu, and D.E. Leckband, *Similarities between heterophilic and homophilic cadherin adhesion.* Proc Natl Acad Sci U S A, 2006. **103**(42): p. 15434-9.
159. Leckband, D. and S. Sivasankar, *Biophysics of cadherin adhesion.* Subcell Biochem, 2012. **60**: p. 63-88.
160. Shi, Q., et al., *Allosteric cross talk between cadherin extracellular domains.* Biophys J, 2010. **99**(1): p. 95-104.
161. Fredette, B.J. and B. Ranscht, *T-cadherin expression delineates specific regions of the developing motor axon-hindlimb projection pathway.* J Neurosci, 1994. **14**(12): p. 7331-46.
162. Ranscht, B. and M.T. Dours-Zimmermann, *T-cadherin, a novel cadherin cell adhesion molecule in the nervous system lacks the conserved cytoplasmic region.* Neuron, 1991. **7**(3): p. 391-402.
163. Ciatto, C., et al., *T-cadherin structures reveal a novel adhesive binding mechanism.* Nat Struct Mol Biol, 2010. **17**(3): p. 339-47.
164. Rakshit, S., et al., *Ideal, catch, and slip bonds in cadherin adhesion.* Proc Natl Acad Sci U S A, 2012. **109**(46): p. 18815-20.
165. Leckband, D. and S. Sivasankar, *Cadherin recognition and adhesion.* Curr Opin Cell Biol, 2012. **24**(5): p. 620-7.
166. Hong, S., R.B. Troyanovsky, and S.M. Troyanovsky, *Cadherin exits the junction by switching its adhesive bond.* J Cell Biol, 2011. **192**(6): p. 1073-83.
167. Rakshit, S. and S. Sivasankar, *Biomechanics of cell adhesion: how force regulates the lifetime of adhesive bonds at the single molecule level.* Phys Chem Chem Phys, 2014. **16**(6): p. 2211-23.
168. Barry, A.K., et al., *alpha-catenin cytomechanics--role in cadherin-dependent adhesion and mechanotransduction.* J Cell Sci, 2014. **127**(Pt 8): p. 1779-91.
169. Chien, Y.H., et al., *Two stage cadherin kinetics require multiple extracellular domains but not the cytoplasmic region.* Journal of Biological Chemistry, 2008. **283**(4): p. 1848-1856.
170. Tabdili, H., et al., *Cadherin point mutations alter cell sorting and modulate GTPase signaling.* J Cell Sci, 2012. **125**(Pt 14): p. 3299-309.
171. Tabdili, H., et al., *Cadherin-dependent mechanotransduction depends on ligand identity but not affinity.* J Cell Sci, 2012. **125**(Pt 18): p. 4362-71.
172. Harrison, O.J., et al., *The extracellular architecture of adherens junctions revealed by crystal structures of type I cadherins.* Structure, 2011. **19**(2): p. 244-56.
173. Haussinger, D., et al., *Calcium-dependent homoassociation of E-cadherin by NMR spectroscopy: changes in mobility, conformation and mapping of contact regions.* J Mol Biol, 2002. **324**(4): p. 823-39.

174. Garcia, A.J. and N.D. Gallant, *Stick and grip: measurement systems and quantitative analyses of integrin-mediated cell adhesion strength.* Cell Biochem Biophys, 2003. **39**(1): p. 61-73.
175. Chyasnavichyus, M.Y., Seth L.; Tsukruk, Vladimir V. , *Recent advances in micromechanical characterization of polymer, biomaterial, and cell surfaces with atomic force microscopy.* Japanese Journal of Applied Physics, 2015. **54**(852): p. 1-13.
176. Leckband, D.E., et al., *Direct measurements of multiple adhesive alignments between cadherin extracellular domains.* Biophysical Journal, 2001. **80**(1): p. 153a-153a.
177. Leckband, D., *Molecular mechanisms of cell adhesion: New perspectives from surface force measurements.* Journal of Adhesion, 2004. **80**(5): p. 409-432.
178. Bayas, M.V., et al., *Lifetime measurements reveal kinetic differences between homophilic cadherin bonds.* Biophysical Journal, 2006. **90**(4): p. 1385-1395.
179. Leckband, D. and A. Prakasam, *Mechanism and dynamics of cadherin adhesion.* Annual Review of Biomedical Engineering, 2006. **8**: p. 259-287.
180. Leckband, D., *From Single Molecules to Living Cells: Nanomechanical Measurements of Cell Adhesion.* Cellular and Molecular Bioengineering, 2008. **1**(4): p. 312-326.
181. Shi, Q.M., et al., *Allosteric Cross Talk between Cadherin Extracellular Domains.* Biophysical Journal, 2010. **99**(1): p. 95-104.
182. le Duc, Q., et al., *Vinculin potentiates E-cadherin mechanosensing and is recruited to actin-anchored sites within adherens junctions in a myosin II-dependent manner.* J Cell Biol, 2010. **189**(7): p. 1107-15.
183. Sivasankar, S., B. Gumbiner, and D. Leckband, *Direct measurements of multiple adhesive alignments and unbinding trajectories between cadherin extracellular domains.* Biophysical Journal, 2001. **80**(4): p. 1758-1768.
184. Bajpai, S., et al., *Loss of alpha-Catenin Decreases the Strength of Single E-cadherin Bonds between Human Cancer Cells.* Journal of Biological Chemistry, 2009. **284**(27): p. 18252-18259.
185. Garcia, A.J., P. Ducheyne, and D. Boettiger, *Quantification of cell adhesion using a spinning disc device and application to surface-reactive materials.* Biomaterials, 1997. **18**(16): p. 1091-8.
186. Garcia, A.J., J. Takagi, and D. Boettiger, *Two-stage activation for alpha5beta1 integrin binding to surface-adsorbed fibronectin.* J Biol Chem, 1998. **273**(52): p. 34710-5.
187. Michael, K.E. and A.J. Garcia, *Cell adhesion strengthening: measurement and analysis.* Methods Cell Biol, 2007. **83**: p. 329-46.
188. Christ, K.V., et al., *Measurement of single-cell adhesion strength using a microfluidic assay.* Biomed Microdevices, 2010.
189. Sniadecki, N.J., et al., *Micropatterning on micropost arrays.* Methods Cell Biol, 2014. **121**: p. 61-73.
190. Han, S.J., et al., *Decoupling substrate stiffness, spread area, and micropost density: a close spatial relationship between traction forces and focal adhesions.* Biophys J, 2012. **103**(4): p. 640-8.
191. Pokutta, S. and W.I. Weis, *Structure and mechanism of cadherins and catenins in cell-cell contacts.* Annu Rev Cell Dev Biol, 2007. **23**: p. 237-61.
192. Nelson, W.J., *Regulation of cell-cell adhesion by the cadherin-catenin complex.* Biochem Soc Trans, 2008. **36**(Pt 2): p. 149-55.

193. Davis, M.A., R.C. Ireton, and A.B. Reynolds, *A core function for p120-catenin in cadherin turnover.* J Cell Biol, 2003. **163**(3): p. 525-34.
194. Xiao, K., et al., *Cellular levels of p120 catenin function as a set point for cadherin expression levels in microvascular endothelial cells.* J Cell Biol, 2003. **163**(3): p. 535-45.
195. Xiao, K., et al., *p120-Catenin regulates clathrin-dependent endocytosis of VE-cadherin.* Mol Biol Cell, 2005. **16**(11): p. 5141-51.
196. Chiasson, C.M., et al., *p120-catenin inhibits VE-cadherin internalization through a Rho-independent mechanism.* Mol Biol Cell, 2009. **20**(7): p. 1970-80.
197. Nanes, B.A., et al., *p120-catenin binding masks an endocytic signal conserved in classical cadherins.* J Cell Biol, 2012. **199**(2): p. 365-80.
198. Cattelino, A., et al., *The conditional inactivation of the beta-catenin gene in endothelial cells causes a defective vascular pattern and increased vascular fragility.* J Cell Biol, 2003. **162**(6): p. 1111-22.
199. Oas, R.G., et al., *p120-Catenin is required for mouse vascular development.* Circ Res, 2010. **106**(5): p. 941-51.
200. Goodwin, M., et al., *Minimal mutation of the cytoplasmic tail inhibits the ability of E-cadherin to activate Rac but not phosphatidylinositol 3-kinase: direct evidence of a role for cadherin-activated Rac signaling in adhesion and contact formation.* J Biol Chem, 2003. **278**(23): p. 20533-9.
201. Iyer, S., et al., *VE-cadherin-p120 interaction is required for maintenance of endothelial barrier function.* Am J Physiol Lung Cell Mol Physiol, 2004. **286**(6): p. L1143-53.
202. Herron, C.R., et al., *p120 regulates endothelial permeability independently of its NH2 terminus and Rho binding.* Am J Physiol Heart Circ Physiol, 2011. **300**(1): p. H36-48.
203. Carmeliet, P., et al., *Targeted deficiency or cytosolic truncation of the VE-cadherin gene in mice impairs VEGF-mediated endothelial survival and angiogenesis.* Cell, 1999. **98**(2): p. 147-57.
204. Anastasiadis, P.Z., *p120-ctn: A nexus for contextual signaling via Rho GTPases.* Biochim Biophys Acta, 2007. **1773**(1): p. 34-46.
205. Beckers, C.M., V.W. van Hinsbergh, and G.P. van Nieuw Amerongen, *Driving Rho GTPase activity in endothelial cells regulates barrier integrity.* Thromb Haemost, 2010. **103**(1): p. 40-55.
206. Anastasiadis, P.Z., et al., *Inhibition of RhoA by p120 catenin.* Nat Cell Biol, 2000. **2**(9): p. 637-44.
207. Noren, N.K., et al., *p120 catenin regulates the actin cytoskeleton via Rho family GTPases.* J Cell Biol, 2000. **150**(3): p. 567-80.
208. Yap, A.S., W.M. Brieher, and B.M. Gumbiner, *Molecular and functional analysis of cadherin-based adherens junctions.* Annual Review of Cell and Developmental Biology, 1997. **13**: p. 119-146.
209. Ehrlich, J.S., M.D. Hansen, and W.J. Nelson, *Spatio-temporal regulation of Rac1 localization and lamellipodia dynamics during epithelial cell-cell adhesion.* Dev Cell, 2002. **3**(2): p. 259-70.
210. Martinez-Rico, C., et al., *Integrins stimulate E-cadherin-mediated intercellular adhesion by regulating Src-kinase activation and actomyosin contractility.* J Cell Sci, 2010. **123**(Pt 5): p. 712-22.
211. O'Toole, T.E., et al., *Integrin cytoplasmic domains mediate inside-out signal transduction.* J Cell Biol, 1994. **124**(6): p. 1047-59.

212. Bodeau, A.L., et al., *A functional comparison of mutations in integrin beta cytoplasmic domains: effects on the regulation of tyrosine phosphorylation, cell spreading, cell attachment and beta1 integrin conformation.* J Cell Sci, 2001. **114**(Pt 15): p. 2795-807.
213. Cheung, L.W., P.C. Leung, and A.S. Wong, *Cadherin switching and activation of p120 catenin signaling are mediators of gonadotropin-releasing hormone to promote tumor cell migration and invasion in ovarian cancer.* Oncogene, 2010. **29**(16): p. 2427-40.
214. Garcia, A.J., F. Huber, and D. Boettiger, *Force required to break alpha5beta1 integrin-fibronectin bonds in intact adherent cells is sensitive to integrin activation state.* J Biol Chem, 1998. **273**(18): p. 10988-93.
215. Ridley, A.J., et al., *The small GTP-binding protein rac regulates growth factor-induced membrane ruffling.* Cell, 1992. **70**(3): p. 401-10.
216. Ridley, A.J., *Rho GTPases and cell migration.* J Cell Sci, 2001. **114**(Pt 15): p. 2713-22.
217. Tan, W., et al., *An essential role for Rac1 in endothelial cell function and vascular development.* FASEB J, 2008. **22**(6): p. 1829-38.
218. Noren, N.K., et al., *Cadherin engagement regulates Rho family GTPases.* J Biol Chem, 2001. **276**(36): p. 33305-8.
219. Kovacs, E.M., et al., *Cadherin-directed actin assembly: E-cadherin physically associates with the Arp2/3 complex to direct actin assembly in nascent adhesive contacts.* Curr Biol, 2002. **12**(5): p. 379-82.
220. Gallant, N.D. and A.J. Garcia, *Model of integrin-mediated cell adhesion strengthening.* J Biomech, 2007. **40**(6): p. 1301-9.
221. Ades, E.W., et al., *HMEC-1: establishment of an immortalized human microvascular endothelial cell line.* J Invest Dermatol, 1992. **99**(6): p. 683-90.
222. Kalman, D., et al., *Ras family GTPases control growth of astrocyte processes.* Mol Biol Cell, 1999. **10**(5): p. 1665-83.
223. Gallant, N.D., et al., *Micro- and nano-patterned substrates to manipulate cell adhesion.* J Nanosci Nanotechnol, 2007. **7**(3): p. 803-7.
224. Gallant, N.D. and A.J. Garcia, *Quantitative analyses of cell adhesion strength.* Methods Mol Biol, 2007. **370**: p. 83-96.
225. Zar, J.H., *Biostatistical analysis*. 1999: Prentice Hall.
226. Chen, C.S., et al., *Geometric control of cell life and death.* Science, 1997. **276**(5317): p. 1425-8.
227. Ingber, D.E., *Tensegrity: the architectural basis of cellular mechanotransduction.* Annu Rev Physiol, 1997. **59**: p. 575-99.
228. Ingber, D.E., *The architecture of life.* Sci Am, 1998. **278**(1): p. 48-57.
229. Dike, L.E., et al., *Geometric control of switching between growth, apoptosis, and differentiation during angiogenesis using micropatterned substrates.* In Vitro Cell Dev Biol Anim, 1999. **35**(8): p. 441-8.
230. Ingber, D.E., *The origin of cellular life.* Bioessays, 2000. **22**(12): p. 1160-70.
231. Wurm, F.M., *Production of recombinant protein therapeutics in cultivated mammalian cells.* Nat Biotechnol, 2004. **22**(11): p. 1393-8.
232. Jayapal, K.P., et al., *Recombinant protein therapeutics from CHO cells-20 years and counting.* Chemical Engineering Progress, 2007. **103**(10): p. 40.
233. Omasa, T., M. Onitsuka, and W.D. Kim, *Cell engineering and cultivation of chinese hamster ovary (CHO) cells.* Curr Pharm Biotechnol, 2010. **11**(3): p. 233-40.
234. Gibbs, J. *Effective Blocking Procedures*. ELISA Technical Bulletin, 2001. **3**, 6.

235. Troyanovsky, S.M., *Mechanism of cell-cell adhesion complex assembly.* Curr Opin Cell Biol, 1999. **11**(5): p. 561-6.
236. Troyanovsky, R.B., J. Klingelhofer, and S. Troyanovsky, *Removal of calcium ions triggers a novel type of intercadherin interaction.* J Cell Sci, 1999. **112 (Pt 23)**: p. 4379-87.
237. Vianay, B., et al., *Single cells spreading on a protein lattice adopt an energy minimizing shape.* Phys Rev Lett, 2010. **105**(12): p. 128101.
238. Levina, E.M., et al., *Cytoskeletal control of fibroblast length: experiments with linear strips of substrate.* J Cell Sci, 2001. **114**(Pt 23): p. 4335-41.
239. Picone, R., et al., *A polarised population of dynamic microtubules mediates homeostatic length control in animal cells.* PLoS Biol, 2010. **8**(11): p. e1000542.
240. Weis, S.M., *Vascular permeability in cardiovascular disease and cancer.* Curr Opin Hematol, 2008. **15**(3): p. 243-9.
241. Vestweber, D., et al., *Cell adhesion dynamics at endothelial junctions: VE-cadherin as a major player.* Trends Cell Biol, 2009. **19**(1): p. 8-15.
242. Huveneers, S., et al., *Vinculin associates with endothelial VE-cadherin junctions to control force-dependent remodeling.* J Cell Biol, 2012. **196**(5): p. 641-52.
243. Xia, P., et al., *Activation of sphingosine kinase by tumor necrosis factor-alpha inhibits apoptosis in human endothelial cells.* J Biol Chem, 1999. **274**(48): p. 34499-505.
244. Xia, P., et al., *Tumor necrosis factor-alpha induces adhesion molecule expression through the sphingosine kinase pathway.* Proc Natl Acad Sci U S A, 1998. **95**(24): p. 14196-201.
245. Fu, J., et al., *Mechanical regulation of cell function with geometrically modulated elastomeric substrates.* Nat Methods, 2010. **7**(9): p. 733-6.
246. Yang, M.T., et al., *Assaying stem cell mechanobiology on microfabricated elastomeric substrates with geometrically modulated rigidity.* Nat Protoc, 2011. **6**(2): p. 187-213.
247. Stapleton, S.C., A. Chopra, and C.S. Chen, *Force measurement tools to explore cadherin mechanotransduction.* Cell Commun Adhes, 2014. **21**(3): p. 193-205.
248. Vedula, S.R., et al., *Emerging modes of collective cell migration induced by geometrical constraints.* Proc Natl Acad Sci U S A, 2012. **109**(32): p. 12974-9.
249. Rabodzey, A., et al., *Mechanical forces induced by the transendothelial migration of human neutrophils.* Biophys J, 2008. **95**(3): p. 1428-38.
250. Liu, Z.J., N.J. Sniadecki, and C.S. Chen, *Mechanical Forces in Endothelial Cells during Firm Adhesion and Early Transmigration of Human Monocytes.* Cellular and Molecular Bioengineering, 2010. **3**(1): p. 50-59.
251. Liu, Z.J., et al., *Mechanical tugging force regulates the size of cell-cell junctions.* Proceedings of the National Academy of Sciences of the United States of America, 2010. **107**(22): p. 9944-9949.
252. Nelson, C.M., et al., *Emergent patterns of growth controlled by multicellular form and mechanics.* Proc Natl Acad Sci U S A, 2005. **102**(33): p. 11594-9.
253. Ganz, A., et al., *Traction forces exerted through N-cadherin contacts.* Biol Cell, 2006. **98**(12): p. 721-30.
254. Sim, J.Y., et al., *Spatial distribution of cell-cell and cell-ECM adhesions regulates force balance while main-taining E-cadherin molecular tension in cell pairs.* Mol Biol Cell, 2015. **26**(13): p. 2456-65.

255. Mertz, A.F., et al., *Cadherin-based intercellular adhesions organize epithelial cell-matrix traction forces.* Proc Natl Acad Sci U S A, 2013. **110**(3): p. 842-7.
256. Kowalczyk, A.P. and B.A. Nanes, *Adherens junction turnover: regulating adhesion through cadherin endocytosis, degradation, and recycling.* Subcell Biochem, 2012. **60**: p. 197-222.
257. Kockx, M., et al., *Pharmacological inhibition of dynamin II reduces constitutive protein secretion from primary human macrophages.* PLoS One, 2014. **9**(10): p. e111186.
258. Kirchhausen, T., E. Macia, and H.E. Pelish, *Use of dynasore, the small molecule inhibitor of dynamin, in the regulation of endocytosis.* Methods Enzymol, 2008. **438**: p. 77-93.
259. Newton, A.J., T. Kirchhausen, and V.N. Murthy, *Inhibition of dynamin completely blocks compensatory synaptic vesicle endocytosis.* Proc Natl Acad Sci U S A, 2006. **103**(47): p. 17955-60.
260. Macia, E., et al., *Dynasore, a cell-permeable inhibitor of dynamin.* Dev Cell, 2006. **10**(6): p. 839-50.
261. Chircop, M., et al., *Inhibition of dynamin by dynole 34-2 induces cell death following cytokinesis failure in cancer cells.* Mol Cancer Ther, 2011. **10**(9): p. 1553-62.
262. Hill, T.A., et al., *Inhibition of dynamin mediated endocytosis by the dynoles--synthesis and functional activity of a family of indoles.* J Med Chem, 2009. **52**(12): p. 3762-73.

VITA

CHIMDIMNMA CHINAZA ESIMAI

ESIMAI was born in Onitsha, Anambra State, Nigeria, to Drs. Charles and Grace Esimai. Immigrating to the United States during junior high school, she graduated from Arlington High School as the first African-American valedictorian in the school district's history in 2004, winning several scholastic and community service awards. Esimai then earned an SB in Biomedical Engineering Sciences (with honors) and a Romance Languages and Literature Citation (specialty in Spanish) from the Faculty of Arts and Sciences of Harvard University, Cambridge, Massachusetts in June 2008. At Harvard, she held many roles, including that of Howard Hughes Medical Institute Research Fellow, president of the Nigerian Students Association, finance coordinator for the Harvard Undergraduate Research Symposium and the Harvard Arise Young Naija Conference, and coordinator of the National Society for Black Scientists and Engineers. For her efforts, she was awarded the Harvard Society of Black Scientists and Engineers Citation for Outstanding Contribution in Science, amongst other accolades. After working in Spain and Portugal during the summer months of 2008, she enrolled in Georgia Tech's Interdisciplinary Bioengineering Program and the Woodruff School of Mechanical Engineering in August 2008. Esimai graduated with a Master's Degree in Mechanical Engineering and Bioengineering in May 2012. At Georgia Tech, Esimai's many leadership roles included but were not limited to being co-organizer for the Life Sciences Track for the Georgia Tech Graduate Technical Symposium, co-organizer and financial coordinator for numerous Bioengineering and Biosciences Unified Graduate Students (BBUGS) Techniques Symposia, co-organizer for the BBUGS Research Committee, president of the Georgia Tech Bethel Campus Fellowship, and coordinator of the NSF REU SURE Program.